INVESTIGATION OF TECHNIQUES FOR IMPROVEMENT OF SEASONAL STREAMFLOW FORECASTS IN THE UPPER RIO GRANDE BASIN

A Dissertation

by

SONG-WEON LEE

Submitted to the Office of Graduate Studies of
Texas A&M University
in partial fulfillment of the requirements for the degree of

DOCTOR OF PHILOSOPHY

August 2004

Major Subject: Civil Engineering

INVESTIGATION OF TECHNIQUES FOR IMPROVEMENT OF SEASONAL STREAMFLOW FORECASTS IN THE UPPER RIO GRANDE BASIN

A Dissertation

by

SONG-WEON LEE

Submitted to Texas A&M University
in partial fulfillment of the requirements
for the degree of

DOCTOR OF PHILOSOPHY

Approved as to style and content by:

Thomas M. Over (Co-Chair of Committee)	Anthony T. Cahill (Co-Chair of Committee)
Andrew G. Klein (Member)	Ralph A. Wurbs (Member)
Paul N. Roschke (Head of Department)	

August 2004

Major Subject: Civil Engineering

ABSTRACT

Investigation of Techniques for Improvement of Seasonal Streamflow Forecasts in the Upper Rio Grande Basin. (August 2004)

Song-Weon Lee, B.A., Kyunghee University;

M.E., Texas A&M University

Co-Chairs of Advisory Committee: Dr. Thomas M. Over
Dr. Anthony T. Cahill

The purpose of this dissertation is to develop and evaluate techniques for improvement of seasonal streamflow forecasts in the Upper Rio Grande (URG) basin in the U.S. Southwest. Three techniques are investigated. The first technique is an investigation of the effects of the El Niño/Southern Oscillation (ENSO) on temperature, precipitation, snow water equivalent (SWE), and the resulting streamflow at a monthly time scale, using data from 1952 to 1999 (WY). It was seen that the effects of ENSO on temperature and precipitation were confined to certain months, predominantly at the beginning and end of the winter season, and that the effect of these modulations of temperature and precipitation by ENSO can be seen in the magnitude and time variation of SWE and streamflow.

The second part is a comparison of the use for snowmelt-runoff modeling of the newly available snowcover product based on imagery from the satellite-borne Moderate Resolution Imaging Spectroradiometer (MODIS) with the long-time standard snowcover product from the National Hydrological Remote Sensing Center (NOHRSC). This

comparison is made using the Snowmelt Runoff Model (SRM) in two watersheds located inside the URG basin. This comparison is important because the MODIS snowcover product could greatly improve the availability of snowcover information because of its high spatial (500m) and temporal (daily) resolutions and extensive (global) coverage. Based on the results of this comparison, the MODIS snowcover product gives comparable snowcover information compared to that from NOHRSC.

The final part is an investigation of streamflow forecasting using mass-balance models. Two watersheds used in the comparison of MODIS and NOHRSC snowcover products were again used. The parameters of the mass-balance models are obtained in two different ways and streamflow forecasts are made on January 1st, February 1st, March 1st and April 1st. The first means of parameter estimation is to use the parameter values from 1990 to 2001 SRM streamflow simulations and the second means is by optimization. The results of this investigation show that mass-balance models show potential to improve the long-term streamflow forecasts in snowmelt-dominated watersheds if dependable precipitation forecasts can be provided.

DEDICATION

This dissertation is dedicated to my parents, wife, brother, sister, father-in-law and mother-in-law for their faith, enthusiasm and enduring support

ACKNOWLEDGMENTS

I would like to express my sincere gratitude to my co-advisor, Dr. Thomas M. Over, for providing constant guidance and encouragement during the course of this work. He has always been a stimulus and shown what research is and how I need to do research. I truly appreciate all the advice and discussions with him. I am also grateful to Dr. Anthony T. Cahill, co-advisor, and Dr. Ralph A. Wurbs for serving as members of my advisory committee. I would like to especially thank Dr. Andrew G. Klein for his guidance, patience, and support. Without his help during the course of this work, my research would have been very hard, and I doubt whether I would have finished my Ph.D dissertation.

I have no words to express my gratitude to my parents who have shown their limitless love, support, and patience throughout the course of my entire life. I am also thankful to my wife, Junghyun Kim for her constant sacrifices and encouragement throughout the years of my study. I thank her parents for giving me this lovable wife and for their great support.

TABLE OF CONTENTS

CHAPTER Page

CHAPTER Page

LIST OF FIGURES

Page

Page

LIST OF TABLES

CHAPTER I

GENERAL INTRODUCTION

Water resources allocation and management is a growing concern for the southwestern United States. As the region's population continues to expand, water resources will remain a major concern into the foreseeable future and may be a limiting factor in the region's future growth. Possible responses to this situation include reducing demand and increasing supply, but also more efficient management of existing water resources based on forecasts of water supply. Accordingly, this dissertation reports an investigation of three techniques for the improvement of seasonal streamflow forecasts from snowmelt-dominated basins, using the Upper Rio Grande (URG) basin as a case study.

The first chapter presents an investigation of the effects of the El Niño/Southern Oscillation (ENSO) phenomenon on climate and hydrology, especially precipitation, temperature, and resulting snowpack and streamflow in the URG basin. These effects could be particularly beneficial for streamflow forecasting, because they offer the possibility of predicting the spring snowpack and resulting summer streamflow volume from previous fall or winter seasons, and thus increasing the lead time of the streamflow forecasts used by water managers. Although there have been many investigations related

---

This dissertation follows the style and format of *Hydrological Processes*.

to ENSO, they have usually demonstrated precipitation, temperature, snow and subsequent streamflow responses to climatic variability over relatively large spatial scales, such as the entire western United States. While helpful in understanding the general climatic responses in large areas, such results are of limited practicality in water resources management because the characteristic response of specific hydrologically important areas within the regions may differ from the regional response to ENSO events, or the response may even differ within the basin of interest. Accordingly, this chapter investigates how the seasonal cycles of precipitation and temperature, and the resultant snow water equivalent (SWE) and streamflow in the URG are modulated by ENSO.

The second chapter of this dissertation approaches the improvement of snowmelt-dominated streamflow forecasting by an investigation of the efficacy of a new remotely-sensed snowcover product for use in snowmelt-runoff modeling. This product is produced from imagery from the satellite-borne Moderate Resolution Imaging Spectroradiometer (MODIS). The investigation compares streamflow simulations with the Snowmelt Runoff Model (SRM) using two different sources of snow covered area (SCA) information: the MODIS snowcover product and the widely-used snowcover product made by the National Operational Hydrologic Remote Sensing Center (NOHRSC) in two watersheds located inside the URG basin. This comparison is important because the MODIS snowcover product could greatly improve the availability of snowcover information because of its high spatial (500m) and temporal (daily) resolutions and extensive (global) coverage, compared to other existing snowcover

products having limited spatial or temporal resolutions. This chapter addresses several specific questions. The first is how, if at all, the timing and volume of simulated snowmelt runoff differs in streamflow simulations that use MODIS and NOHRSC snow maps as SCA inputs? Secondly, can the observed differences in the simulated streamflow be explained by spatial-temporal differences in the mapped snowcover between the two products during the snowmelt period? Thirdly, how do zonal SWE volumes on April 1st calculated using the Modified Depletion Curve (MDC) produced by SRM differ when MODIS and NOHRSC snow maps are used, and how do these estimates compare to *in situ* snowpack telemetry (SNOTEL) observations.

The final part of this dissertation presents an investigation of the potential and limitations of two types of mass-balance models for long-term (April – September) streamflow forecasts on January 1st, February 1st, March 1st and April 1st in the two sub-watersheds of the URG which were used in the comparison of MODIS and NOHRSC snowcover products above. The first type of mass-balance model uses the parameter values from SRM streamflow simulations and the second type obtains its parameters by optimization. The model based on the parameters from SRM streamflow simulations uses SWE values at the time of forecast and forecast period parameter values (snow and rainfall runoff coefficients) obtained through SRM streamflow simulations and precipitation data during the forecast period. The optimized parameter models use historical SWE values at the time of forecast and historical precipitation values during the forecast period in order to get optimized parameter values for four different mass-balance models of increasing complexity during the forecast period. After getting

parameter values for two types of mass-balance models, it is necessary to apply the forecasted precipitation in the forecasting mode. For precipitation forecasts, the observed precipitation amount in the year of interest was first applied to look at the forecast performance apart from the effect of the errors of precipitation forecast although this is not a real forecasting situation. Meanwhile, in the actual forecasting mode, it is difficult to forecast the long-term precipitation amount. So, the ensemble forecasting method was used; that is, the historical precipitation data in each year was applied except for the year of interest and then streamflow forecasts were obtained for each precipitation value. This gives a distribution of streamflow forecasts from which statistics such as mean and standard deviation (i.e., the uncertainty due to precipitation) can be calculated. In addition to these streamflow forecasts, the streamflow forecasts using only SWE and the forecasting for naturalized streamflow from Natural Resources Conservation Service (NRCS) are also presented in order to compare the relative accuracy of streamflow forecasts among the models. Through these investigations, it is possible to see first what are the potential and limitations of these two types of mass-balance model parameterizations in these snowmelt-dominated watersheds; second, comparing streamflow forecast accuracy using the two types of parameterizations, how much improvement in the accuracy of streamflow forecasts can be achieved in the optimized parameter models compared to models which use the parameter values from SRM streamflow simulations and which type of mass-balance model can show the best results related to the long-term streamflow forecasts; third, as previous studies have shown that forecast model performance depends on site-specific characteristics, what

kind of differences in model parameters and performance are obtained and why this kind of difference occurs between these two closely-located watersheds.

The dissertation is organized as follows: Chapter II shows the effects of ENSO on temperature, precipitation, SWE and resulting streamflow in the URG basin. Chapter III evaluates the use of the MODIS snowcover product for simulating streamflow using SRM by comparing streamflow simulation made using the NOHRSC snowcover product in the two watersheds located inside the URG. Chapter IV shows the potential and limitations of mass-balance models for long-term volumetric streamflow forecasts in the same watersheds as those in Chapter III. Finally, general conclusions for this dissertation are provided in Chapter V.

CHAPTER II

EFFECTS OF THE ENSO ON TEMPERATURE, PRECIPITATION, SNOW WATER EQUIVALENT AND RESULTING STREAMFLOW IN THE UPPER RIO GRANDE BASIN*

2.1. Introduction

Water resource allocation and management is a growing concern for the southwestern United States. As the region's population continues to expand, water resources will remain a major concern into the foreseeable future and may be a limiting factor in the region's future growth. Possible responses to this situation include reducing demand and increasing supply, but also more efficient management of existing water resources based on forecasts of water supply. From this perspective, the recognition of the effects of the ENSO phenomenon on western US climate and hydrology, especially precipitation, temperature, and resulting snowpack, is particularly beneficial for water resource management, because it offers the possibility of predicting the spring snowpack, and thus increasing the lead time of the streamflow forecasts used by water managers (Brown, 1998; Cayan, 1996; Cayan and Webb, 1992; Groisman and Easterling, 1994;

---

*Reprinted with permission from "Effects of the El Nino-southern oscillation and temperature, precipitation, snow water equivalent and resulting streamflow in the Upper Rio Grande river basin" by Songweon Lee, Andrew Klein, and Thomas Over, 2004. *Hydrological Processes*, **18**:1053-1071. 2004 by Wiley.

Kahya and Dracup, 1993; Dracup and Kahya, 1994; Cayan et al., 1999; Woolhiser et al.,1993; Clark et al., 2001;Redmond and Koch, 1991; Ropelewski and Halpert, 1986).

For the southwestern United States, it is generally observed that during the negative phase of ENSO (El Niño), there is higher precipitation, higher streamflow, and lower temperatures, while during positive ENSO phase (La Niña), precipitation is lower, streamflow is reduced, and temperatures are higher. Considerable research has examined the relationship between climate, snow conditions, and resulting streamflow with ENSO on a regional scale in the western United States. Redmond and Koch (1991) found negative correlations between average October-March monthly precipitation and June-November averaged SOI and positive correlations over the same period between temperature and SOI in the desert southwest. Ropelewski and Halpert (1986, 1989), Kahya and Dracup (1993) and Dracup and Kahya (1994) detected consistent response regions in the United States in terms of precipitation, temperature, and streamflow for El Niño and La Niña periods through harmonic and composite analysis. More recent papers have investigated how daily precipitation, temperature, and streamflow frequency and volume is affected by ENSO phase (Woolhiser et al., 1993; Gershunov, 1998; Gershunov and Barnett, 1998; Cayan et al., 1999). For example, Cayan et al. (1999) found a higher than average frequency of occurrence of high precipitation and streamflow in the desert southwest during El Niño years, and the opposite during La Niña years. Cayan (1996) noted that there are more significant differences in April 1st SWE between La Niña and neutral years rather than between El Niño and neutral years in five regions encompassing the western US, especially in the Rocky Mountains.

Brown (1998) also demonstrated the differences in snow conditions during El Niño and La Niña periods using satellite and climate station data throughout the United States. Clark et al. (2001) showed that differences in the seasonal changes and intensities of SWE response to each ENSO phase exist in several smaller regions of the desert southwest.

This previous research has demonstrated precipitation, temperature, snow and subsequent streamflow responses to climatic variability over relatively large spatial scales, such as the western United States. While helpful in understanding the general climatic responses in large areas, it is of limited practicality in water resource management because the characteristic response of specific hydrologically important areas within the regions may differ from the regional response to ENSO events, or the response may even differ within the basin of interest. Accordingly, this paper investigates how the seasonal cycles of precipitation and temperature, and the resultant snowpack and streamflow in the URG basin are modulated by variable sea surface temperatures in the tropical Pacific Ocean (i.e., ENSO).

The URG (**Figure 2-1**) of southern Colorado and northern New Mexico, defined here as the area draining the Rio Grande at Espanola, NM (at the downstream end of HUC 130201), has an area of approximately 43,000 km^2 including a non-contributing area in the northeast, and elevations ranging from approximately 1600 to 4200 m, with highest elevations found in the northwest corner of the basin along the continental divide. Snow formation usually begins in late October, with the snowpack

approaching its maximum near April 1st as measured by SWE values from snowcourse sites scattered across the basin and in more recent years also at SNOTEL sites.

Several factors led to the selection of this basin as the study area. The primary reason is that all reaches of the Rio Grande are heavily utilized as a water resource. The ground water resources in the Middle Rio Grande Basin, which is just downstream and supplies water to the Albuquerque metropolitan area, have recently been determined to be significantly less than previously believed (Thorn et al., 1993; Bartolino and Cole, 2002), putting further pressure on the surface water supply from the URG. In addition, as mentioned above, it is not clear that the results of the rather large-scale studies of the influence of ENSO on climate and streamflow can be successfully scaled down to this basin, especially because the URG lies near the northern limit of the southwestern US region as defined in previous studies.

This study combines meteorological data from National Weather Service (NWS) stations, which are located at lower elevations (**Table 2-1**) with SWE data from snowcourse sites, which are located at higher elevations (**Table 2-2**). Meteorological observations are combined with streamflow data from United States Geological Survey (USGS) streamgaging stations (**Table 2-3**) having long records. Both stations on the Rio Grande River itself and in tributary basins with limited direct human influence are investigated. The locations of all observation sites are shown in **Figure 2-1**. Analysis begins in 1952 because prior to this date the temperature and precipitation timeseries at NWS stations are very incomplete.

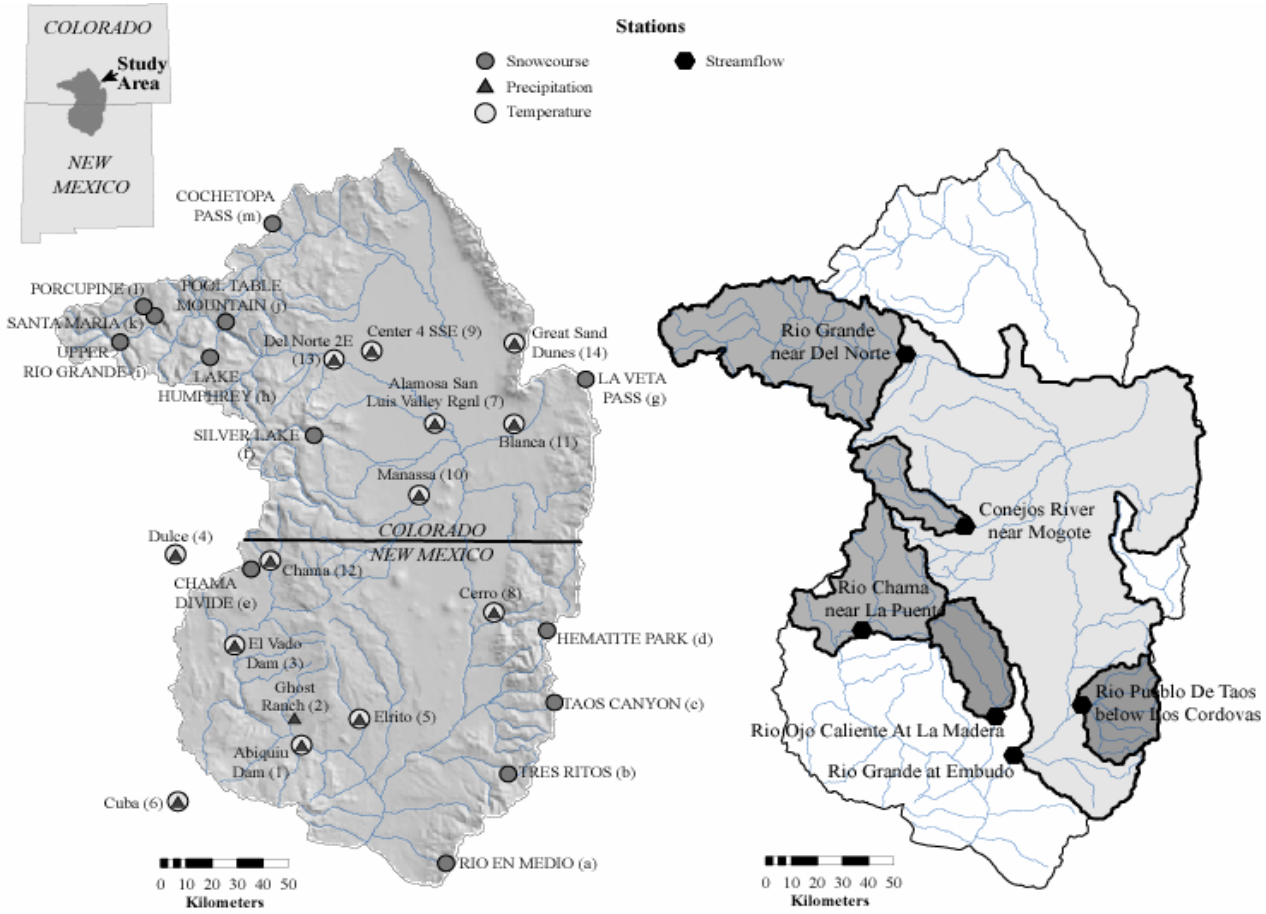

Figure 2-1. Maps of the Upper Rio Grande basin showing the gauging sites used in this study: (a) NWS temperature and precipitation stations and snowcourse sites (left); (b) USGS streamflow gauging stations and their drainage basins (right)

Combining temperature and precipitation observations with long-term snow course measurements and streamflow enables investigation of how variations in ENSO are associated with differences in monthly precipitation and temperature, which in turn affect SWE and streamflow. It is hoped that by better understanding these relationships, streamflow prediction in the URG can be improved. It is also hoped that a better understanding of these relationships can improve modeling of how the magnitude and timing of streamflow in the URG basin may be altered by anthropogenic climate changes such as global warming.

Table 2-1. Temperature and precipitation stations

Number	Name	Elevation (m)	Mean Annual Temp. (^{o}C)	Mean Annual Precip. (mm)
(1)	Abiquiu Dam	1945	10.28	251
(2)	Ghost Ranch	1969	*	288
(3)	El Vado Dam	2054	7.05	372
(4)	Dulce	2071	6.88	450
(5)	Elrito	2094	9.34	314
(6)	Cuba	2147	7.79	336
(7)	Alamosa San Luis Valley Rgnl	2296	5.14	185
(8)	Cerro	2332	6.85	329
(9)	Center 4 SSW	2339	5.04	183
(10)	Manassa	2344	5.74	200
(11)	Blanca	2362	5.66	222
(12)	Chama	2393	5.57	545
(13)	Del Norte 2E	2399	6.22	262
(14)	Great Sand Dunes Natl. Mon.	2475	6.43	287

*data not available.

Table 2-2. Snowcourse sites

Number	Name	Elevation (m)
(a)	Rio En Medio	3139
(b)	Tres Ritos	2621
(c)	Taos Canyon	2774
(d)	Hematite Park	2896
(e)	Chama Divide	2384
(f)	Silver Lakes	2896
(g)	La Veta Pass	2877
(h)	Lake Humprey	2743
(i)	Upper Rio Grande	2865
(j)	Pool Table Mountain	2999
(k)	Santa Maria	2926
(l)	Porcupine	3133
(m)	Cochetopa Pass	3048

Table 2-3. Characteristics of streamgaging stations

Station	USGS Number	Period of Record (WY)	Station Elevation (m)	Drainage Area (km^2)	Annual Average Streamflow (m^3/s)	Linear Trend in Standardized [1] annual average streamflow (yr^{-1})	Station Summary
Rio Chama Near La Puente	08284100	1956 – 99	2159	1229	10.25	**0.0097** [2]	Diversions for irrigation of about 41.6 km^2
Rio Ojo Caliente At La Madera	08289000	1952 – 99	1938	1073	1.94	0.0088	Diversions for irrigation of about 14 km^2
Rio Grande At Embudo	08279500	1952 – 99	1765	19098	22.87	**0.0122**	Irrigation of about 2504.8 km^2 in Colorado and 161 km^2 in New Mexico
Rio Pueblo De Taos Below Los Cordovas	08276300	1958 – 99	2028	973	1.89	**0.0180**	Diversions for irrigation of about 48.5 km^2
Rio Grande Near Del Norte	08220000	1952 – 99	2432	3379	24.00	**0.0067**	Small diversions for irrigation, storage in 4 reservoirs (0.156 km^3 total capacity), and some incoming interbasin transfers
Conejos River Near Mogote	08246500	1952 – 99	2521	722	8.81	0.0031	Small diversions for irrigation

[1]Streamflows are standardized by dividing by mean annual streamflow.

[2]Slopes in bold face are significant at the 90% level.

2.2. Methods

2.2.1. ENSO Designation Criteria

Determination of ENSO phase has historically been accomplished using the Southern Oscillation Index (SOI), which is based on deviations in the sea level pressure differences between the island of Tahiti and Darwin, Australia. In this study, water years (October-September) in the period 1952-1999 were assigned to one of three ENSO phases, El Niño, neutral and La Niña by three different methods, which employ two different indices: the Climate Prediction Center (CPC) SOI and the Troup SOI for the period 1952-1999 (WY). If at least one of the three methods designated a year as either El Niño or La Niña it was considered as such, otherwise it is considered as neutral. The designation of ENSO phase based on these three criteria is shown in **Figure 2-2**. The three methods occasionally differ in their assignment of ENSO phase to each water year. However, conflict never occurs between El Niño and La Niña, only between El Niño or La Niña and neutral. In the first method, when the 5-month running mean of the CPC SOI is in the lower (upper) 25% of its distribution for five consecutive months in a calendar year (CY), then the following WY is designated as an El Niño (La Niña) year (Ropelewski and Jones, 1987; Dracup and Kahya, 1994). This method suffers from the problem that ENSO designation may change through time as additional years are added. The second method uses the Troup SOI. When average Troup SOI values for the period running from April of the previous WY to March of current WY fall below –5, the current year is designated as an El Niño year. When average SOI values for the April-

March period are above +5, the year is designated as a La Niña year (Chiew et al., 1998). The third method follows the criteria used in Redmond and Koch (1991) and Cayan et al. (1999). When the average CPC SOI of June to November of the previous CY is –0.5 or less, then the present WY is designated as El Niño. If it is greater than or equal to +0.5, then the present WY is designated as La Niña. June to November SOI values are selected because SOI values for these months exhibit the strongest correlation with winter climate over the western United States among the averages of leading 6-month SOI values prior to the winter in question.

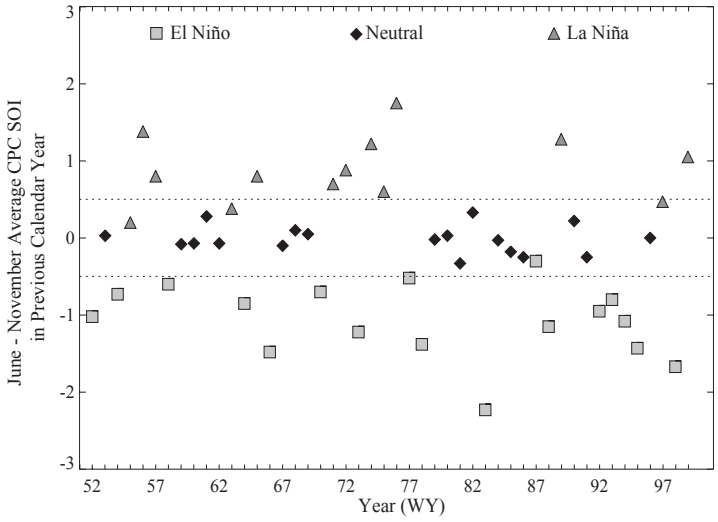

Figure 2-2. Designation of ENSO phases in each year. Symbols show designation of the ENSO phase of each year following the criteria described in the text. Location of symbols gives the June-November average CPC SOI. The dashed lines, at +/-0.5, separate the years into La Niña (top), neutral (middle), and El Niño (bottom), according to the CPC SOI criterion

To check the randomness of assigned ENSO phase through time, two runs tests were performed (Davis, 1986). In each, the years of one ENSO phase (El Niño or La Niña) were assigned the value of one and the other two assigned a value of 0. The randomness of this binomial distribution was then tested using a runs test. The Z statistic and associated probability were 0.33 and 0.37, respectively for El Niño years, indicating they occur randomly throughout the study period. For La Niña years the Z statistic and its probability were –1.47 and 0.07, respectively, indicating La Niña years are not randomly distributed over the study period, but are rather clumped in a few periods. That is, there is a possibility that these clumped La Niña years could result in periods of higher or lower values of the interest variables in terms of long-term trends. Therefore, it was necessary to remove any long-term trends in the climate variables to isolate ENSO effects from background climate variability.

2.2.2. Data

Figure 2-1 shows the locations of the NWS, snowcourse, and streamgaging stations that provide the temperature, precipitation, SWE, and streamflow records used in this study, and **Tables 2-1, 2-2** and **2-3** provide basic information about them. All NWS stations are located at relatively low elevations in the basin between 1945 and 2475 m a.s.l. while snowcourse sites are located relatively higher in the basin at elevations between 2384 and 3139 m a.s.l. Only those NWS and snowcourse stations with records covering the period from 1952 to 1999 and with a small percentage of missing days were used in the analysis.

To create uniform time series of temperature and precipitation, small gaps in missing data were replaced. Gaps in NWS daily average temperatures were filled at the daily time scale using regressions against another station with a complete or nearly complete record. Daily average temperatures were then averaged up to monthly values. NWS daily precipitation depths were summed to monthly totals with months having ten or more missing days considered to be missing months. These months were then filled at the monthly time scale by the normal-ratio method (e.g., McCuen, 1998) using the average of monthly to annual total precipitation. Snowcourse SWE exists as individual measurements taken once per month, near the end of the months of January through March or April. No attempt was made to replace missing snowcourse measurements. Monthly streamflow data were taken as published by the USGS, so no replacement of missing periods was performed.

2.2.3. Removal of Long-Term Trends

Following creation of monthly data sets as described above, long-term trends in each variable of interest were removed. This was done to isolate the effect of short-term and potentially ENSO-related fluctuations from longer-term factors such as the Pacific Decadal Oscillation as stated above. Long-term temporal trends were estimated by fitting first and second-order polynomials to the monthly temperature, precipitation, and SWE data, and to annual streamflow time series. Except in the case of streamflow, for each station, a long-term trend was computed separately for each month. In the first-order analysis of temperature and precipitation, a significant fraction of station-months

(25% for both temperature and precipitation) had slopes significant at the 90% level. Linear temperature trends for individual station-months had ranged from –0.052 to 0.078 $^{\circ}C$ per year, and monthly averages of slopes over all stations ranged from –0.016 (October and June) to 0.044 (March) $^{\circ}C$ per year. As an example, **Figure 2-3** shows the slopes of the linear trends in average temperature for each station during October and March. The average linear temperature increase over all stations and months was just 0.002 $^{\circ}C$ per year.

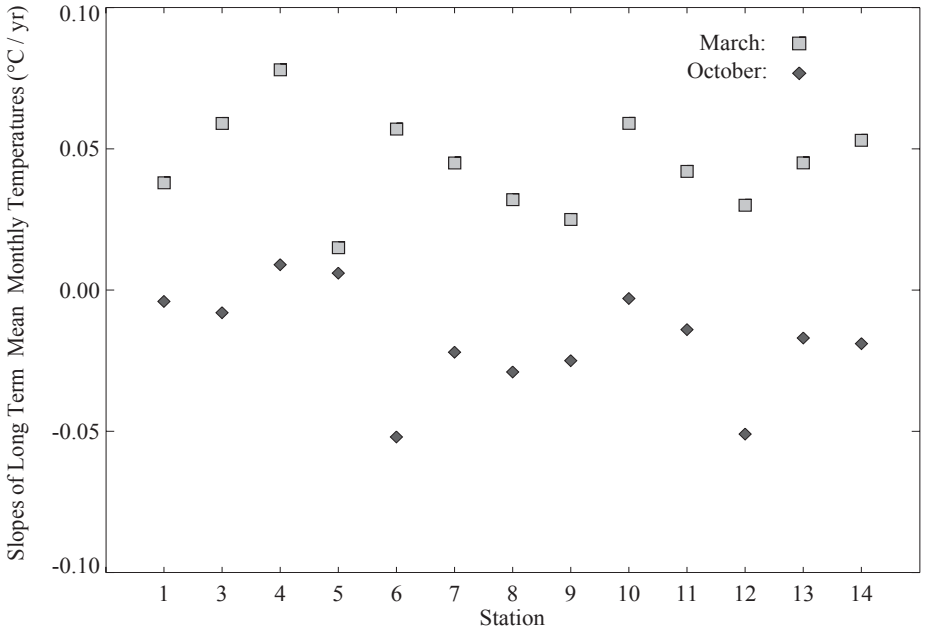

Figure 2-3. Slopes of October and March monthly average temperature versus time, obtained by linear regression. October is the month having the smallest slope averaged over the stations, and March is the month with the largest averaged slopes

Linear trends for individual precipitation station-months ranged from –0.280 to 0.644 mm/yr, and monthly averages ranged from –0.064 (December) to 0.327 (September) mm/yr, with an average over all stations and months of 0.137 mm/yr. Due to a larger variance relative to precipitation, only 3 of 39 (7.7%) station-months of SWE values had significant linear trends, with slope values ranging from –2.1 to 2.1 mm/yr. As given in **Table 2-3**, standardized linear trends in streamflow had slopes ranging from 0.0031 per year at the Conejos River station to 0.018 per year at the Rio Pueblo station. In all but the Conejos River and Rio Ojo station, trends were significant at the 90% level.

Similar levels of significance were found for both coefficients in the second-order analysis. However, the removal of linear trends in temperature and streamflow were deemed to be sufficient, as subsequent composite analysis (described below) was found to be relatively insensitive to the use of first vs. second-order residuals.

Streamflow exhibits both a strong annual cycle and large, non-Gaussian variation at the monthly time scale; therefore long-term trends in streamflow were obtained and subtracted only at the annual (water year) time scale. Monthly residuals were then computed using a downscaling technique, in which the annual residual for a given year was divided into monthly residuals by multiplying the year's residual by the monthly fraction of that year's annual streamflow in the original data. Analytically, if the annual residual for year T is denoted as $\varepsilon_Q(T)$ and defined in the usual way through $Q(T) = a_Q + b_Q T + \varepsilon_Q(T)$, where $Q(T)$ is the annual average streamflow in year T and

a_Q and b_Q are the constants defining the estimated linear trend, then the monthly residual for month *t* in year *T*, $\delta(t,T)$, is computed as

$$\delta(t,T) = \frac{q(t,T)}{12Q(T)}\varepsilon_Q(T) \tag{2.1}$$

where $q(t,T)$ is the average streamflow in month *t* in year *T*. Where appropriate, results using the streamflow residuals given below have been standardized by dividing by the root-mean-square-residuals (*RMSR*), defined as

$$RMSR = \sqrt{\frac{1}{N}\sum_{T=1}^{N}\varepsilon_Q^2(T)} \tag{2.2}$$

where *N* is the number of years of record, and other symbols are defined as before.

2.2.4. Tests for Dependence on ENSO

After residuals were obtained by subtracting the linear trend, two types of analyses were performed to test dependence of the variables on ENSO. First, continuous dependence on ENSO was tested by plotting the residuals versus June to November average CPC SOI. Second, a composite analysis was performed in which separate averages of the residuals for El Niño, neutral, and La Niña years were obtained for each variable, month, and station, according to the ENSO phase designations shown in **Figure 2-2**.

2.3. Results

2.3.1. Continuous Dependence on CPC SOI

Among the meteorological variables (maximum and average monthly temperatures and total monthly precipitation) the number of station-months exhibiting linear dependence (i.e., correlation) on CPC SOI at various significance levels is similar for both the original variables and detrended residuals. For example, for average monthly temperature, the fraction of station-months having significant correlation at the 90% level is 12.8% for the original variables and 15.4% for the residuals, while for monthly total precipitation, these fractions are 17.3% and 12.2%, respectively. Using maximum monthly temperatures as opposed to average monthly temperatures greatly increases the number of station-months having significant correlation; for this variable, the fractions are 23.7% for the original variables and 24.4% for the residuals.

2.3.1.1. Temperature and Precipitation

As in the analysis of temporal trends above (and in the composite analysis below), certain months stand out as having the most significant linear dependence on CPC SOI. For average monthly temperature, these months are March and November. The correlations of March average temperature residuals versus CPC SOI are positive at all stations with an average slope of 0.526 $^{\circ}C$ per SOI unit (note from **Figure 2-2** that the total range of CPC SOI is about four units), and are significantly positive at the 90%

level at 10 of the 13 stations. This indicates colder temperatures in El Niño years and warmer ones in La Niña, as expected. Similarly, for the residuals in November, all correlations are again positive with an average slope of 0.401 $^{\circ}C$ per SOI unit, but the significance is not as high: only two are significant at the 90% level, but 11 of 13 are significant at the 70% level. The results are similar in the original variables for November, but not as strong for March. Combining November and March, four stations have the weakest relationship to the CPC SOI: Dulce, El Vado Dam, Blanca, and Chama (stations 3, 4, 11 and 12). As can be seen in **Figure 2-1,** the first three of these stations are clustered in the upper reaches of the Rio Chama drainage basin in the west-central portion of our study area.

For precipitation, the months with the strongest linear dependence on CPC SOI were November, December, and March. The correlations of total monthly precipitation residuals versus CPC SOI are negative for all stations during these months, with average slopes of -3.53, -3.11, and -4.08 mm per SOI unit, respectively. This indicates these months are wetter in El Niño versus La Niña years. These correlations are significant at the 90% level at 3 of 14 stations in November and December, and at 8 of 14 in March. The number of significant slopes jumps to 12, 10, and 12 in November, December, and March, respectively, if the 70% significance level is considered. The results are somewhat stronger in the case of precipitation residuals than in the original variable. Unlike temperature, there is not a clear geographical clustering of the stations that fail to have significant slopes.

2.3.1.2. Snow Water Equivalent

Whether residuals or original values are considered, no snowcourse stations have significant (at the 90% level) correlations of SWE with SOI for January and February, but several do have significant negative correlations during (late) March. The latter are the snowcourse stations in the eastern portion of the study area (stations a-d and g). This implies larger snow storage in El Niño versus La Niña years. As will be discussed in the composite analysis below, this is the result of a decrease in SWE from February to March in La Niña years, apparently caused by warmer March temperatures and lower March precipitation.

2.3.1.3. Streamflow

Annual streamflow and its residuals at all the stations exhibit negative correlation with June to November CPC SOI, implying more runoff in El Niño years, as would be expected (see **Figure 2-4** for the results in the residuals). This dependence is significant at the 90% at the Rio Chama station, Rio Grande at Embudo, and the Rio Pueblo station for the original variables, but only at the Rio Pueblo and Rio Ojo stations in the residuals. The four southernmost stations (all stations except Rio Grande near Del Norte and the Conejos River station) have slopes that are significant at the 70% level, whether original variables or residuals are considered.

The lack of significance of the Rio Grande near Del Norte can be understood in terms of the SWE results discussed above, since the cluster of snowcourse stations in its

drainage basin did not show a significant correlation between SWE and the June to November CPC SOI. Because no meteorological stations are situated in this watershed (the Del Norte NWS station is near the streamgage and thus is unlikely to characterize of the entire drainage basin), it is difficult to characterize streamflow in this basin in terms of temperature and precipitation. Human regulation of streamflow may also be an influence on the dependence of streamflow on ENSO in this watershed.

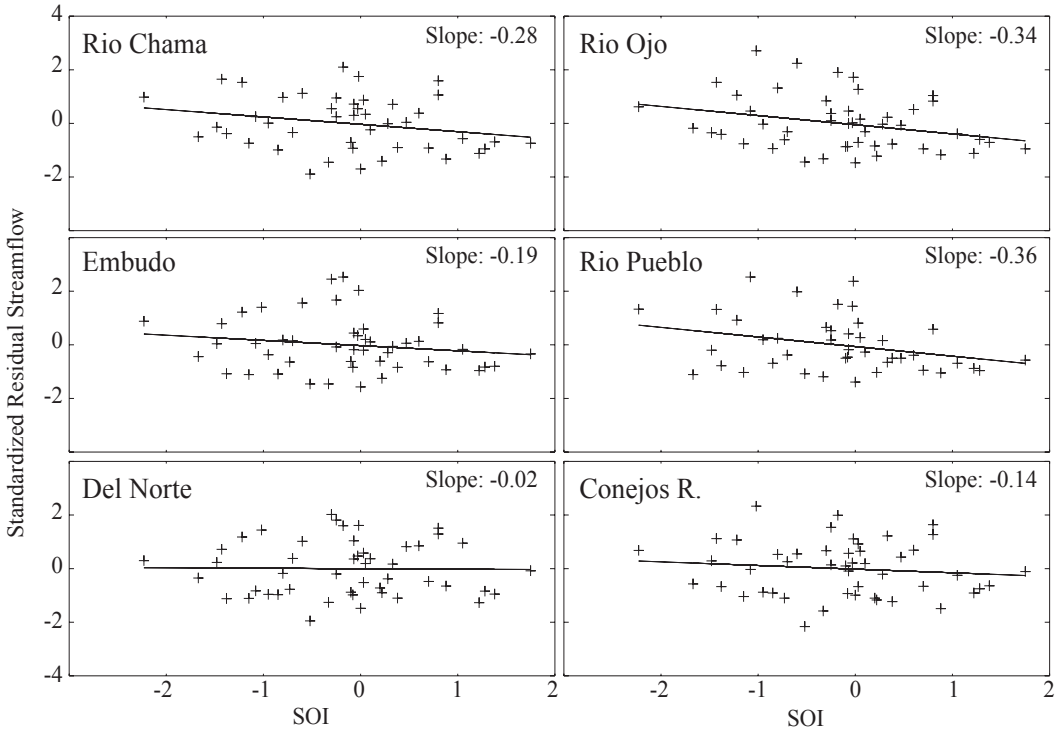

Figure 2-4. Regression of standardized annual streamflow residuals versus June-November average CPC SOI. Standardization here is by division by the stations's RMSR (see Equation (2.2) for definition)

2.3.2. Composite Analysis

Composite Analysis is the analysis of composites created by separating instances of a climatic phenomenon into classes based on some criterion, and then combining, usually by averaging, the instances falling into each class (Brown, 1998; Dracup and Kahya, 1994; Kahya and Dracup, 1993; Clark etc., 2001). Here we apply composite analysis to the weather and hydrology in the URG by first separating the years into El Niño, neutral, La Niña years, according to the criterion described in the ENSO designation section above, and then by combining the years by averaging the temperature, precipitation, SWE, and streamflow data separately for each ENSO phase, primarily to test if statistically significant differences exist between the ENSO phases.

2.3.2.1. Temperature and Precipitation

An overview of the composite analysis results for temperature and precipitation residuals are shown in **Figures 2-5 and 2-6**. The statistically significant months are the same as observed above in the linear dependence of these variables versus CPC SOI. In **Figure 2-5**, it may be seen that El Niño years are colder vis-a-vis neutral years in November and March while La Niña years are warmer vis-a-vis neutral years in March, but without much difference in November. **Figure 2-6** shows that El Niño years are unusually wet (wetter than neutral years) in November, while in December and March it is La Niña years that are unusually dry (drier than neutral years).

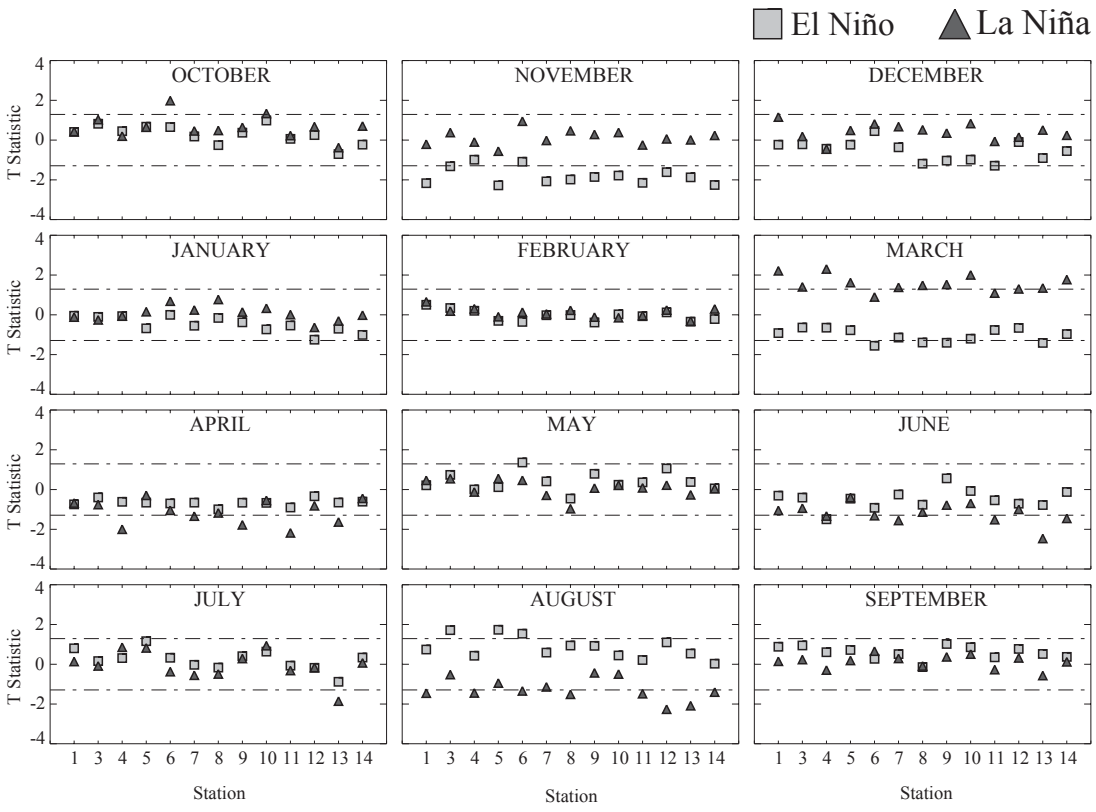

Figure 2-5. The *t*-statistics of differences of composite average monthly temperature residuals between El Niño and neutral years and between La Niña and neutral years

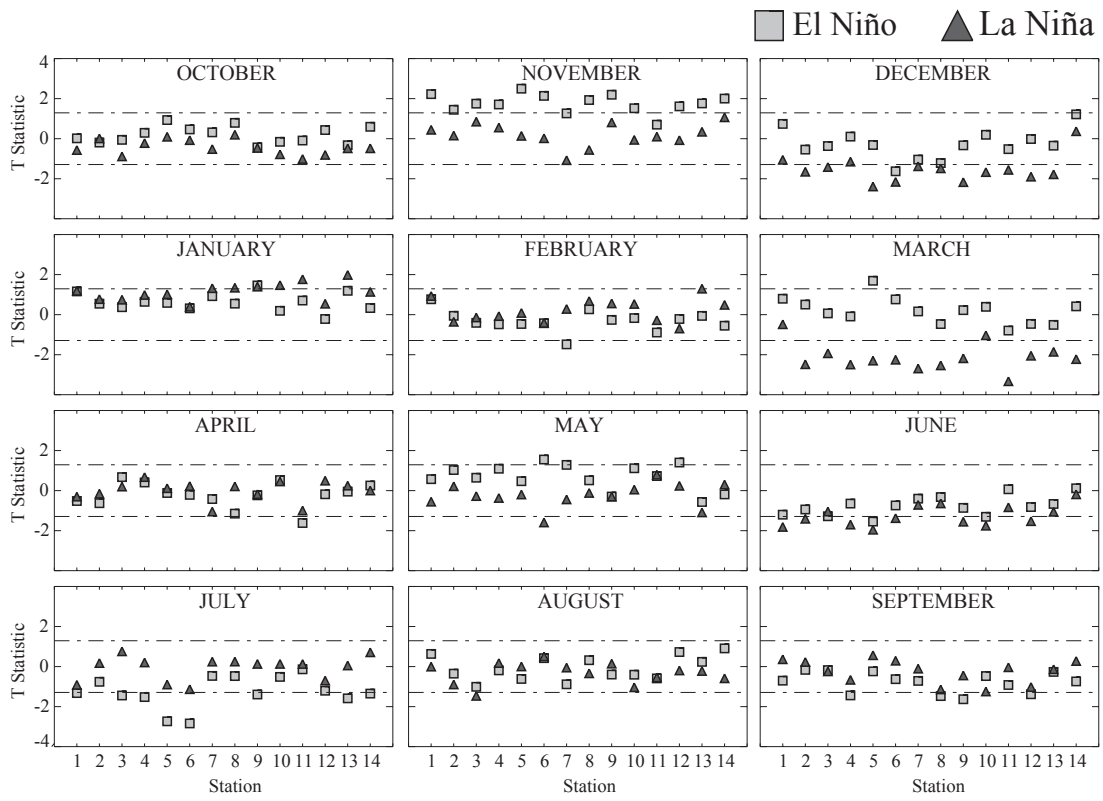

Figure 2-6. The *t*-statistics of differences of composite average monthly precipitation residuals between El Niño and neutral years and between La Niña and neutral years

Spatial patterns in temperature and precipitation residuals between ENSO phases across the basin are illustrated in **Figure 2-7** and **2-8**, respectively. **Figure 2-7** suggests the presence of two inter-basin geographical patterns in the residual temperatures. The first is a spatial variability in the colder El Niño November temperatures. During El Niño years, stations in the northern and eastern sections of the basins appear to have colder temperatures than other stations. This is consistent with *t*-test statistic result (**Figure 2-5**). November El Niño temperature residuals are smallest

for stations in the southwestern portion of the basin, which is consistent with the CPC SOI dependences for these stations.

Stations across the entire basin show March temperature of La Niña years to be warmer than neutral or El Niño years. Thus warmer temperatures during March in La Niña years appear to be more spatially uniform than the colder El Niño November temperatures. However, warmer temperatures in the southwestern portion of the basin appear slightly smaller than those in the northeast.

A map of composite average precipitation residuals from October to September is illustrated in **Figure 2-8**. Overall, spatial patterns in the monthly precipitation residuals are less obvious than those for the temperature residuals. However, during the snow season, March precipitation during La Nina years is most notably lower in the southwestern stations, but a more mixed response is seen at the other stations. Stations in the southern half of the basin also tend to experience a greater increase in precipitation during November of El Niño years, but the response is not seen at all stations.

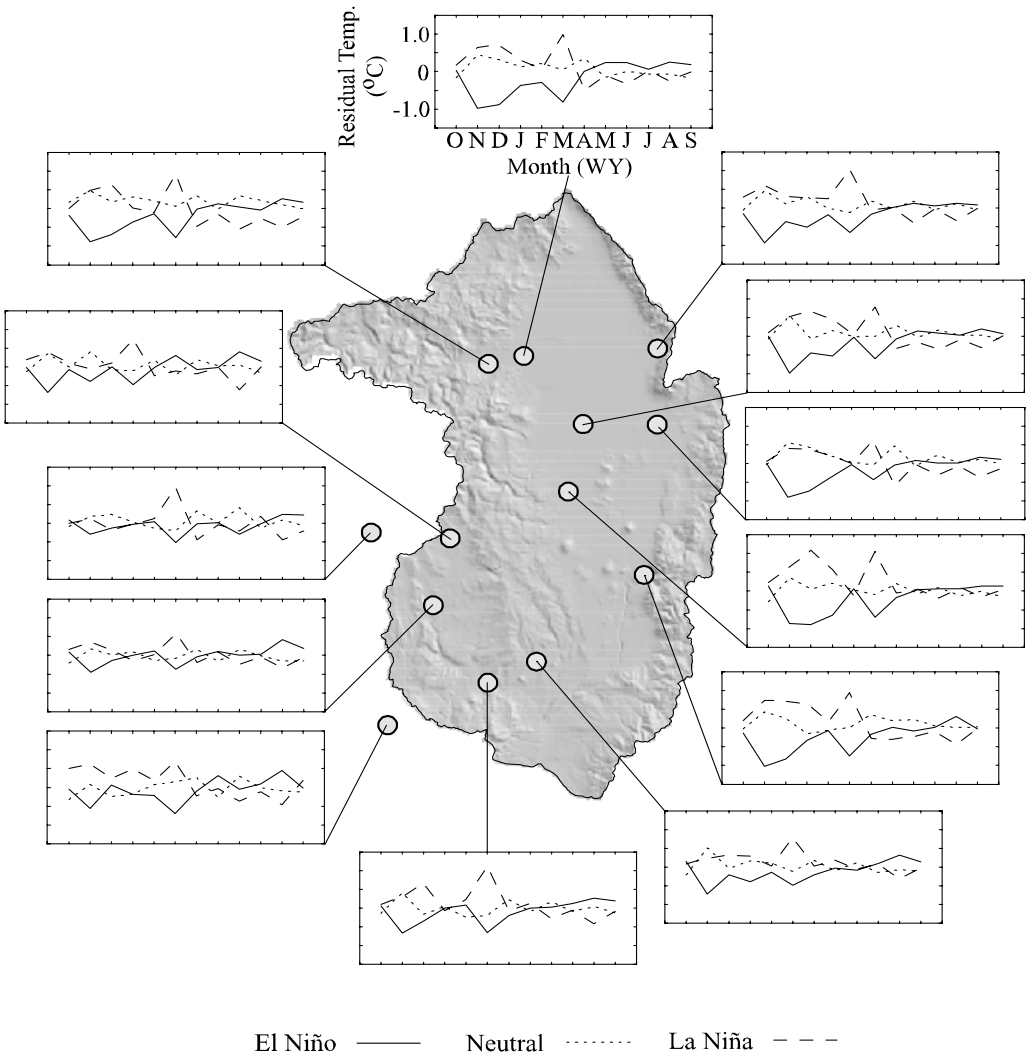

Figure 2-7. Map of composite average monthly temperature residuals at each station from October through September for El Niño (solid), neutral (dotted), La Niña (dashed) years

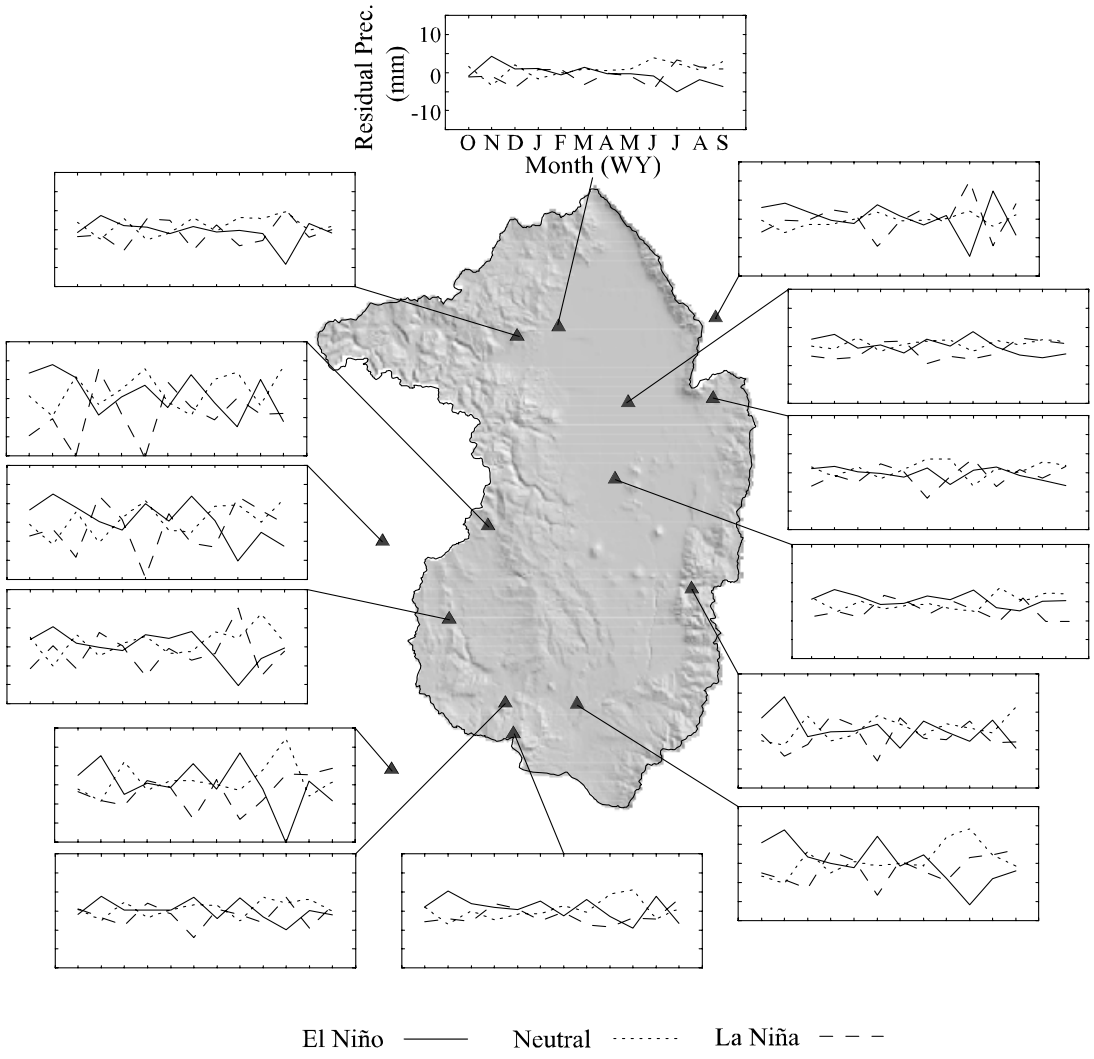

Figure 2-8. Map of composite average monthly total precipitation residuals at each station from October through September for El Niño (solid), neutral (dotted), La Niña (dashed) years

2.3.2.2. Snow Water Equivalent

Composite averages of SWE residuals at the snowcourse stations are shown in **Figure 2-9** in which exhibit consistent spatial patterns. With a single exception, Silver Lake, all stations with small SWE residuals for the January through March period occur along the URG's western side. The stations with the largest decrease in March SWE during La Niña years occur on the basin's eastern side. A one-tailed *t*-test (not shown) indicates that either or both of the differences between El Niño or La Niña and neutral years are significant at about the 90% level for March at these eastern stations. This is consistent with the analysis of the linear dependence of SWE on CPC SOI.

2.3.2.3. Streamflow

Composite average analyses of annual residual streamflow are shown in **Figure 2-10**. As expected, El Niño years have higher residual streamflow than La Niña years, except at Rio Grande at Del Norte. Standardizing the residuals by dividing by the station's RMSR as in **Figure 2-10** gives a more realistic picture of the significance of the differences, where, according to a *t*-test (not shown), the streamflow in La Niña years is significantly less at about a 90% level than that in the neutral years at all stations except Rio Grande at Del Norte. The difference between La Niña and neutral years at Conejos River near Mogote is a bit deceiving, however, since at this station the composite average streamflow residual in neutral years is larger than that during El Niño years.

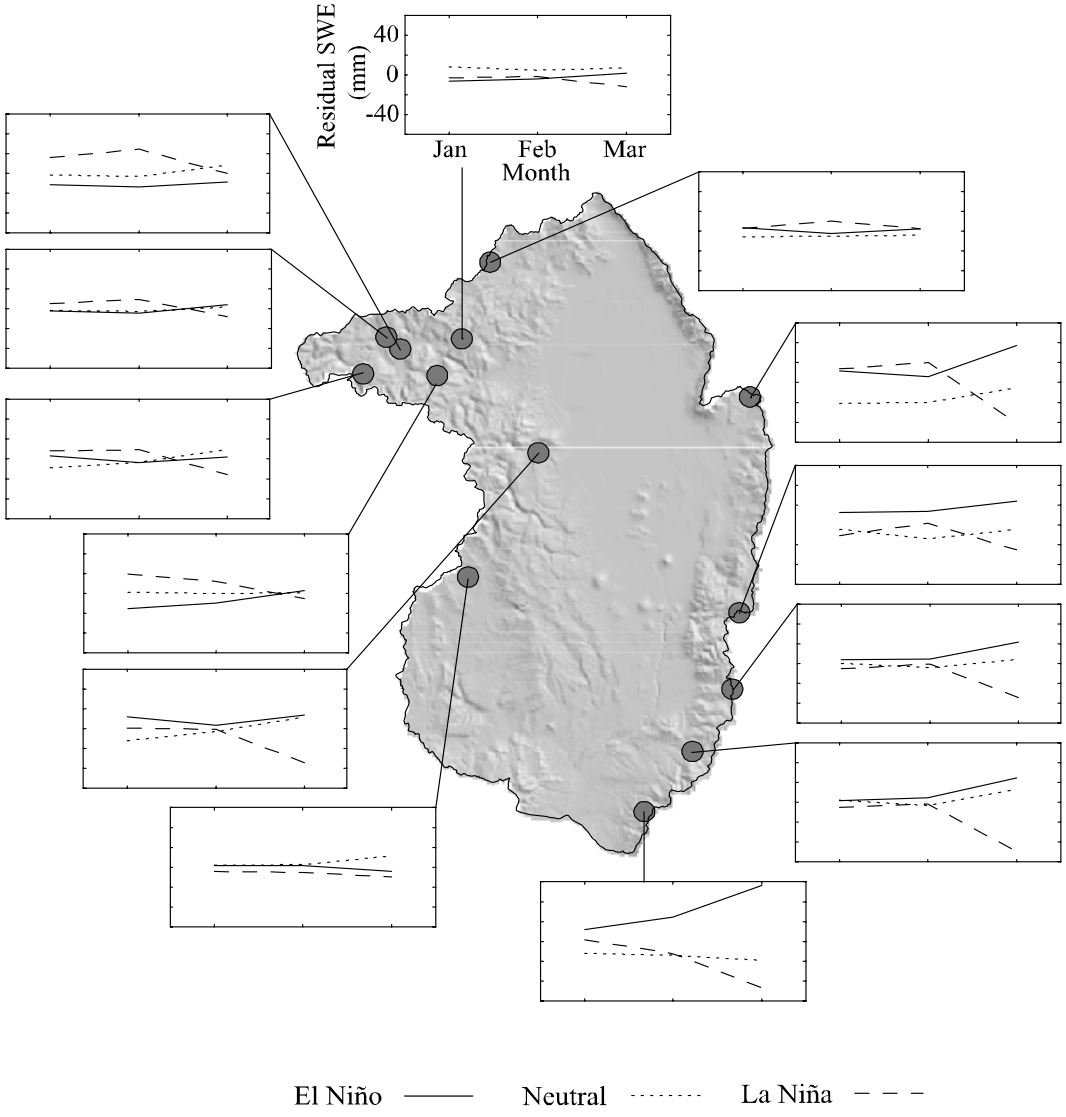

Figure 2-9. Map of composite average SWE residuals at each snowcourse station for January, February and March

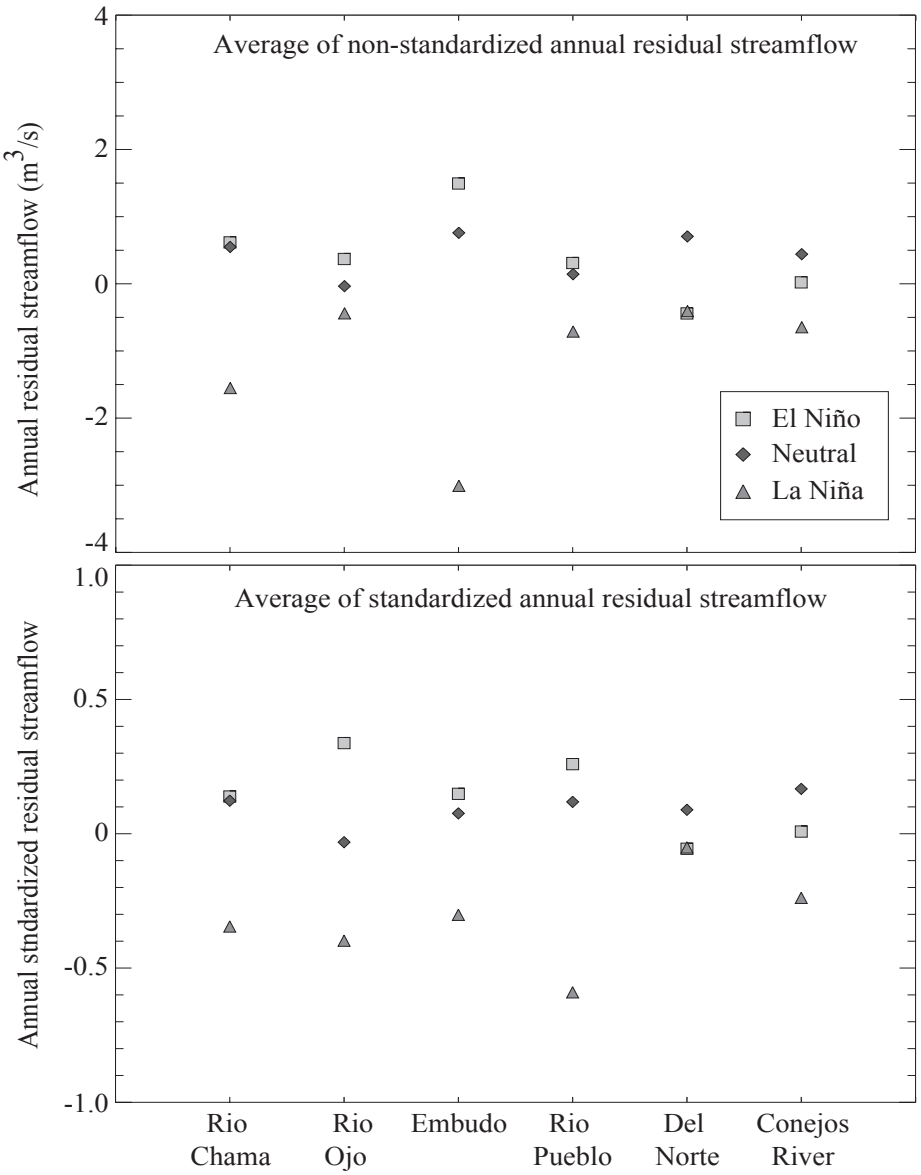

Figure 2-10. Composite average of annual streamflow residuals: (above) not standardized; (below) standardized by dividing by RMSR

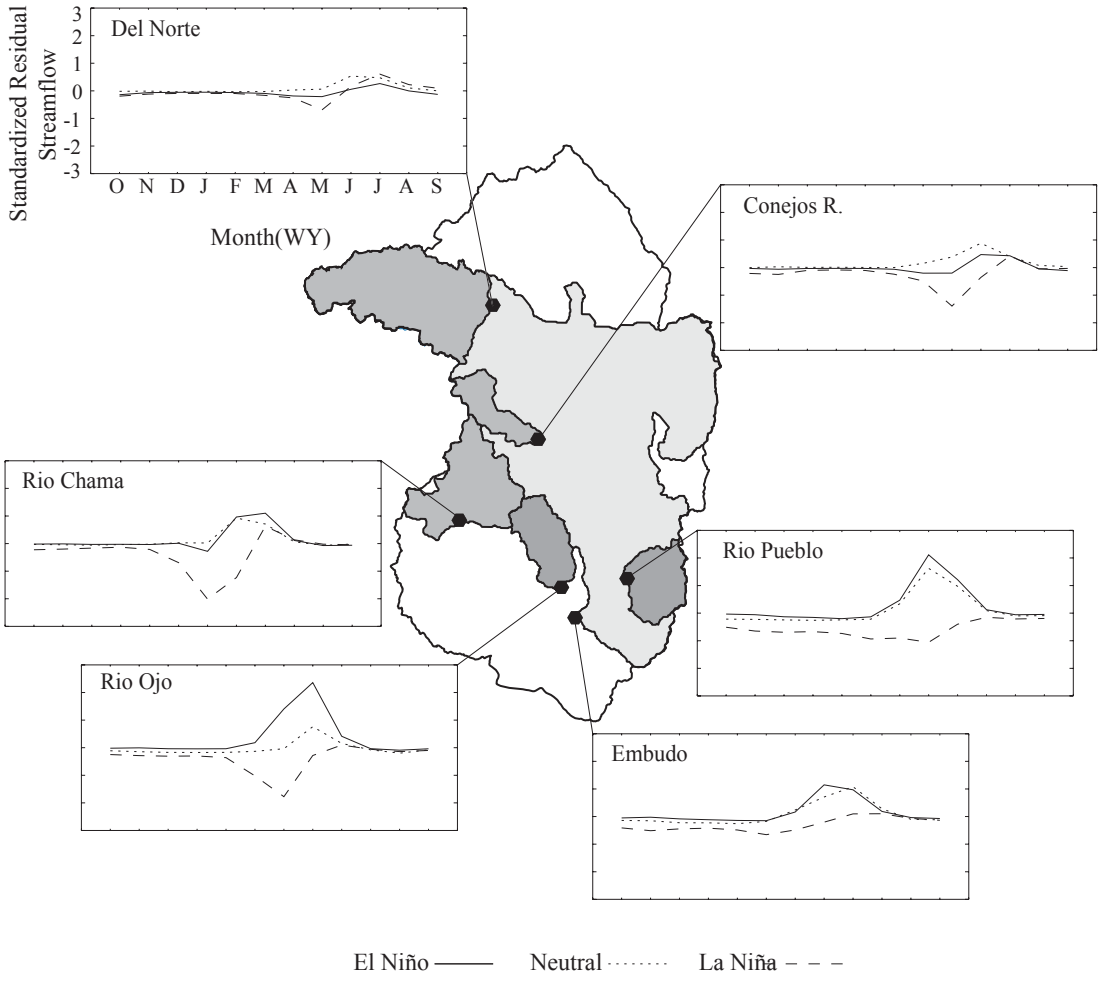

Figure 2-11. Map of composite average of monthly streamflow residuals standardized by dividing by RMSR for each of the gauging stations studied

Figure 2-11 shows the composite average of the standardized monthly streamflow residuals in the map. In interpreting these plots, it is important to remember the definition of the monthly residual, given above in equation (2-1). Based on this definition, it can be seen that the monthly residual for a certain ENSO phase is the combined effect of the size of the annual residuals for that phase and the proportion of the annual flow volume in that month. Thus, for example, the large negative La Niña residual in April at the Rio Chama station implies that this station has relatively large average annual residuals in La Niña years and that a large proportion (in fact, the largest of any month) of annual flow volume occurs during April. More subtly, the positive monthly average La Niña residual in June at this station is due to a few La Niña years having positive residuals and relatively significant streamflow during June, whereas most La Niña years have negative residuals and relatively little streamflow during June. This same situation occurs in July at the Rio Grande near Del Norte and the Conejos River near Mogote. An analogous situation obtains for the negative composite average residual streamflow in April during El Niño years at the Rio Chama station.

These monthly composite average residual plots therefore show certain subtle features at each basin that make generalization difficult. The Rio Chama and Rio Ojo stations, which are the two smaller basins in the southwestern portion of the study area, show strong evidence of a lag in the maximum streamflow month between La Niña and El Niño years, with the La Niña maximum streamflow month occurring earlier in the year, as generally warmer March temperatures and lower March SWE values at the snowcourse stations on the east side of the URG would suggest. However, the

snowcourse station actually within the Rio Chama basin (Chama Divide) does not show lower March SWE values, and the stations with the strongest tendency to have reduced March SWE are in the region of the Rio Pueblo in the southeast, which does not exhibit a lag in the maximum month between La Niña and El Niño. However, the Rio Pueblo station shows significant winter streamflow during La Niña years (and very little during winter in other ENSO phases), as does Rio Grande at Embudo, to which the Rio Pueblo is a nearby tributary.

The most northern Conejos River and Rio Grande near Del Norte stations show rather similar behavior: rather weaker separation of composite average annual residuals (especially at Rio Grande near Del Norte), an earlier maximum month during La Niña years (May) compared to El Niño and neutral years (June or July), and a higher or equally high maximum during neutral compared to El Niño years. These behaviors correspond to the warmer March during La Niña years, combined with little difference in SWE values: apparently the average total snowpack affecting flow at these stations is rather independent of ENSO phase (again especially at Rio Grande near Del Norte), but it melts somewhat earlier during La Niña years.

2.4. Conclusions

Examination of two important climatic factors, temperature and precipitation, along with streamflow volumes and estimates of SWE at snowcourse stations, over the years of 1952-1999 demonstrates that ENSO appears to modulate temperature and precipitation across the basin, affecting snow accumulation and melt and the resulting

streamflow in the URG river basin. Through these sequential observations of ENSO impacts, it is possible to demonstrate how the important climatological factors of temperature and precipitation are modulated by ENSO and how these climatological differences are embodied in the form of SWE and resultant streamflow differences among ENSO phases.

Comparing this research with previous work highlights some important characteristics concerning temperature and precipitation responses to ENSO episodes specific to the URG. First, temperature differences between the three ENSO phases are not uniform throughout the entire winter, but are concentrated at its beginning and end - only in November and March. Second, El Niño years as compared to neutral years, the URG experiences lower temperatures especially in the basins northern and eastern sections. Third, during La Niña years March temperatures are warmer across the entire basin. With respect to temperature at least, it can be said that ENSO in the URG affects the length of winter rather than its severity.

Statistically significant increases in monthly precipitation totals were found to occur only during November. Significantly lower precipitation occurred in La Niña years during December and March. So, as with temperature mentioned above, climatological precipitation differences during El Niño, neutral and La Niña years are confined to certain months, predominantly at the beginning and end of the winter season.

Differences in snow water equivalent among ENSO phases were found to exist only during March. While meteorological variations in observed ENSO response were primarily temporal with relatively weak geographical variability, SWE dependence on

ENSO was seen to vary geographically very strongly, with snowcourse stations on the east side of the URG showing a strong ENSO signal, while those on the west side did not.

These findings are also important in another respect. The URG has been the site of several studies investigating the effect of increased temperatures caused by anthropogenic climatic change (van Katwijk, et al., 1993; Rango, 1992; Rango and Martinec, 1997). Many of these studies have employed the Snowmelt Runoff Model (SRM), which is one of most popular models to simulate and predict snowmelt in mountainous areas. SRM has been used to model predict changes in the streamflow regime caused by temperature changes (e.g. global warming). In these studies, temperatures changes have usually been considered uniform. However, our work suggests that assuming a uniform warming may be overly simplistic, and future modeling efforts may be able to predict climatically-induced streamflow variations more accurately if existing variations caused by ENSO are considered.

March during La Niña years is the critical month in determining differences in annual hydrograph in the URG. Higher temperatures and lower precipitation result in lower, and usually earlier, streamflow, compared to that of neutral and El Niño years. March therefore needs to be given special attention when modeling scenarios of streamflow under altered climatic conditions.

There are variable time lags between ENSO-modulated differences in temperature and precipitation and the resultant streamflow. Colder temperatures and greater precipitation in November of El Niño may result in more snow storage over the

winter and higher streamflow during the following snowmelt season – a time lag of several months. However, the impact of warmer and drier conditions during March of La Niña years on streamflow is more immediate, with almost no lag time occurring between ENSO modulated meteorological differences and the resultant streamflow.

Finally, La Niña years experience decreased annual streamflow compared to both El Niño and neutral water years. However, examination of the reduction of runoff during La Niña phase on a monthly basis reveals different responses at different stations. At most stations, with the exception of the Rio Grande at Embudo and Rio Pueblo, the peak streamflow month during La Niña years is earlier, though the size of the differences varies. At the Rio Grande near Del Norte, the effect of ENSO is rather slight, matching small differences in SWE between El Niño and La Niña years in this drainage basin. At the Rio Grande at Embudo and at Rio Pueblo, winter streamflow during La Niña years is greatly increased and the spring peak is attenuated.

The above observations demonstrate that improved streamflow forecasting using ENSO phase information, which has in the past been observed for the western US in general, should indeed be possible specifically for the URG. Particular features of the differences between El Niño, neutral and La Niña water years in terms of temperature and precipitation and resulting SWE and streamflow that can contribute to the improved forecasting have been provided by this research. However, responses vary in strength and in timing, and cannot be completely characterized in terms of meteorological and SWE data, given the sparseness of the long-term data network.

CHAPTER III

COMPARISON OF MODIS AND NOHRSC SNOWCOVER PRODUCTS FOR SIMULATING STREAMFLOW USING SNOWMELT RUNOFF MODEL

3.1. Introduction

Snowmelt is a dominant water resource for runoff and groundwater recharge in wide areas of the world and therefore it is very beneficial to obtain more accurate forecasts of snowmelt magnitude and timing. The utilization of snowcover information as an important source of data for runoff prediction started in 1930's with the use of aerial photographs (Potts, 1937). Many daily regional scale satellite-derived estimates of snow covered area (SCA) have become available since 1972 with the advent of National Oceanic and Atmospheric Administration - Advanced Very High Resolution Radiometer (NOAA-AVHRR) (Rango, 1986; Rango, 1996) and have been serving as input into snowmelt runoff models or weather prediction models around the world (Rango, 1980; Dey et al., 1983; Baumgartner et al., 1987; Richard and Gratton, 2001; Landesa and Rango, 2002). Especially in data-sparse regions such as the Himalayan or Andean Mountains, satellite-derived SCA information is the best routinely available SCA input for snowmelt runoff estimates (Rango, 1985; Compagnucci and Vargas, 1998).

Beginning in 1986, a 1 km snowcover product for the conterminous United States and portions of Canada has been operationally produced by the NOHRSC (Hartman et al., 1996; Hall et al., 2000; Bitner et al., 2002; Klein and Barnett, 2003; Maurer et al., 2003). A number of new satellite-derived snowcover maps covering all or portions of the Northern Hemisphere are currently produced including: the NOAA's 23 km Interactive Multisensor Snow and Ice Mapping System (IMS) charts (Ramsay, 2000), the 25 km Near Real-Time SSM/I EASE-Grid Daily Global Ice Concentration and Snow Extent from National Snow and Ice Data Center (NSIDC) made from Defense Meteorological Satellite Program (DMSP) F13 Special Sensor Microwave/Imager (SSM/I) passive microwave measurements (Chang et al., 1987; Armstrong and Brodzik, 2001), and new automated 5 km snowcover maps produced by the National Environmental Satellite, Data, and Information Service (NESDIS) using Geostationary Operational Environmental Satellite (GOES) and SSM/I (Romanov et al., 2000; Bitner et al., 2002) data.

A suite of snowcover products is also currently being produced from data collected by the MODIS instrument including a 500 m global daily product which is used here. NASA's MODIS began collecting science data from onboard the Terra (formerly known as EOS-AM1) spacecraft on February 24, 2000 and from onboard the Aqua (formerly known as EOS-PM1) spacecraft on June 24, 2002. MODIS has 36 spectral bands in the visible, near- and short-wave infrared and thermal portions of the electromagnetic spectrum and it views the earth's entire surface ranging from every day at high latitudes to every other day at low latitudes (Justice et al., 1998). The Distributed

Active Archive Center (DAAC) at the NSIDC currently distributes the snowcover products produced from MODIS (Scharfen et al., 1997; Hall et al., 2000). Their global extent and daily coverage enable these global MODIS snow products to augment existing remote-sensing derived continental and regional scale snowcover maps and provide high resolution snowcover information for areas of the world where snowcover maps are not currently produced.

A number of comparisons between different satellite-derived snow maps have been conducted (Baumgartner et al., 1987; Hall et al., 2000; Bitner et al. 2002; Rango et al., 2002; Klein and Barnett, 2003; Maurer et al., 2003; Rango et al., 2003). These studies have examined the relative snow-mapping accuracy of various snowcover maps or the relationship between snow-mapping accuracy and spatial resolution, ruggedness, or landcover type. **Table 3-1** lists recent studies which evaluate snowcover mapping techniques and assess the accuracy of these techniques either through the comparison of different snowcover products or the comparison between satellite-derived snow products and ground-truth observations using SNOTEL or NOAA Cooperative Observer meteorological network stations.

Among these studies, Klein and Bartnett (2003) found good overall agreement between snowcover maps produced using the 500-m resolution MODIS snowcover product used here and NOHRSC snow maps for the URG basin of Colorado and New Mexico. They showed that the MODIS product typically mapped a higher proportion of the basin as snow covered than did the NOHRSC product. However, whether the differences in these two remote sensing-derived snow maps produce significant

differences in the timing and volume of snowmelt in the URG was not addressed. Since an important use of snowcover maps is for water resource estimates, it is useful to compare snowmelt runoff simulations using MODIS and NOHRSC snowcover maps as input, both against each other and against observed streamflow. The SRM is used in these simulations because of its long and successful history of use in one northwestern watershed of the URG basin (Martinec 1985; Rango and van Katwijk 1990; Rango 1992; van Katwijk et al., 1993; Martinec and Rango, 1995; Rango and Martinec, 1997; Rango et al., 2002; Rango et al., 2003).

Table 3-1. Papers evaluating satellite-derived snowcover products

Manuscript	Sensors or snowcover products	Study region
Baumgartner et al., 1987	Landsat-MSS and NOAA/AVHRR	Rhein-Felsberg (Alps), Switzerland
Hall et al., 2000	Landsat-TM (30m and 1km) using MODIS SNOWMAP algorithm, NOHRSC snow products, SSM/I	Saskatchewan, Canada; New England, Idaho, North and South Dakota, USA
Rango et al., 2002	NOAA/AVHRR, Landsat-TM and Terra-MODIS	Upper Rio Grande, Colorado and New Mexico, USA
Bitner et al., 2002	NOHRSC, Terra-MODIS, and new automated snowcover maps from NESDIS	Entire conterminous USA and northwest and north central USA
Rango et al., 2003	NOAA/AVHRR and Terra-MODIS	Noguera Ribagorzana basin, central Pyrenees, Spain
Maurer et al., 2003	NOHRSC and Terra-MODIS	Columbia and Missouri river basins, USA
Klein and Barnett, 2003	NOHRSC and Terra-MODIS	Upper Rio Grande, Colorado and New Mexico, USA

The research addresses several specific questions. The first is how, if at all, the timing and volume of simulated snowmelt runoff differs in streamflow simulations that use MODIS and NOHRSC snow maps as SCA inputs? Secondly, can the observed differences in the simulated streamflow be explained by spatial-temporal differences in the mapped snowcover between the two products during the snowmelt period? Thirdly, how do zonal SWE volumes on April 1st calculated using the MDC produced by SRM, differ when MODIS and NOHRSC snow maps are used, and how do these estimates compare to *in situ* SNOTEL observations. To answer these questions, streamflow simulations were performed with SRM using NOHRSC snow products from 1990 to 2000, and representative (average) coefficient or factor values obtained from these streamflow simulations were used to parameterize streamflow simulations made using MODIS and NOHRSC snowcover products as inputs for the year 2001. While another MODIS snowcover product has been produced from a different snow-mapping algorithm (Rango et al., 2002; Landesa and Rango, 2002; Rango et al., 2003), this research evaluates standard MODIS snowcover product because this product is readily available to the cryospheric research community and does not require remote sensing expertise to use. Therefore, this investigation can help assess whether standard MODIS snow product provides suitable SCA information for input into SRM in less well-studied portions of the world.

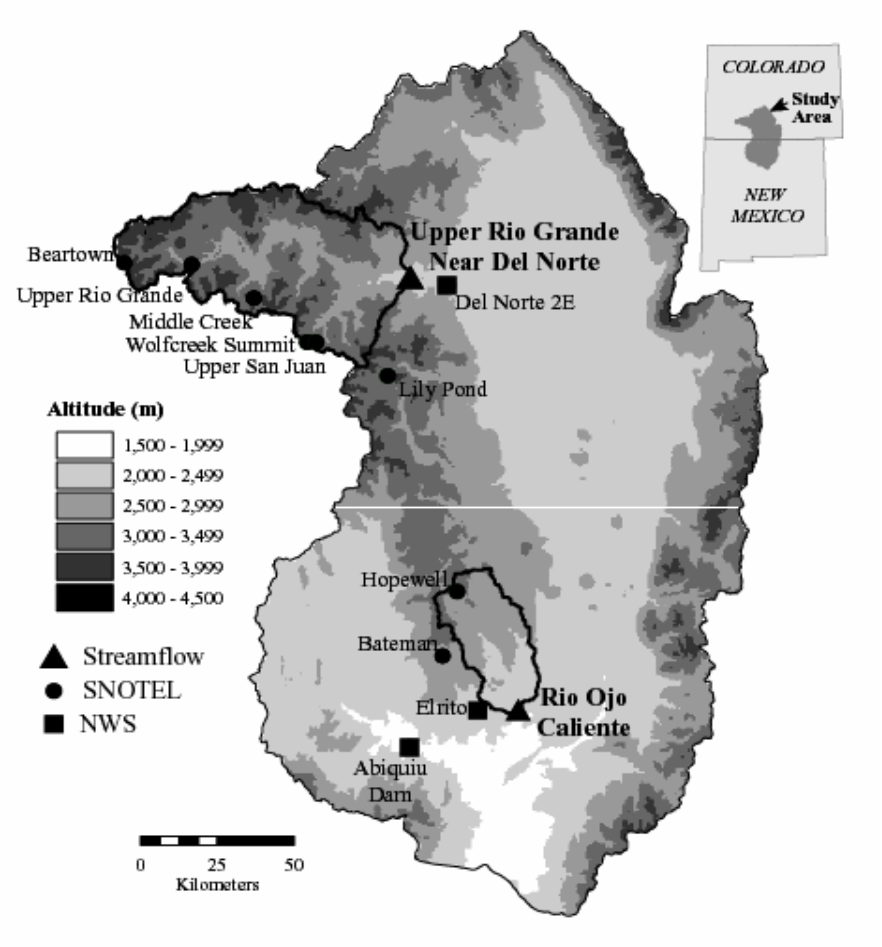

Figure 3-1. Digital elevation model of the Upper Rio Grande basin showing the location of the two study basins and the gauging stations used in this study

3.2. Study Site

Two tributary watersheds of the URG basin in Colorado and New Mexico were selected for this study (**Figure 3-1**). One watershed located in the northern part of URG has been a main research watershed for SRM-related research and has been utilized for development and testing of SRM techniques (e.g. Rango and van Katwijk, 1990; Rango, 1992; van Katwijk et al., 1993; Rango and Martinec, 1997; Rango et al., 2002; Rango et al., 2003). It thus provides an ideal setting for evaluating the performance of SRM using MODIS and NOHRSC snow maps as model inputs.

In the URG, snow formation usually begins in late October, with the snowpack approaching its maximum SWE near April 1st as has been measured at snowcourses scattered across the basin and in more recent years also at SNOTEL sites. The exact timing of peak SWE accumulation varies spatially across the URG basin and from year to year. This study only considers the period from April 1st to the end of the snowmelt season.

The larger of the two studied watersheds is Rio Grande upstream of the USGS gauge near Del Norte, Colorado (hereafter referred to simply as the Rio Grande). The smaller and more southerly watershed is the Rio Ojo Caliente upstream of USGS gauge at La Madera, New Mexico (hereafter referred to as the Rio Ojo). The pertinent geographic characteristics of the two watersheds are listed in **Table 3-2** and the proportion of each landcover class covering each of the three SRM elevation zones in each basin is listed in **Table 3-3**. Both of the watersheds meet the 100-500 km^2

minimum recommended area for the use of SRM given the spatial resolutions (500 m and 1000 m) of the snowcover maps being investigated (Rango, 1985; Martinec et al., 1998). In the SRM modeling, each watershed is separated into three approximately 500 m altitudinal zones and SRM inputs (daily temperature, precipitation, and SCA) are allowed to vary between zones. In both watersheds, the 2nd zone area comprises approximately 50% of each basin (**Table 3-2**). Landcover is similar in the two basins for the lower two SRM zones (zones 1 and 2). However, in the 3rd (upper) SRM zone of the Rio Grande grassland occupies the majority of the area (53%) while evergreen forests dominate landcover in the 3rd zone of the Rio Ojo.

3.2.1 Rio Grande Watershed

The Rio Grande watershed is located in the northwestern portion of the basin and has been a site of several snowmelt runoff modeling studies using SRM (e.g. Rango and van Katwijk, 1990; Rango, 1992; van Katwijk et al., 1993; Rango and Martinec, 1997; Rango et al., 2002; Rango et al., 2003) and contains both NWS meteorological sites and SNOTEL sites. Moreover, this watershed has a large altitudinal range, variable slopes, and *in situ* observations over a wide range of environmental conditions. Klein and Barnett (2003) showed SCA differences to exist between MODIS and NOHRSC snow maps for the winter of 2000-2001, especially at the lower elevations.

3.2.2 Rio Ojo Watershed

Unlike most other tributary watersheds located in the southern portions of URG, the Rio Ojo has several meteorological stations located in or in close proximity to the watershed. Klein and Barnett (2003) showed the upper portion of this watershed to have significant differences in the areas mapped as snow by MODIS and NOHRSC. Moreover, the Rio Ojo watershed is much smaller and drier of the two watersheds; therefore, the effect of these factors on differences in runoff simulation can be examined.

Table 3-2. Geographic characteristics of selected watersheds

Zone	Rio Grande		Rio Ojo	
	Area (km^2)	Elevation (m)	Area (km^2)	Elevation (m)
1st	777 (23%)[1]	2438 – 2937	294 (30%)	1950 - 2449
2nd	1628 (48%)	2938 – 3437	573 (58%)	2450 - 2949
3rd	964 (29%)	3438 – 4069	128 (12%)	2950 - 3247
Total	3369	2438 – 4069	995	1950 - 3247

[1]Percentages are the proportions of each zone relative to its total basin area.

Table 3-3. Proportion of major landcover classes for two studied watersheds determined from USGS North American Landcover Data. The 1st zone in each watershed is the lowest, the 3rd zone the highest

	Rio Grande			Rio Ojo		
Zone	1st	2nd	3rd	1st	2nd	3rd
Evergreen Forests	45%	64%	32%	47%	67%	54%
Shrublands	9%	3%	2%	3%	18%	18%
Grasslands	35%	22%	53%	25%	14%	26%
Deciduous Forests	6%	7%	2%	0%	0%	0%
Others	5%	4%	11%	25%	1%	2%

3.3. Method and Data

3.3.1 Snowmelt Runoff Model (SRM)

Among many snowmelt runoff models which use snowcover information, the deterministic SRM is one of the most widely used models in both simulation and forecasting modes (e.g. Rango and Martinec 1979; Shafer et al. 1982; Martinec 1985; Hall and Martinec, 1985; Rango and van Katwijk, 1990; Martinec and Rango, 1995; Rango and Martinec, 1997; Ferguson 1999). It was first applied to small European basins beginning in 1975 and since has been successfully used in approximately 80 mountainous basins in 25 countries worldwide (Martinec, 1975; Martinec et al., 1998). SRM is a degree-day based model for daily runoff simulations and forecasts in the mountainous areas in which snowmelt is the major runoff contributor (Rango and

Martinec, 1981; Martinec et al., 1998; Mitchell and DeWalle, 1998). The degree-day method employed by SRM has been used in different ways for more than 60 years (Clyde, 1931; Collins, 1934), and Rodriguez (1994) points out that SRM and HBV-2 model (Bergstrom, 1975) are two mostly widely used models using degree-day method (Rango and Martinec, 1995). The degree-day method has also proven to be very efficient in determining the average zonal or basin SWE for a specific day (Martinec and Rango, 1981; Martinec and Rango, 1987; Martinec, 1991).

Assuming there is an 18-hour time lag between the meteorological inputs on day n and the resulting streamflow on day n+1, SRM calculates the daily streamflow separately for each zone as follows:

$$Q_{n+1} = [c_{Sn} \cdot a_n (T_n + \Delta T_n) S_n + c_{Rn} P_n] \frac{A \cdot 10000}{86400} (1 - k_{n+1}) + Q_n k_{n+1} \qquad (3.1)$$

In Eq. (3.1), the daily average discharge on day n+1 (Q_{n+1}) [$m^3 s^{-1}$] is calculated as the sum of three quantities from the preceding day (n): (1) snowmelt calculated as the product of the degree-day factor a [$cm \cdot {}^oC^{-1} \cdot d^{-1}$], the representative zonal degree-days ($T + \Delta T$) [$^oC \cdot d$], the ratio (S) of the SCA to the total basin area (A) [km^2], and the snowmelt runoff coefficient C_S; (2) precipitation contributing to runoff [cm], calculated as the product of measured precipitation P and the rainfall runoff coefficient C_R; and (3) discharge on the preceding day (Q_n), weighted by the recession coefficient k. ($T + \Delta T$) represents extrapolated degree-days calculated at the hypsometric average elevation of the zone from the degree-days measured at the meteorological stations. The snowmelt and rainfall runoff coefficients C_S and C_R are defined as the fraction of snowmelt and

rainfall, respectively that become streamflow. The recession coefficient on day n+1, k_{n+1}, is defined, as can be seen in Eq. (3.1), as the ratio of streamflow on day n+1 to that on day n when there is no input of runoff. The factor $\frac{10000}{86400}$ represents a conversion from $cm \cdot km^2 \cdot d^{-1}$ to $m^3 s^{-1}$. If a watershed contains multiple altitudinal zones, as were used in this research, Eq. (3.1) is applied separately to each zone and the discharges are summed. If a lag-time other than 18 hours is needed for the basin being modeled, SRM adjusts the input data appropriately as explained in the SRM manual (Martinec, et al., 1998); for example, for a 6-hour lag, SRM uses an average of the input data from days n and n+1, as 12 hours of each day is appropriate. In addition to the coefficients and input data appearing in Eq. (3.1), other parameters such as critical temperature, rainfall contributing area also need to be specified in SRM.

When streamflow simulations are made using SRM, SRM gives users a freedom to modify the values used at different times during melt season unlike other calibration models (Ferguson, 1999). Related to these characteristics of SRM, Ferguson (1999) described SRM as the model which falls in between the fully calibration-based hydrological models which are fitted from data and have no physical interpretations and fully physics-based models which are physical constants or measurable real-world quantities so that no fitting is involved.

3.3.2. Determination of SCA Variation

The shape of a snow depletion curve (changes in SCA over time during the melt season) depends on several factors including initial snow reserves and meteorological conditions as well as intermittent precipitation during the melt season (Leaf, 1967; Hall and Martinec, 1985). The snow depletion curves required as input into SRM only consider the depletion of seasonal snowcover which has been present for some weeks and therefore has undergone a process of densification. 'Transient' intermittent snow that falls during the ablation season is treated in SRM as precipitation, and therefore sudden and short-lived increases in SCA should not be included in the snow depletion curve. During the 2001 water year, several intermittent one or two day snowfall events occurred during the melt season. By comparing snow maps from the preceding and following days, it can be determined that this snowfall was a transient event relative to the seasonal snowcover. Therefore, although the streamflow simulations begin on April 1st, it is necessary to inspect both MODIS and NOHRSC snow maps beginning earlier in the snow season and consider several neighboring snow maps simultaneously in order to decide whether each available snow map is affected by 'transient' intermittent snowcover.

Although there is one equation that has been developed to model the snow depletion curve (Hall and Martinec, 1985; Rango et al., 2003), this equation also requires subjective decisions of the modeler. Therefore, the construction of the snow depletion curves used in this research follows the general procedures outlined in the

SRM manual (Martinec et al., 1998), and the following specific approach was used. First, the SCA as a percentage of each zone's total area was obtained from all cloud-free days using MODIS and NOHRSC snow maps. In here, cloud-free days were mainly determined by modeler's subjective decisions through visual inspection, and some cases in which cloud is reclassified as snow will be described below. Secondly, an initial snow depletion curve was constructed for each zone, using visual analysis to remove days affected by transient intermittent snow. Thirdly, starting on April 1st, the values of SCA were interpolated at 10-day intervals from this initial snow depletion curve. Finally, a final smoothed snow depletion curve was created by fitting a spline function through the interpolated points.

3.3.3. MODIS Snow Cover

As one aim of this study is to evaluate the suitability of the standard MODIS snowcover product as an input into SRM, MODIS daily snowcover product (MOD10A1 version 3) were used as one source of snowcover information. Each daily MOD10A1 file is a single tile of 500m gridded, georeferenced cells covering a 1200 km x 1200 km area. The MOD10A1 product indicates the presence of snow, no snow, and cloud using all MODIS observations covering each pixel during a day using the SNOWMAP, the MODIS snow-mapping algorithm. In SNOWMAP, surface reflectance and a cloud mask serve as the basic inputs to the MODIS swath products with other ancillary inputs such as land/water mask or geographic adjustment, cloud mask analysis, decision rules and quality assurance analysis added to the algorithm to construct the daily and weekly

snowcover products (Hall et al., 1995). Snow detection in SNOWMAP is accomplished several spectral tests incorporating at-satellite reflectances in visible to mid-infrared wavelengths. A normalized difference snow index (NDSI) employing MODIS bands 4 (0.545-0.565 μm) and 6 (1.628-1.652 μm) is the primary snow-classification criteria:

$$NDSI = \frac{(MODIS4 - MODIS6)}{(MODIS4 + MODIS6)} \tag{3.2}$$

Non-forested pixels whose NDSI ≥ 0.4 and reflectance in MODIS band 2 (0.841-0.876 μm) is >11% will be mapped as snow. However, snow-covered forests may have lower NDSI values. To better map these snow-covered forests, a combination of the normalized difference vegetation index (NDVI) computed using MODIS bands 1 (620-670 μm) and 2 (841-876 μm) and the NDSI are used. Pixels falling in a polygon region in NDVI-NDSI space may be mapped as snow when the NDSI is < 0.4. However, to prevent very dark forests from being erroneously mapped as snow the reflectance in MODIS band 4 must be greater than <10% even if other criteria are met. A split-window technique employing MODIS thermal bands 31 (10.780-11.280 μm) and 32 (11.770-12.270 μm) is used to mask misclassified pixels whose temperature is too high to contain snow. Details concerning the SNOWMAP algorithm can be found in Hall et al., (1995, 2001) and a complete description of the suite of MODIS snowcover products are described in Hall et al. (2002).

In the MOD10A1 snow products, cloud masking is accomplished using the MODIS cloud mask. The MODIS cloud-masking algorithm uses a series of visible, mid

and thermal infrared thresholds and consistency tests to specify the confidence with which a MODIS observation provides an unobstructed view of the surface. The actual cloud screening tests employed vary depending on the underlying surface and other conditions. A complete description of the cloud mask algorithm is presented in Ackerman et al. (1998).

3.3.4. NOHRSC Snow Cover

During the northern hemisphere snow season, snowcover maps are created for the conterminous United States, Alaska, and the southern portions of Canada by NOHRSC since 1986, primarily for use in hydrological forecasting. Currently, the NOHRSC daily nationally-gridded product is available the day after the satellite observations are made (Bitner et al., 2002). Snow detection is accomplished via a semi-automated multispectral snow classification algorithm (theta) that is designed to distinguish snow from cloud, land, and water over North America. Typically, two GOES images per day (GOES 10 for western USA and GOES 8 for eastern USA) and images from AVHRR are combined (Hartman et al., 1996; Maxson et al., 1996; Cline and Carroll, 1999; Hall et al., 2000; Bitner et al., 2002). NOHRSC daily snow maps are produced at a nominal resolution of approximately 1 km and are available via the internet.

NOHRSC snowcover products serve as a useful comparison for MODIS snow maps because NOHRSC snowcover products have been used for almost 20 years. While Landsat Thematic Mapper (TM) and AVHRR images have been most commonly used

for deriving SCA information for input into SRM, Mitchell and DeWalle (1998) did employ NOHRSC snow maps in SRM streamflow simulations for the Towanda creek basin located in Pennsylvania, USA.

3.3.5. Landcover

It is known that landcover affects the snow mapping accuracy of both MODIS and NOHRSC in the URG (Klein and Barnett, 2003). In this research, land cover information for the two watersheds was obtained from the National Land Cover Data (NLCD) produced by USGS (http://landcover.usgs.gov/natlland cover.asp). This data set was produced from 30 m Landsat TM multi-band mosaics using an unsupervised clustering algorithm along with aerial photography and ground observations. The 21 land cover classes of the NLCD are based on the Anderson Level III land-use and land-cover classification system; however, some Anderson Level II classes have been consolidated into a single NLCD class (Vogelmann et al., 2001). The NCLD was used to obtain the proportions of major landcover classes for each zone of the two watersheds (**Table 3-3**). The pixels falling in each altitdinal zone were determined using the 30 m spatial resolution National Elevation Dataset (NED) by United States Geological Survey (USGS) (http://gisdata. usgs.net/NED/default.asp).

3.3.6. Meteorological Observations

In addition to zonal daily SCA, zonal daily temperature and precipitation data are also needed to run SRM. These data values were obtained from SNOTEL and NWS

stations around or inside the watershed. For the Rio Grande watershed, 6 SNOTEL stations and 1 NWS station were used while 2 SNOTEL stations and 2 NWS stations were used in the Rio Ojo watershed. **Figure 3-1** gives the locations of SNOTEL and NWS stations used. Although they are not located within the study watersheds, one or two NWS stations were used to characterize meteorological conditions in each basin's lower elevations because SNOTEL stations are restricted to higher elevations.

Zonal daily temperatures were calculated as follows. First, average monthly temperatures at each station were computed from average daily temperatures. Monthly temperature lapse rates were then computed by linear regression of the mean monthly temperatures observed at all the available NWS and SNOTEL stations against their elevations. The lowest elevation stations (Del Norte 2E (NWS, 2399m) and Abiquiu Dam (NWS, 1945m)) were selected as the base stations of the Rio Grande and Rio Ojo watershed, respectively. For each day of a month, the difference between the monthly average temperature at the base station and monthly temperature at the base station's elevation predicted by the regression equation (i.e., the regression residual at the base station) was applied to the base station's daily temperature to obtain a modified daily temperature at the base station. Then the daily temperature for each zone was found by extrapolating from the modified daily temperature at the base station using the monthly regression slope to the hypsometric mean elevation of each zone.

To determine zonal daily precipitation, the average daily precipitation from all the available stations was first calculated and assigned to the average elevation of all the stations. Then average daily precipitation was extrapolated to the mean hypsometric

elevations of the respective zones by an assumed elevation gradient of 3.5% per 100m (Martinec et al., 1998).

3.3.7. Parameterization of SRM

To effectively simulate runoff, SRM requires the determination of several coefficients: the snow (C_S) and rainfall (C_R) runoff coefficients and the degree-day factor (a) in Eq. (3-1) which vary both inter- and intra-annually depending on hydrometeorological and snow conditions. An extensive literature describing the procedures for obtaining physically-realistic values for these coefficients exists (Rango and Martinec 1979; Shafer et al., 1982; Hall and Martinec, 1985; Martinec and Rango, 1986; Martinec et al., 1998; Mitchell and DeWalle, 1998).

Streamflow simulations from 1990 to 2000 using the NOHRSC snow products were first performed in the Rio Grande watershed. The coefficient values in each year were obtained from the modifications of values used in the sample simulation for this same watershed which is included in the SRM program (version 4.06), starting with the modification of the runoff coefficients if there is general under or over-prediction of streamflow. And then degree-day factor (a) or other parameters were modified if unsatisfactory streamflow simulation were obtained after the modification of runoff coefficients. The degree-day factor (a) and snow runoff coefficient (C_S) were allowed to vary between zones, while identical rainfall runoff coefficient (C_R) was applied to the whole basin. In the case of Rio Ojo watershed, because two watersheds are located near to each other, the time variation and values of coefficients in the Rio Grande watershed

were used as a starting point in the determination of coefficient values in the Rio Ojo watershed and then the same procedure was applied, i.e., adjustment of the runoff coefficients if there was general over- and under-prediction of streamflow and then other coefficients each year. In the case of the recession coefficient (*k*), this important coefficient was parameterized as a function of streamflow using daily streamflow rates measured in the USGS gauge station from 1990 to 2000, following the procedure explained in Martince et al. (1998).

Figure 3-2 illustrates how the derived coefficients vary at half-month interval beginning on April 1st in the 2nd zone or all zones of each basin depending on the coefficient, and **Table 3-4** shows two statistical criteria used to assess the SRM streamflow simulations for each of the 11 years. Although degree-day factor should increase linearly with time during the melt season in both watersheds (Kustas et al., 1994; Ferguson, 1999; DeWalle et al., 2002), runoff coefficients show, in **Figure 3-2**, some differences in terms of time variation between the two watersheds. The probable reasons are relatively thinner snow cover due to more southerly latitude, lower average elevation, and the differences of soil moisture recharge in an initial early season of melt due to the higher aridity in the Rio Ojo compared to the Rio Grande watershed. As can also be seen in **Figure 3-2**, there is less intra-annual variation in the determined coefficients for the larger Rio Grande watershed as compared to the smaller Rio Ojo watershed. It can be expected that the smaller watershed would have larger intra-annual variations because it is more likely to be influenced by meteorological variations such as irregular snowfalls and spatial variability in surface characteristics in addition to

geographic conditions mentioned above. This highly variable situation in the Rio Ojo watershed is also evidenced by multiple high streamflow events during the snowmelt period. That is, while the Rio Grande always experiences a single peak streamflow each year, the Rio Ojo experienced two to four similar amount of peak streamflow events each year, which makes the determination of appropriate coefficients more difficult and streamflow simulations less accurate.

3.4. Results

3.4.1 Snow Depletion Curves

The study employed MODIS and NOHRSC snow maps for the period from January 1st to July 31st, 2001 (**Figure 3-3**). Visual inspection of the daily snow images was deemed to be the most appropriate method for selecting appropriate images for determining SCA because many MODIS and NOHRSC daily snow maps suffer from cloud contamination. In cases where it seemed reasonable to assume that snow had been misclassified as cloud, like the cases of the cloudy pixels which are located totally inside the snow pixels or cloudy pixels in the transition zone between snow and land which will be explained later, the cloudy pixels were reclassified as snow in creating the snow depletion curves.

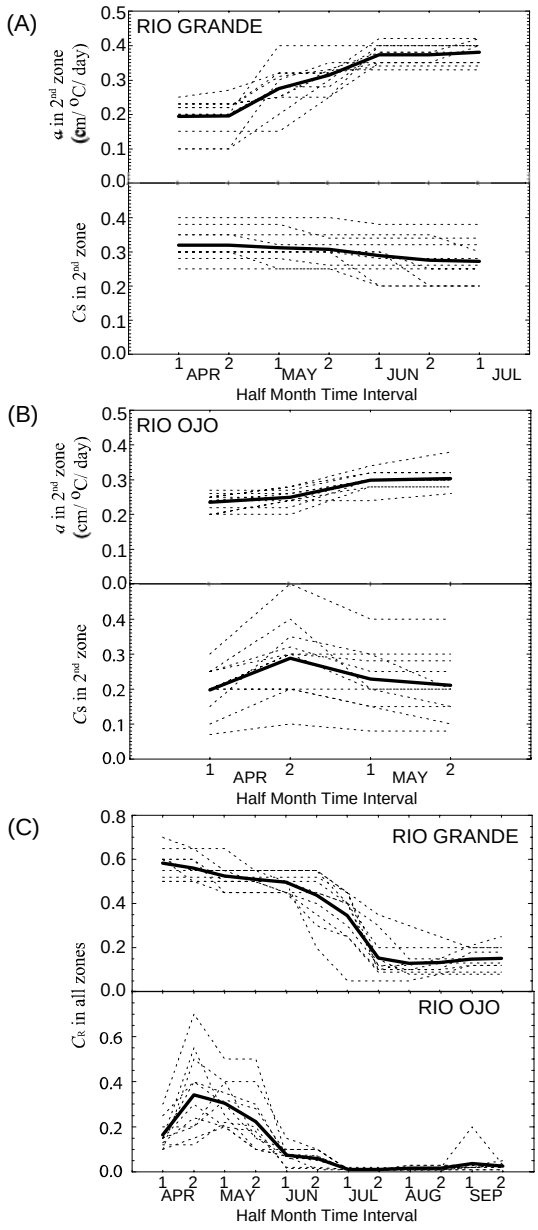

Figure 3-2. Time variations in the calculated SRM parameters for individual years (dashed lines) in an eleven-year period (1990-2000) as well as their arithmetic means (solid lines) over the same period. Degree-day factor (a) and snow runoff coefficient (C_S) in the 2nd zone for the Rio Grande (A) and for the Rio Ojo (B) watershed, and basinwide rainfall runoff coefficients (C_R) for both watersheds (C)

Table 3-4. SRM simulation statistical results using NOHRSC derived SCA values from April 1st to September 30th

Rio Grande												
	1990	1991	1992	1993	1994	1995	1996	1997	1998	1999	2000	Ave.
Goodness of Fit (R^2)[1]	0.93	0.89	0.83	0.82	0.79	0.87	0.90	0.85	0.95	0.85	0.82	0.86
Vol. Diff $D_v(\%)$[2]	-0.23	5.99	3.82	0.08	5.49	0.94	2.66	-0.63	1.19	-0.20	5.06	2.39
Rio Ojo												
	1990	1991	1992	1993	1994	1995	1996	1997	1998	1999	2000	Ave.
Goodness of Fit (R^2)	0.67	0.28	0.89	0.67	0.67	0.77	0.82	0.88	0.91	0.80	0.83	0.75
Vol. Diff $D_v(\%)$	-3.28	44.89	9.87	35.75	13.13	12.63	12.08	-0.10	6.70	2.17	1.83	12.95

[1]Goodness of Fit is defined as $R^2 = 1 - \frac{\sum_{i=1}^{n}(Q_i - Q_i')^2}{\sum_{i=1}^{n}(Q_i - \overline{Q})^2}$, where Q_i is the measured daily discharge, Q_i' is the computed daily discharge, and $\overline{Q}$ is the average measured daily discharge of the snowmelt season (Martinec et al., 1998).

[2]Volume Difference (Vol. Diff) in percent is defined as $D_v(\%) = \frac{V_R - V_R'}{V_R} \cdot 100$, where V_R is the measured seasonal discharge volume, and V_R' is the computed seasonal discharge volume (Martinec et al., 1998).

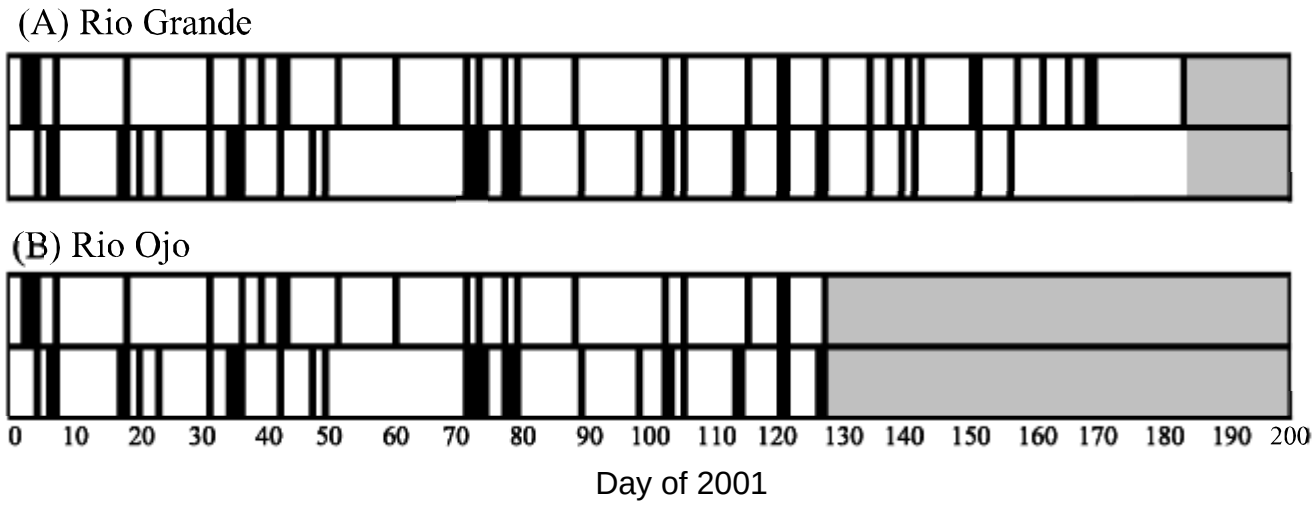

Figure 3-3. Dates of the MODIS and NOHRSC snowcover maps selected for (A) the Rio Grande and (B) the Rio Ojo watersheds. For each watershed, the black lines in the upper and lower panels indicate the dates for NOHRSC and MODIS snowcover maps, respectively. Gray area indicates snow-free periods

Example MODIS and NOHRSC snowcover maps from 4 dates (**Figure 3-4**) illustrate the progressive snowmelt pattern observed in the study basins. One interesting phenomenon in the MODIS snow maps is that cloudy pixels which were reclassified as snow in this research, are often located in the transition zone between snow-covered and snow-free areas as was previously noted by Riggs and Hall (2002) and Klein and Barnett (2003). In the discussion of the problem of misclassification of snow as clouds in the standard MODIS snow products by Riggs and Hall (2002), they noted that the transition zone between snow and land is usually covered by thin or fractional snow. In addition, they proved that misclassified clouds at the edges of SCA can be eliminated using a less strict cloud masks. So, the reclassification from cloud to snow in the transition zone between snow-covered and snow-free land is a reasonable assumption.

In general, MODIS snowcover products exhibit more consistent patterns of snow retreat as a function of elevation than do NOHRSC snow maps. Comparing the SCA images from April 13th or May 1st (**Figure 3-4**) with a DEM of the URG (**Figure 3-1**) shows that the transient snowline on these two dates occurs at much more uniform elevations in the MODIS snow maps than in the NOHRSC snow maps. **Figure 3-5** compares the snow extent mapped by MODIS and NOHRSC as a function of aspect for both watersheds for the days illustrated in **Figure 3-4**. Although there are some differences in the area mapped as snow by MODIS and NOHRSC at some aspects, overall there are strong similarities in the patterns of snow mapped as a function of aspect by the two algorithms. Therefore, it can be expected that aspect does not play a

significant role on the pattern of snowcover mapped by the two approaches in these two watersheds.

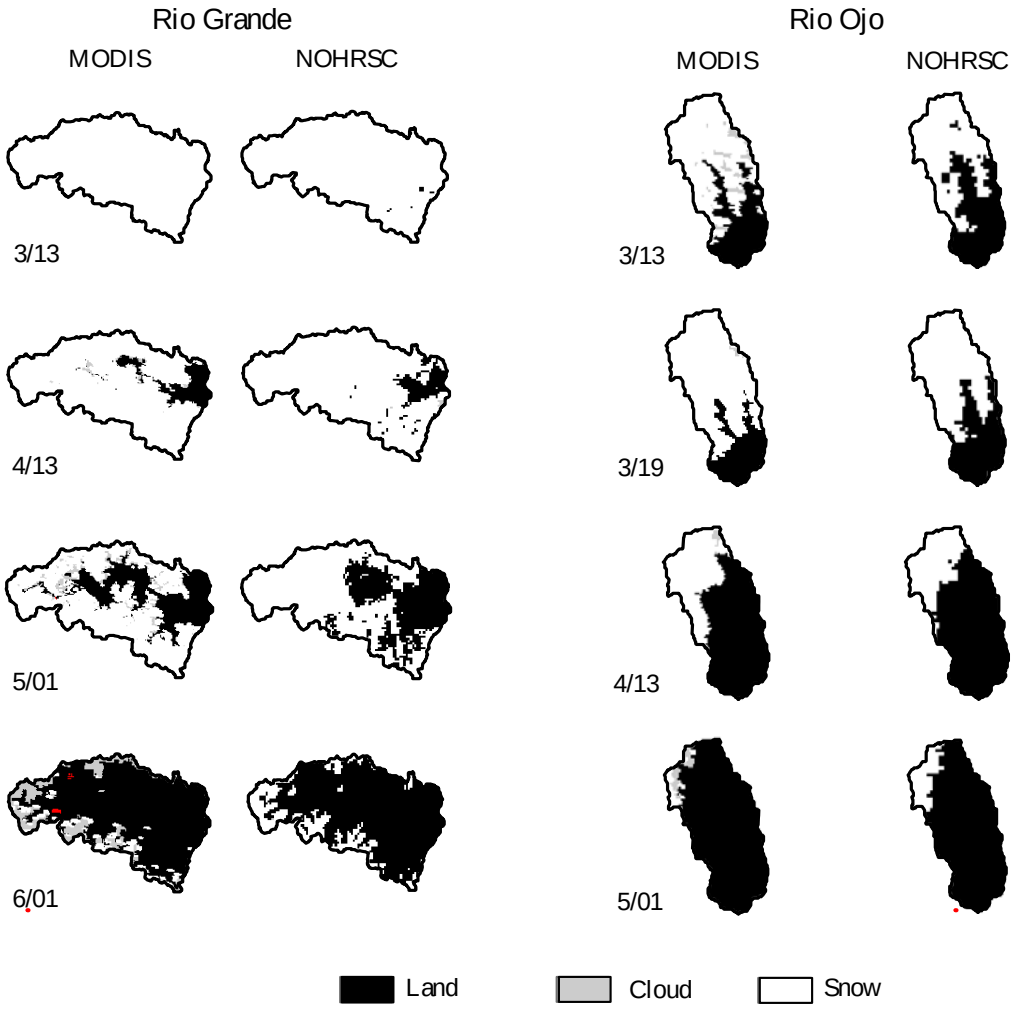

Figure 3-4. MODIS and NOHRSC snow maps for selected days in 2001 for (A) the Rio Grande and (B) the Rio Ojo watersheds. White indicates snow and gray cloud and black land

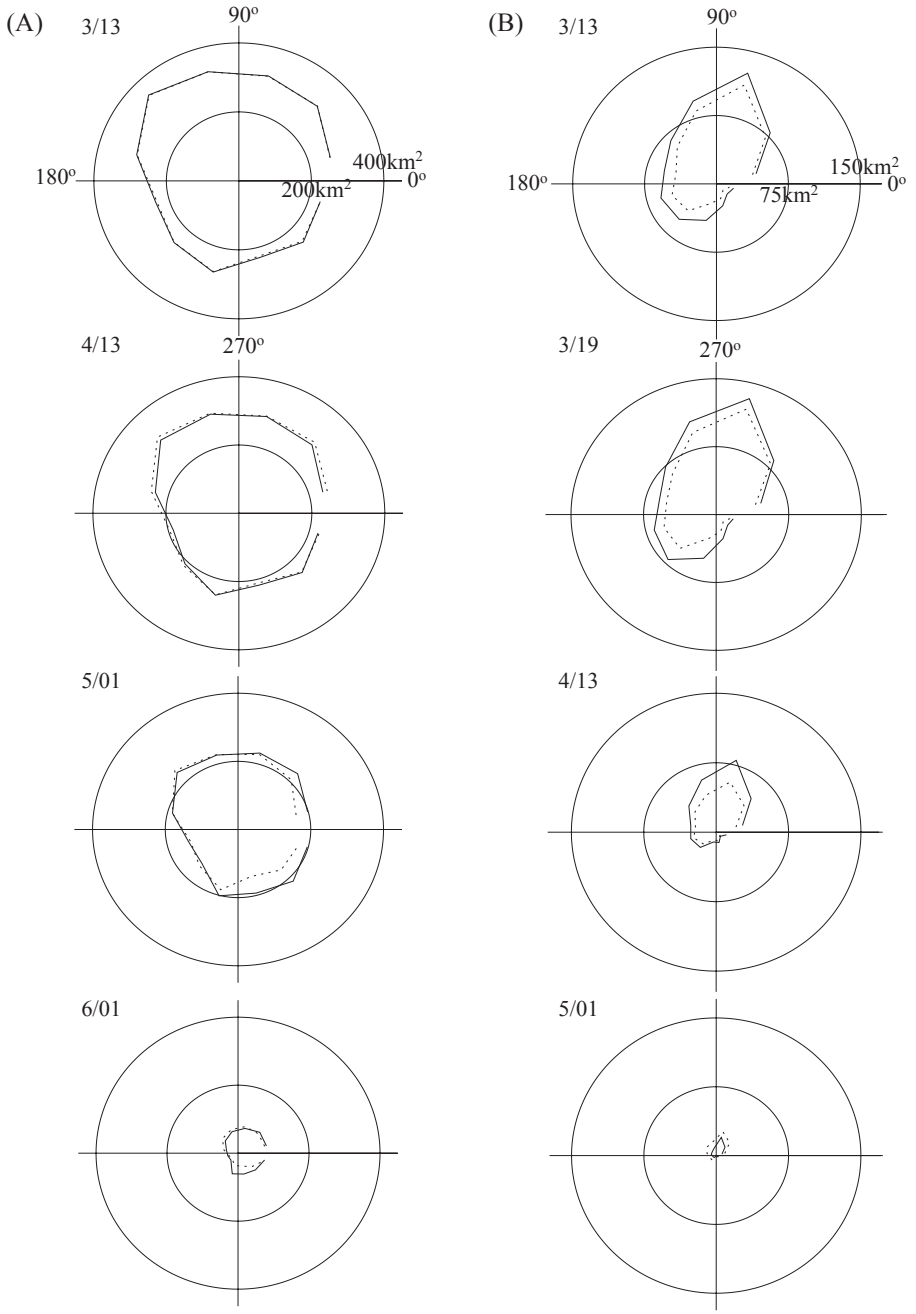

Figure 3-5. Polar plot (bin size: 30°) showing the dependence of SCA as a function of aspect for (A) the Rio Grande and (B) the Rio Ojo watersheds for MODIS (solid line) and NOHRSC (dotted line). Selected days are the same as those of Figure 3-4

The daily snow depletion curves used in the SRM simulations beginning from April 1st and individual SCA observations beginning from March 1st derived from MODIS and NOHRSC snowcover maps are shown in **Figure 3-6**. Individual SCA observations are shown beginning from March 1st in order to identify transient intermittent snowfalls as described above. The methodology used to produce the snow depletion curves does result in some differences between the observed SCA and the final depletion curves for both MODIS and NOHRSC (**Figure 3-6**) due to both the avoidance of transient snow and temporal smoothing. However, the differences between the individual observations and the snow depletion curves were similar for both snow products.

In 2001, the snow depletion curve in the Rio Grande watershed was much easier to characterize than the Rio Ojo watershed because the Rio Grande had considerably more snow and the snowmelt season lasted much longer than in the Rio Ojo. In the Rio Ojo watershed, it was difficult to determine the actual SCA in the lowermost zone on April 1st because only one cloud-free NOHRSC snow map was acquired within 10 days of this date. Unfortunately, this image also appears to be affected by a transient intermittent snowfall event as both MODIS and NOHRSC snow maps for previous and subsequent dates show considerably less snow.

Differences between the MODIS and NOHRSC snow depletion curves are observed in **Figure 3-6**. In the lowermost (1st) zone of the Rio Grande watershed, MODIS mapped less snow than did NOHRSC in the initial stages of snowmelt and more snow during the final stages of snowmelt. In the middle (2nd) zone of the Rio Grande

watershed, MODIS showed snow persisting longer into the melt season than did NOHRSC. This difference is significant because this zone occupies 48% of the basin's total area and will significantly affect the simulated streamflow. In the upper (3rd) zone of the Rio Grande watershed, MODIS shows more snow persisting into through the end of May than does NOHRSC. However, through the remainder of the melt season similar snow retreat can be observed in both snow products.

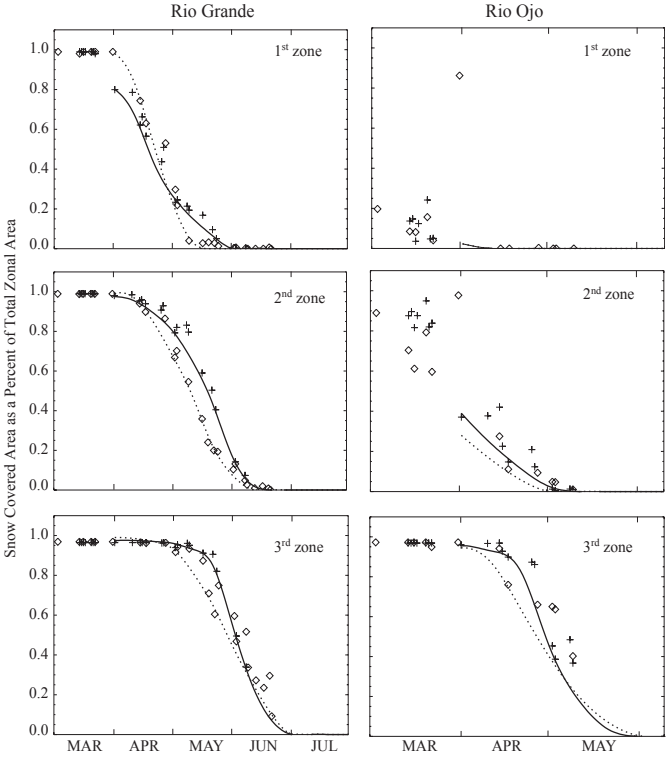

Figure 3-6. Snow depletion curves for MODIS (solid lines) and NOHRSC (dashed lines) showing changes in SCA as a percentage of the total area of each zone from April 1st, 2001 until the end of the melt season. Also shown are individual SCA observations for selected days from MODIS (cross) and NOHRSC (diamonds)

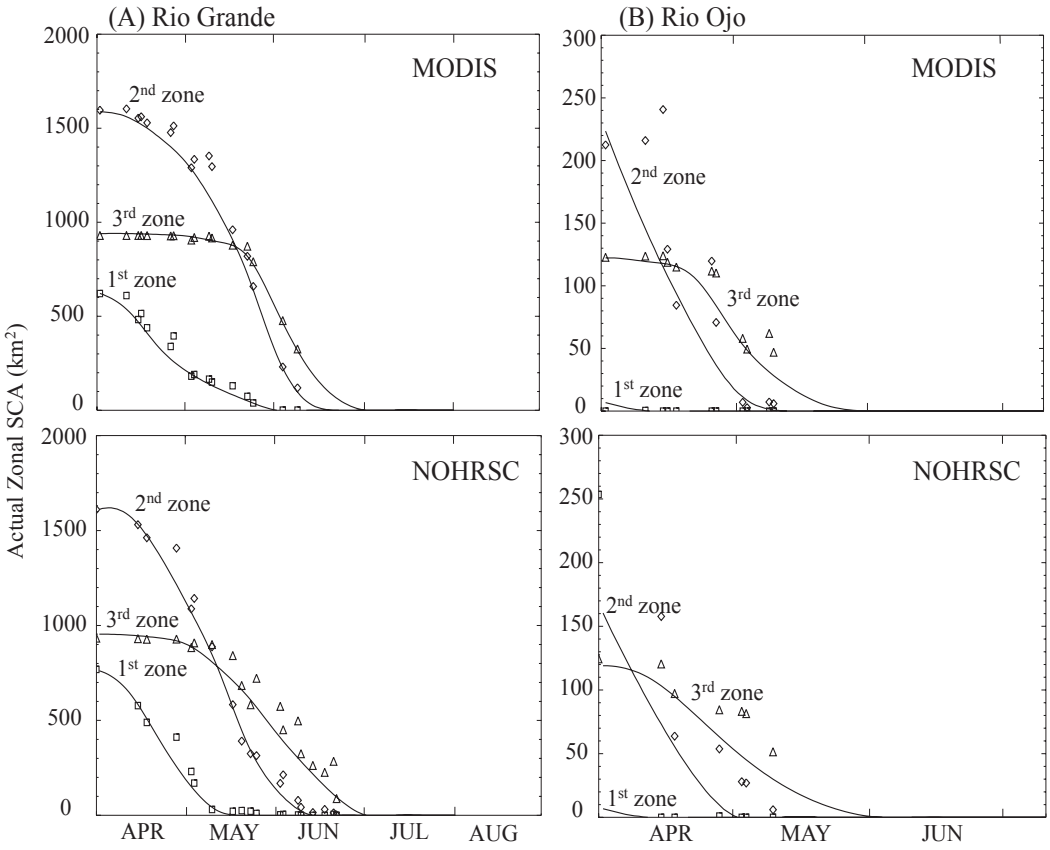

Figure 3-7. Total SCA in each zone of the (A) Rio Grande and (B) Rio Ojo watersheds as derived from MODIS (upper panels) and NOHRSC (lower panels) snow maps for the period from April 1st, 2001 until the end of the melt season. Square for the 1st zone, diamond for the 2nd zone and triangle for the 3rd zone

Similar differences are seen between the two snowcover products for Rio Ojo watershed. In the lowermost (1st) zone, both MODIS and NOHRSC show SCA to be < 5% of the total zonal area. In the middle (2nd) zone MODIS shows more snow and shows it persisting longer into the melt season. However, there is large scatter in the

actual SCA values for both products in this zone. In the highest (3rd) zone, MODIS shows a slower snowmelt in the April, but slightly faster snow retreat in May. However, because the number of observations at the end of the melt season is limited, the zonal snow depletion curves in this period were more subjective than those earlier in the snowmelt season.

From a snowmelt runoff perspective, depicting changes in the actual area covered by snow is often more useful than simply examining changes in the snowcover fraction in each zone. As can be seen in **Figure 3-7**, snowcover in the 2nd zone of both studied watersheds will dominate the simulated streamflow from April 1st to approximately May 15th in the Rio Grande and from April 1st to April 15th in the Rio Ojo watershed simply due to much larger SCA in this zone. After these periods, the 3rd zone dominates the simulated streamflow in both watersheds. In the Rio Grande, the lowermost (1st) zone seems to have some effects on the simulated streamflow during the first half of April and MODIS shows SCA in this zone decreasing more slowly than does NOHRSC. Meanwhile, in the Rio Ojo, the contribution to simulated streamflow from this zone is very small.

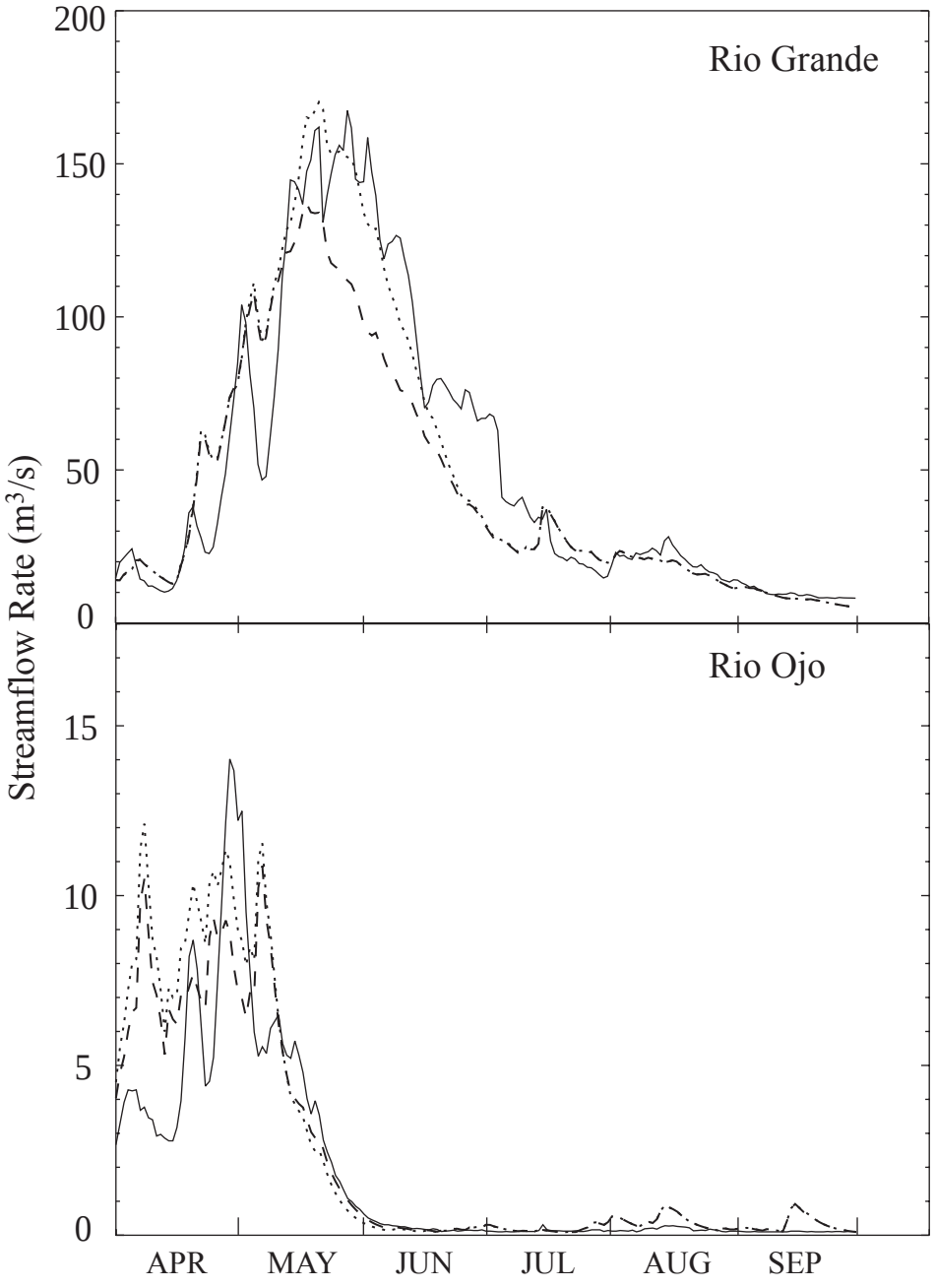

Figure 3-8. Measured (solid line) and SRM simulated streamflow using MODIS- (dotted line) and NOHRSC- (dashed line) derived SCA inputs and the representative parameter values

3.4.2. Runoff Simulation Comparisons

Using the developed MODIS and NOHRSC snow depletion curves, runoff was simulated from April 1st to September 30th, 2001 for both watersheds using SRM and the representative coefficient values obtained from 1990 to 2000 simulations (**Figure 3-2**). **Figure 3-8** illustrates the daily runoff simulations using the two snow products along with measured discharge, and **Table 3-5** summarizes the simulation result statistics for both watersheds. In the case of Rio Grande watershed, all of the simulation result statistics are fairly good even though the simulations were conducted using coefficient values that do not account for the specific hydrometeorological characteristics of the study year. The volume differences (measured – simulated) between the measured and simulated discharge are 2.6% and 14.0% for MODIS and NOHRSC, respectively. When measured streamflow depth from April 1st to September 30th in 2001 is compared with average measured streamflow depth from 1990 to 2000 in **Table 3-5**, higher streamflow depth happened during the year 2001 in the Rio Grande watershed. Therefore, it is reasonable for the simulated streamflow using representative coefficient values to have less streamflow depth compared to the measured one in 2001. The MODIS and NORHSC streamflow simulations compared for the Rio Grande watershed are quite comparable in their ability to successfully simulate the climbing limb of hydrograph. Large differences between the two simulations start approximately just before the peak annual streamflow. Moreover, on the hydrograph's falling limb, the streamflow simulation using MODIS snow products more closely match observed variations in

streamflow. Meanwhile, both snow products fail to catch some secondary and minor streamflow peaks on the falling limb.

Table 3-5. Result statistics of SRM simulations, April 1st - September 30th

	Rio Grande		Rio Ojo	
	MODIS	NOHRSC	MODIS	NOHRSC
Measured streamflow volume, 2001 (10^6 m^3)	808		28.7	
Measured streamflow depth, 2001 (m)	.240		.0288	
Average measured streamflow depth, 1990-2000 (m)	.193		.0532	
Measured precipitation during simulation period, 2001 (m)	.363		.208	
Computed streamflow volume, 2001 (10^6 m^3)	787	695	38.1	34.0
Average measured discharge, 2001 (m^3/s)	51.1		1.81	
Average computed discharge, 2001 (m^3/s)	49.8	44.0	2.41	2.15
R^2 Goodness of Fit[1] between measured and computed daily discharge, 2001	.89	.80	.57	.68
Volume difference[2], 2001 (%)	2.6	14.0	-33.1	-18.6

[1, 2]See Table 3-4 for definition.

In the Rio Ojo watershed, there are greater differences between simulated and measured runoff when two snowcover products are used. Both MODIS and NOHRSC SRM simulations significantly overpredict discharge with volume differences being -33.1% for MODIS and -18.6% for NOHRSC and cannot model the peak streamflow. This situation can be also explained by much smaller measured streamflow depth in

2001 compared to average measured streamflow depth from 1990 to 2000 (**Table 3-5**). These results, compared to the better results for the Rio Grande watershed, would appear to be due to two factors in addition to above hydrological situation in 2001: (1) the Rio Ojo watershed is much drier than the Rio Grande, as can be seen by its much smaller runoff depth (**Table 3-5**), its smaller fractional area of snowcover (**Figure 3-6**), and smaller estimated depth of SWE on April 1st (**Table 3-6**, to be discussed below) and to a smaller degree, (2) its smaller size (smaller watersheds are more easily affected by meteorological variations, spatial variability in surface characteristics and consequently changes in the SRM coefficients). The small amount of runoff observed in the Rio Ojo implies that loss processes (evaporation and the portion of infiltration that does not re-appear as baseflow) are relatively more important in the watershed, yet these were modeled relatively crudely in SRM, as compared to the computation of snowmelt runoff. These characteristics of small watershed are also seen in large intra-annual variability in the coefficient values (**Figure 3-2**).

Figure 3-8 shows that the simulated discharge from SRM using MODIS snow products is greater than simulated discharge using NOHRSC during peak runoff periods in both watersheds. The greater peak flow in mid-May in the Rio Grande is not surprising as the largest SCA differences between MODIS and NOHRSC snow maps occur during May, when snowcover is still extensive, air temperatures are rising significantly and are consistently above freezing. In the lower and more southerly Rio Ojo watershed, the largest differences between MODIS and NOHRSC snowcover occur during April and these differences result in the higher peak SRM simulated discharge

using MODIS snow products. Moreover, daily SRM-generated streamflow is calculated by combining the previous day's streamflow modified by the recession coefficient with the current day's calculated runoff. The consideration of previous day's runoff is shown in the second-term in Eq. (3-1). So if a previous day's runoff is overestimated, this overestimation will propagate to following days, helping to exaggerate the differences in the simulated streamflow.

Examining differences between the MODIS- and NOHRSC-based SRM simulations yields two important observations. The first is that discharge is higher in the MODIS simulations due to greater SCA in the middle (2^{nd}) and highest (3^{rd}) zone. Differences in total streamflow volume between SRM simulations using MODIS- and NOHRSC-derived snow depletion curves are 12% and 11% ((MODIS – NOHRSC) / MODIS) for the Rio Grande and Rio Ojo watershed, respectively. However, both simulations show very similar temporal pattern discharges for both watersheds. In fact, the correlation coefficients between discharges simulated using MODIS and NOHRSC snowcover products are remarkably high at 0.99 for both watersheds.

3.4.3 Estimate of Total SWE Accumulation on April 1st

Several papers have discussed determining areal average SWE from accumulated daily snowmelt depths and daily SCA variations (Martinec and Rango, 1981; Martinec et al., 1987; Martinec, 1991). In SRM the relationship between accumulated snowmelt depth and SCA variations is described by MDC. MDC quantifies the relationship between daily-accumulated snowmelt depth calculated from air

temperatures and a degree-day factor, and daily reductions in basinwide or zonal SCA. That is, the y-axis is just daily 'observed' fractional SCA (basically given in **Figure 3-6**) and the x-axis shows the cumulative melt depth M on day n, according to Eq. (3-1), $M(n) = \sum_{m=1}^{n} a_m (T_m + \Delta T_m)$. **Figure 3-9** illustrates MDCs for each zone in the two studied watersheds employing MODIS and NOHRSC snow depletion curves and representative coefficient values.

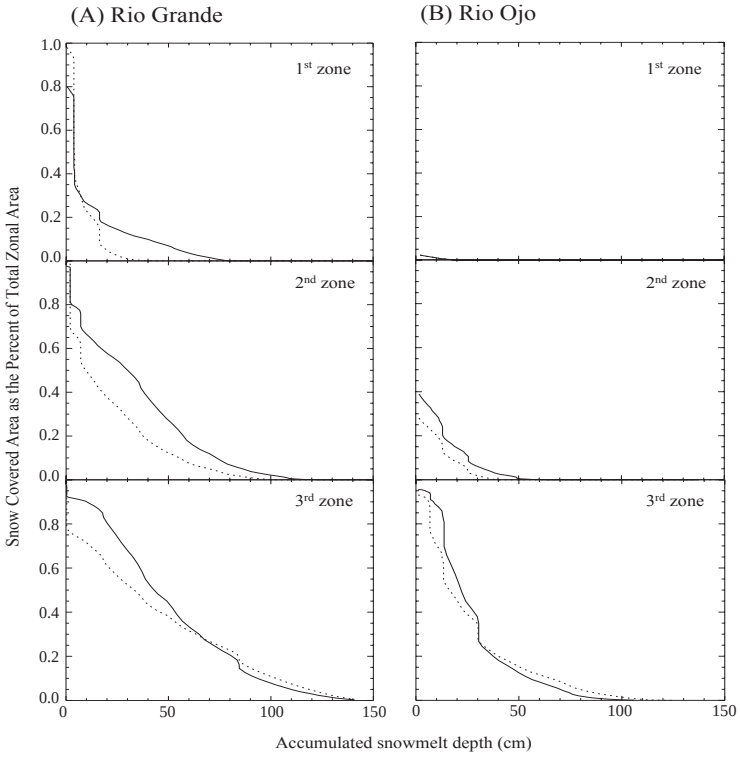

Figure 3-9. Modified Depletion Curves calculated using MODIS (solid line) and NOHRSC (dotted line) snow depletion curves for the (A) Rio Grande and (B) Rio Ojo watersheds

Spatially-averaged SWE, either for an entire basin or a single zone, for a specific day, in this case April 1st, 2001, can be calculated by integrating the area under the MDC. Calculating SWE by this method can help assess the representativeness of snowcourse or SNOTEL SWE as well as to better determine winter precipitation total in mountainous areas and detection of differences of snow accumulation across a basin (Martinec and Rango, 1981; Martinec, 1991). Therefore, it is interesting to examine how SRM estimates of total basin SWE on April 1st, which is near the time of maximum snow accumulation, differ when MODIS and NOHRSC snow maps are used as SRM inputs. It is also useful to compare these SWE estimates to those made from *in situ* SNOTEL measurements.

Comparing the snow depletion curves illustrated in **Figure 3-7** with the modified depletion curves in **Figure 3-9** reveals similar temporal trends in snow retreat. Meanwhile, in the lowermost (1st) zone in the Rio Grande watershed, the MODIS-based MDC shows snow cover to persist to much higher level of accumulated melt than does the NOHRSC-based MDC, and thus seems to exaggerate snow accumulation differences between the two products. Higher air temperatures in this zone compared to zones 2 and 3 and slower snow retreat as mapped in the MODIS snow products in later snowmelt season seem to be the cause of this exaggerated difference in the MDC.

Table 3-6 lists the zonal average SWE values and total April 1st SWE calculated from SRM using representative SRM coefficient values. Average measured SWE from the SNOTEL sites located within the 3rd zone of both watersheds is also shown. As expected from the simulation results and **Figure 3-9**, higher total and zonal April 1st

SWE accumulations are found in the MODIS-based SRM simulations. For the Rio Grande and Rio Ojo, NOHRSC-based basinwide SWE volume estimates were 27% and 25%, respectively, lower than SWE calculated from MODIS-based depletion curves.

Comparisons between SRM calculated SWE values and *in situ* SNOTEL-measured SWE could only be made in the 3rd zone because SNOTEL stations are restricted to higher elevations. As can be seen in **Table 3-6**, SRM calculated SWE values using both MODIS and NOHRSC are less than those observed in the 3rd zone of each watershed when average coefficient values are applied. However, when zonally-averaged SWE values calculated from the MODIS and NOHRSC-based MDCs are compared, the observed differences are insignificant except in the 2nd zone of both watersheds. However, because this zone occupies approximately 50% of the total area in both watersheds, some differences in total SWE accumulation do occur between the two snow products.

Table 3-6. April 1st SWE in the two watersheds

Rio Grande		Average SWE (m) in each zone			SWE volume: Area * SWE (m^3)	
Zone	Zone Area (km^2)	MODIS	NOHRSC	Measured [1]	MODIS	NOHRSC
1st zone	777	.11	.07		8.55E+07	5.44E+07
2nd zone	1628	.32	.20		5.22E+08	3.26E+08
3rd zone	964	.48	.42	.62	4.63E+08	4.05E+08
Watershed Total	3369	.32	.23		1.07E+09	7.85E+08

Rio Ojo		Average SWE (m) in each zone			SWE volume: Area * SWE (m^3)	
Zone	Zone Area (km^2)	MODIS	NOHRSC	Measured [2]	MODIS	NOHRSC
1st	294	.002	.002		5.88E+05	5.88E+05
2nd	573	.07	.04		4.01E+07	2.29E+07
3rd	128	.26	.25	.34	3.33E+07	3.20E+07
Watershed Total	995	.074	.056		7.40E+07	5.55E+07

[1]Average of SWE values from four SNOTEL stations located in the 3rd zone.

[2]Average of SWE values from two SNOTEL stations located in the 3rd zone.

3.5. Conclusions

This paper investigates how differences in snow maps produced by NOHRSC and from MODIS are translated into differences in simulated runoff and zonally averaged April 1st SWE by the widely-used snowmelt runoff model SRM for the snowmelt season of the year 2001. Differences in mapped snow cover during the melt season lead to differences in the simulated runoff and zonally averaged SWE. The MODIS product generally maps more snow at higher elevations in the studied watersheds than does NOHRSC, while both products map similar snow amounts at

lower elevations. The greater amount of snow mapped by MODIS leads to higher simulated discharge volumes from April to September in SRM simulations than when NOHRSC snow depletion curves are used. Similarly, the calculated zonally averaged April 1st SWE from MODIS is higher than that calculated using NOHRSC snow maps. MODIS-derived snow maps show more consistent patterns of snow cover retreat with respect to elevation than do the NOHRSC snowmaps. This is probably due to their higher spatial resolution of the MODIS product, which enables it to provide a more detailed picture of snow cover in these high relief basins (**Figure 3-4**). Meanwhile, no significant effects of aspect on mapped snowcover between the two products were observed in the two watersheds (**Figure 3-5**).

The large number of cloudy days in both snow products necessitates making some subjective decisions in the construction of SRM snow depletion curves. Despite some subjectivity, the developed curves do a reasonable job of capturing real differences in SCA between the two products (**Figure 3-6**). Overall, the snow depletion curves developed from MODIS and NORSC snowcover maps provide consistent and comparable patterns of snow retreat in the two studied watersheds.

For the larger and wetter of the two watersheds, the Rio Grande, satisfactory simulations can be obtained by using representative coefficient values. The MODIS-based simulations show higher discharge simply because MODIS maps more snow in the watersheds. Meanwhile, SRM was unable to satisfactorily simulate observed streamflow in the smaller Rio Ojo watershed. For the Rio Ojo, it appears that these coefficient values should be determined for the hydrometeorological conditions of the

current year to obtain good matches between simulated and observed streamflow, and it appeared to be difficult to model the multiple-peaked hydrograph in SRM. Nevertheless, when the time-variation of simulated MODIS- and NOHRSC-based discharges are compared, the correlation coefficients between them are remarkably high at 0.99 for both watersheds.

The observed differences MODIS- and NOHRSC-based simulated streamflow for both watersheds can be traced to spatial-temporal differences in SCA in a single SRM zone within each watershed. The middle elevation zone (2^{nd}) covers approximately 50% of the area of both watersheds. In this zone of both watersheds, MODIS consistently maps more snow. Because this zone also occupies a high proportion of each watershed's area, small fractional SCA differences lead to differences in simulated streamflow.

Total basin April 1^{st} SWE calculated using MODIS-based snow depletion curves show a little more difference compared to the difference in the amount of simulated streamflow. Again, the 2^{nd} zone in each watershed contributes most significantly. There are small differences between SRM zonally averaged SWE and SNOTEL measured SWE located in the uppermost (3^{rd}) zone.

Snowcover information obtained from MODIS and NOHRSC maps and discharge simulated using the SRM is quite comparable both in terms of total seasonal discharge and in daily streamflow variations for two tributary basins of the URG. Thus it appears that standard MODIS snowcover product can provide sufficient-quality SCA

information for streamflow simulation using SRM in the snowmelt dominated watersheds.

This research focused on the standard MODIS snowcover product because of its widespread availability to the cryospheric community. Moreover, the MODIS snow-mapping algorithm is not static but is evolving. One potential area of improvement in MODIS snow cover products is to include subpixel estimates of snow cover fraction which would improve SCA over the current MODIS snow products and make more accurate snowmelt runoff simulations or forecasts possible. Several approaches to subpixel (fractional) snowcover calculations using MODIS have been recently undertaken (Barton et al., 2000; Kaufman et al., 2002; Landesa and Rango, 2002; Rango et al., 2003). Meanwhile, Rango et al. (2002, 2003) developed a different algorithm to derive a MODIS snow product at the swath level (level - 2) using the same spectral regions as when AVHRR (channels 1 and 2) or Landsat TM (channels 2 and 4) image data are used. Thus there is great potential for improved MODIS estimates of SCA compared to what is provided by the current algorithm. Indeed, Rango et al. (2002) asserted that MODIS offers the best potential for snow mapping on regular basis with respect to temporal and spatial resolution and data availability.

Finally, while satisfactory streamflow forecasting using only SCA information was obtained in the Himalayas (Dey et al., 1983), the worldwide use of SRM to simulate or forecast snowmelt runoff also requires reliable temperature and precipitation measurements which provides additional constraints to its use even if MODIS can provide adequate measurement of snowcover extent. Therefore, if the above conditions

(adequate temperature and precipitation measurements) are satisfied and the watersheds of interest are snowmelt-dominated ones, these results show that SRM simulations using snowcover maps from MODIS can be successfully applied to other parts of the world.

CHAPTER IV

POTENTIAL AND LIMITATIONS OF MASS-BALANCE MODELS FOR FORECASTING LONG-TERM STREAMFLOW VOLUME IN THE UPPER RIO GRANDE BASIN

4.1 Introduction

The considerable interannual variation of precipitation and runoff is part of the natural variability of climate and hydrological systems, and must be considered in efficiently managing water resources and coping with risks to maximize benefits and minimize damages (Chiew et al., 2003). Among various tools for management of water resources systems, long-term streamflow forecasts can be used in the allocation of irrigation water, negotiation of hydropower contracts, and in the evaluation and implementation of mitigation measures such as water conservation contingency plans or risk-based management decisions to improve the management of water resources systems (Maidment, 1992). As an example of anticipated financial benefits of improved long-term streamflow forecasts, Hamlet et al. (2002) found that reservoir model simulations based on new climate forecasts increased non-firm energy production from the major Columbia River hydropower dams by as much as 5.5 million megawatt-hours/year, resulting in an average annual revenue increase of approximately $153 million per year. In addition to these financial benefits, the allocation and management

of water resources through streamflow forecasting is directly related to a region's current and future growth. For example, the population in the southwestern United States continues to expand and efficient water resources management is an essential to region's development. If efficient water resources management is not achieved, they will be a limiting factor in the region's future growth.

Operational monthly to seasonal streamflow forecasts in the western United States are usually performed by two methods, one by the Natural Resources Conservation Service (NRCS) and the other by the National Weather Service (NWS). The NRCS method relies on a regression-based forecasting method (also known as the index-variable method), in which the volumetric streamflow during the forecast period is related to accumulated precipitation in the form of snow storage or soil moisture at the time of forecast. The NWS method uses conceptual hydrologic/hydraulic simulation models to capture the hydrologic/hydraulic memory, as reflected in soil moisture, snow storage and reservoir conditions and then assumes, explicitly or implicitly, climatological average conditions during the forecast period. The climatological averages are assumed during the forecast period because it is difficult to obtain accurate climatological variable forecasts with long lead times (Garen, 1992; Lettenmaier et al., 1990; Maidment, 1992; Stedinger et al., 1989; Twedt et al., 1977).

The winter accumulation of snow in mountainous snowmelt-dominated watersheds such as those in Sierra Nevada or the Rocky Mountains in the western United States facilitates seasonal forecasts of streamflow volumes because of the direct relationship between winter accumulated snow amount and resulting summer

streamflow (Maidment, 1992). Accordingly, useful streamflow forecasts can be usually achieved in the watersheds having significant snow accumulation and small liquid precipitation during the forecast period.

However, there are several basic sources of errors in streamflow forecasts even in snowmelt-dominated basins (Maidment, 1992). The first error source is the determination of snow reserves at the time of forecast. It is not easy to accurately determine the snow covered area and average snow water equivalent (SWE) in a watershed, especially in mountainous regions. The second and most problematic error source is the difficulty of predicting precipitation during the forecast period. The third error source is incorrect model conceptualization of the relationships among variables affecting streamflow generation (Maidment, 1992; Martinec and Rango, 1995). Problems related to model conceptualization occur because there are some unexplainable relationships among variables affecting streamflow which are not embedded in the model, and each year has its own hydrological characteristics. Finally, there are also some problems related to the model parameterization. That is, even under the condition that appropriate model conceptualization has been obtained, it is difficult to obtain proper parameters for the model.

In order to investigate the effects of the various sources of errors (or uncertainties), this chapter investigates potential of several simple mass-balance models for seasonal streamflow forecasting in the two sub-watersheds of the URG basin which were also used in the Chapter III. The concept of a mass-balance model is that runoff in a future forecast period is determined by the amount of water presently in storage in a

watershed (here snow accumulation) as well as forecast period precipitation and water losses through evapotranspiration and groundwater percolation in the watershed.

In this chapter, two ways of obtaining the parameters of the mass-balance models are examined. The forecasts obtained by use of the split-sample method due to short period record of historical observation. The first means of parameter estimation is to use the parameter values from SRM streamflow simulations which were discussed in the Chapter III, and the second means is by optimization. Further the effect of forecast lead time is considered by comparison of streamflow forecasts made on January 1st, February 1st, March 1st and April 1st. Forecasts are made for both observed and ensemble-forecasted precipitation in order to separate the effect of precipitation forecast uncertainty. For data, the models mainly use historical SWE on April 1st and precipitation amount from April 1st to September 30th from 1981 to 2001 observed in several NWS and SNOTEL sites located inside or very close to the watersheds.

The models based on the parameters from SRM streamflow simulations (hereafter referred to SRM mass-balance model) use SWE at the time of forecast and forecast period parameter values (snow and rainfall runoff coefficients) obtained through SRM streamflow simulations from 1990 to 2001 and precipitation during the forecast period. The optimized parameter models use historical SWE values at the time of forecast and historical precipitation during the forecast period in order to get optimized parameter values (usually snow and rainfall runoff coefficients) for the mass-balance models during the forecast period. Through streamflow forecasts using SRM mass-balance model, it is possible to see whether the parameter values obtained from

SRM streamflow simulations effectively represent time-varying hydrometeorological characteristics of these two watersheds in the forecasting mode. However, it is not necessarily true that the parameter values from SRM streamflow simulations are optimal for forecasting. Therefore, mass-balance models which have several assumptions and constraints related to the parameters and input variables (SWE on April 1st and precipitation amount from April 1st to September 30th) were developed to check whether optimization can give more satisfactory results in terms of long-term streamflow forecasts.

In addition to the above mentioned streamflow forecasts, two additional streamflow forecasts are also presented for purposes of comparison in this chapter. The first is the simple index-variable method which uses the relationship between average SWE on the first day of each month (January, February, March, April) at several SNOTEL stations and streamflow volume from April 1st to September 30th, and the other comes from the NRCS. The reason to examine the streamflow forecasts using simple index-variable method is to compare the results from above two types' mass balance models with those from simple method which do not consider the hydrological conditions during the forecast period to see how much improvement using mass balance models can be achieved. NRCS streamflow forecasts forecast naturalized streamflow which is not affected by upstream water management such as reservoirs or irrigation. Therefore, although our results can not be directly compared with these streamflow forecasts, it is possible to examine the relative accuracy of our models.

Through this investigation, it will be possible to examine first what are the potential and limitations of above mentioned two types of mass-balance model parameterizations in these snowmelt-dominated watersheds; second, by comparing streamflow forecast accuracy using the two types of parameterizations, how the improvement in the accuracy of streamflow forecasts can be achieved in the optimized parameter models compared to SRM mass-balance model and which type of mass-balance model shows the best results for seasonal streamflow forecasts; third, as previous studies (Lettenmaier and Garen, 1979; Stedinger et al., 1989) have shown that forecast model performance shows dependence on site-specific characteristics, what kind of differences in model parameters and performance are obtained in these two closely-located watersheds and why this kind of difference occurs.

4.2. Study Site

The two sub-watersheds (Rio Grande and Rio Ojo watersheds) located inside the URG basin used in Chapter III are again used in this chapter. The elevation ranges and landcover types of these two watersheds were described in detail in section 3.2 along with the historical SRM studies that have been conducted in the Rio Grande watershed. **Figure 3-1** also shows the outlines and locations of these two watersheds.

4.3. Data and Method

4.3.1. Meteorological Observations

To perform SRM streamflow simulations from 1990 to 2001, daily temperature and precipitation data from NWS meteorological stations and SNOTEL stations were used. Detailed information regarding the data used, for example, how many stations in each watershed were used and how zonal temperature and precipitation were calculated, were explained in section 3.3.6. Meanwhile, in order to forecast volumetric stremflow amounts from 1981 to 2001 as is done in this chapter, the historical precipitation and SWE from 1981 to 1989 were also used in addition to the 1990 – 2001 data used in Chapter III. The 1981 to 1989 data were also obtained from NWS and SNOTEL stations, and the same method was applied to compute zonal precipitation data in both watersheds from 1981 to 1989.

4.3.2. Snow Cover

NOHRSC snowcover product from 1990 to 2001 was used for the SRM streamflow simulations. The characteristics of the NOHRSC snowcover product and how SCA daily time variations were determined are explained in detail in section 3.3.4 and section 3.3.2, respectively. **Figure 3-4** illustrates four examples of snowcover maps for both watersheds and **Figure 3-6** illustrates the NOHRSC zonal daily SCA variation used for an SRM streamflow simulation in 2001.

4.3.3. Snowmelt Runoff Model (SRM)

The SRM mass-balance model uses the parameter values which come from the SRM streamflow simulations from 1990 to 2001. Detailed explanations regarding SRM are found in section 3.3.1.

4.3.4. Parameterization of SRM

Several parameters are required when SRM streamflow simulations are performed. Each parameter has its own characteristics such as physically-realistic range or time variation. Section 3.3.7 illustrates details about the parameterization of SRM, and **Figure 3-2** shows the time variation of SRM parameters from 1990 to 2000 over the same period. One thing to be noticed is that when SRM streamflow simulation was also conducted in 2001, the time-variation shape of parameters follows the same pattern as other years. **Table 3-4** lists the SRM simulation result statistics from 1990 to 2000 using two statistical criteria.

4.3.5. Streamflow Forecasts Using SRM Mass-Balance Model

The starting point for the parameter values used in the forecasting investigation in this chapter is the values obtained for the use of SRM to model snowmelt runoff as discussed in Chapter III. How these parameter values were obtained is fully described in section 3.3.7. To review briefly, the bimonthly-varying snow runoff coefficients (C_S) applied to each zone and the bimonthly-varying one rainfall runoff coefficients (C_R)

applied to all the zones were obtained from 1990 to 2001 SRM simulations. A bimonthly-varying degree-day factor (a) for each zone was obtained (this parameter is not used in the SRM mass-balance model). Therefore, three zonal bimonthly-varying C_S values, a values and one bimonthly-varying spatially constant C_R value were obtained through SRM streamflow simulations from 1990 to 2001.

The following is the mass-balance equation expressing SRM mass-balance model for runoff integrated over the snowmelt season which uses the parameter values obtained from 1990 to 2001 SRM streamflow simulations (Martinec and Rango, 1995).

$$\Re = \sum_i R_i = A_i \left(HW_i C_{S,i} + \sum_t C_{R,t} P_{i,t} \right) \qquad (4.1)$$

$\Re$: Total forecasted streamflow volume from April 1st to September 30th

R_i: Forecasted streamflow volume from April 1st to September 30th in zone i

i: Zonal index (i = 1, 2, 3)

t: Bimonthly time step from April 1st to September 30th

HW_i: Average zonal snow water equivalent on April 1st (m) in zone i

$P_{i,t}$: Forecasted precipitation from April 1st to September 30th in zone i and time step t

A_i: Area (m^2) in zone i

$C_{S,i}$: Runoff coefficient for snow in zone i

$C_{R,t}$: Runoff coefficient for rainfall at time step t

This mass balance equation is suitable for use in these two watersheds because maximum snow accumulation in these two watersheds occurs on approximately April 1st, and it is reasonable to assume that maximum snow accumulation on April 1st, total precipitation from April 1st to September 30th, and losses through evapotranspiration or groundwater percolation which are expressed as runoff coefficients for rain and snow are the main factors affecting the streamflow amount from April 1st to September 30th. One thing to be noticed in the above equation is that annually averaged zonal values are used in the case of C_S values while in the case of C_R values, bimonthly-varying spatially constant values are used. That is, C_S values are separated by zone while C_R values are separated by time in the above equation. The reason to use annually averaged zonal C_S values is to make the equation simplified. Meanwhile, the reason to use bimonthly-varying spatially constant C_R values is that it was difficult to estimate annually-averaged C_R values in the forecasting mode which will be explained later.

Using this mass balance equation, to compute volumetric streamflow amount from April 1st to September 30th requires knowledge of averaged SWE on April 1st, annually-averaged zonal C_S, bimonthly-varying but spatially constant C_R, and bimonthly precipitation totals from April 1st to September 30th. However, for a forecast on April 1st, the only available information is the observed SWE at the SNOTEL stations at that date and meteorological data such as temperature, precipitation and streamflow for earlier months. Therefore, it is necessary to estimate the other parameter values (1st, 2nd, 3rd zonally-averaged SWE values on April 1st, annually-averaged zonal C_S values and bimonthly-varying spatially constant C_R values) from the relationship between these

parameter values and average observed SWE in the 3rd (upper) zone of both watersheds. The reason only to use SWE in the 3rd zone although there are other SNOTEL stations in the watershed is due to the fact that the number of SNOTEL stations located in other zones is very small compared to the size of zonal area, especially in the 2nd zone.

First, it is necessary to obtain the relationship between observed SWE at SNOTEL stations from 1990 to 2001 and zonally-averaged April 1st SWE in the 3rd zone through MDC derived from SRM simulations (Martinec et al., 1998) because there are differences between these two SWE values. This relationship in both watersheds is illustrated in **Figure 4-1(a)**. As can be seen, there is a significant relationship between average measured SWE and SRM calculated zonally-averaged SWE in the 3rd zone of both watersheds, which can be used to estimate zonally-averaged SWE in the 3rd zone. Secondly, to forecast annually-averaged zonal C_S from average observed SWE, the relationship between annually-averaged zonal C_S obtained from the 1990-2001 SRM simulations and average measured SWE on April 1st was used. As an example, **Figure 4-1(b)** illustrates this relationship for C_S in the 2nd zone of each watershed. As can be seen, a first-order linear relationship is appropriate between average observed SWE in the 3rd zone and annually-averaged C_S in the 2nd zone. A similar relationship is also valid for the other two zones. This relationship is reasonable because high SWE on a specific day will give high C_S in following days. Therefore, the linear regression to forecast annually-averaged C_S from average measured SWE was used in each zone. Estimates of zonally-averaged SWE in the 1st and 2nd zones are also needed. In this case, the ratios between the SRM-calculated SWE in the 1st and 2nd zones and the SRM-calculated SWE

in the 3rd zone were calculated from each year's simulation and then the average of above ratios for each zone were used to estimate the 1st and 2nd zonally-averaged SWE from the estimated 3rd zonally-averaged SWE in the forecasting mode.

No relationship exists between C_R and average measured SWE because C_R is related to the precipitation total from April 1st to September 30th, not to April 1st SWE. One possibility would be to predict annually-averaged C_R as a function of the observed precipitation from April 1st to September 30th. However, as illustrated in **Figure 4-1(c)**, the observed relationship was poor as compared to that between C_S and April 1st SWE. This difference appears to be related to hydrological differences between snowmelt and rainfall runoff in both watersheds. Compared to precipitation, snowmelt occurs in a short time period and therefore the relationship between snowmelt and C_S is not affected by many other hydrological factors in these watersheds. However, precipitation occurs throughout the period of April to September and therefore many other factors can affect the relationship between precipitation and C_R during wet and dry periods. Therefore, bimonthly-varying spatially constant C_R from 1990-2001 SRM streamflow simulations were averaged in bimonthly time scale, and then used in the forecasting mode.

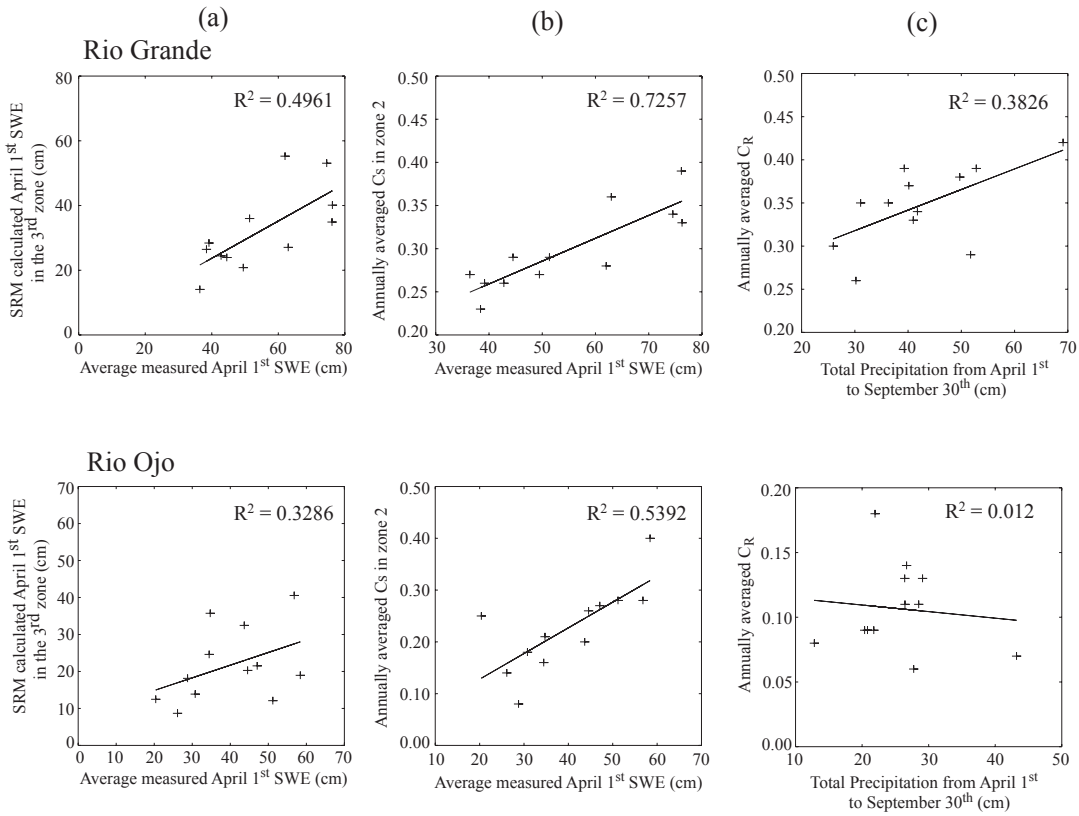

Figure 4-1. Relationships between several parameter values obtained from streamflow simulations and average observed 3rd zonal April 1st SWE at SNOTEL stations in both watersheds from 1990 to 2001. a) Linear relationship between average observed April 1st SWE and SRM calculated April 1st zonally averaged SWE. b) Linear relationship between average observed April 1st SWE and annually averaged C_S in the 2nd zone. c) Linear relationship between averaged observed April 1st SWE and annually-averaged spatially constant C_R

After setting up the above procedure to estimate parameter values from average observed SWE in the 3rd zone, the split-sample method (also known as the jack-knife method) was used. For example, to forecast the streamflow volume from April 1st to September 30th in 1990, the linear relationships among the above-mentioned parameters and average observed SWE in the 3rd zone from 1991 to 2001 were used. Then average observed SWE on April 1st in 1990 was applied to each linear regression equation to obtain the parameters for 1990. This procedure is applied in sequence for the years 1990 to 2001. However, in the case of streamflow forecast for 1981 to 1989, it was unnecessary to use the split-sample method because the streamflow simulation started from 1990. For the years prior to 1990, the relationship using all the data from 1990 to 2001 was used to obtain the parameter values.

In the case of precipitation term in the SRM mass-balance model, the observed precipitation amount in the year of interest was first applied to look at the forecast performance apart from the effect of the errors of precipitation forecast. That is, if the forecast of streamflow amount in 1990 is of interest, the precipitation observed in 1990 was applied to above mass balance equation with the parameter values obtained through the split-sample method. In the actual forecasting mode a precipitation forecast is required. However, it is difficult to forecast the long-term precipitation amount. So, the ensemble forecasting method is used; that is, the historical precipitation in each year from 1981 to 2001 was applied except for the year of interest and then streamflow forecasts were obtained for each precipitation value. This gives a distribution of streamflow forecasts from which statistics such as mean and standard deviation (i.e., uncertainty due to precipitation) can be calculated.

Finally, in the case of January 1st, February 1st, and March 1st streamflow forecasts, the univariate linear regression between the observed SWE on each of these days and the observed SWE on April 1st at each SNOTEL station from 1981 to 2001 was used following the split-sample method described above. After obtaining the forecasted SWE on April 1st in the 3rd zone, the same procedure as when the observed SWE in the 3rd zone on April 1st were used in order to forecast volumetric streamflow amount from April 1st to September 30th.

Table 4-1. Characteristics of optimized models

Models	Assumptions	Optimized coefficients	Constraints of optimized coefficients
Model 1	- C_S, C_R are intra- and inter-year constants and are spatial constants (same value is applied to all the zones) - 3rd zonal average measured SWE (*HW*) and 3rd zonal average measured precipitation (*P*) are applied to all the zones	C_S, C_R	$0 \le C_S \le 1$ $0 \le C_R \le 1$
Model 2	- a, b, c, d are intra- and inter-year constants and are also spatial constants - 3rd zonal average measured SWE (*HW*) and 3rd zonal average measured precipitation (*P*) are also applied to all the zones - Snow and rainfall runoff coefficients are both proportional to the 3rd zonal average measured SWE and 3rd zonal average measured precipitation from April 1st to September 30th	a, b, c, d	$0 \le C_S (= a + b \cdot HW) \le 1$ $0 \le C_R (= c + d \cdot P) \le 1$
Model 3	- C_S, C_R are intra- and inter-year constants and are spatial constants - 1st, 2nd zonal SWE values are optimized as the proportions on the 3rd zonal measured SWE, and zonal precipitation which was used in the SRM simulation is again used	C_S, C_R, e (SWE 1 / SWE 3), f (SWE 2 / SWE 3)	$0 \le C_S \le 1$ $0 \le C_R \le 1$ $0 \le e \le 1$ $0 \le f \le 1$
Model 4	- a, b, c, d are intra- and inter-year constants and are spatial constants - 1st, 2nd zonal SWE values are optimized from the proportions to the 3rd zonal measured SWE, and zonal precipitation which was used in the SRM simulations is again used - Snow(rainfall) runoff coefficients are both proportional to measured and optimized SWE values and average measured precipitation from April 1st to September 30th in each zone	a, b, c, d, e (SWE 1 / SWE 3), f (SWE 2 / SWE 3)	$0 \le C_{S,i} (= a + b \cdot HW) \le 1$ $0 \le C_{R,t} (= c + d \cdot P) \le 1$ $0 \le e \le 1$ $0 \le f \le 1$

4.3.6. Streamflow Forecasts Through Parameter Optimization of Mass-Balance Models

Although the SRM mass-balance model is a reasonable one to forecast volumetric streamflow amount from April 1st to September 30th, it is difficult to ascertain that the parameter values obtained through SRM simulations and above linear relationships are the optimal ones. Therefore, the next step is to develop models based on mass-balance which have optimized parameters. The following equations describe four models in order from the simplest to the most complicated, and **Table 4-1** gives detailed explanations about the corresponding assumptions and constraints of each model. In this optimization procedure, the goal of optimization was to minimize the sum of the squared differences between optimized and measured streamflow amount during all the available years. Here, "optimized streamflow" amount means the streamflow amount in each year after optimization process.

$$\text{Model (1):}\quad \hat{\Re} = A \cdot (C_s \cdot HW + C_r \cdot P)$$

$$\text{Model (2):}\quad \hat{\Re} = A \cdot ((a + b \cdot HW) \cdot HW + (c + d \cdot P) \cdot P)$$

$$\text{Model (3):}\quad \hat{\Re} = \sum_i R_i = \sum_i \left[A_i \cdot (C_s \cdot HW_i + C_r \cdot P_i)\right]$$

$$\text{Model (4):}\quad \hat{\Re} = \sum_i R_i = \sum_i \left\{A_i \cdot \left[(a + b \cdot HW_i) \cdot HW_i + (c + d \cdot P_i) \cdot P_i\right]\right\}$$

Models 3 and 4 are zonally separated forms of models 1 and 2, respectively. The difference between models 1 and 3 and models 2 and 4 is that models 1 and 3 optimize C_S and C_R directly, while in models 2 and 4, C_S and C_R are estimated as linear functions of SWE (*HW*) and precipitation, respectively. The reason to use these relationships to estimate C_S and C_R instead of C_S and C_R directly in the models 2 and 4 is that there is a linear relationship between C_S and SWE on April 1st as was mentioned above, and it can be accordingly hypothesized that a similar relationship could exist between annually-averaged C_R and April 1st to September 30th precipitation although above SRM streamflow simulations from 1990 to 2001 failed to show it. This relationship can be considered because, all other things being equal, the fraction of runoff increases with the amount of rainfall, since some losses reach a maximum at some rain amount. Although numerous models modifying above mass balance equations exist, the above four models provide the general characteristics of many possible optimized mass-balance models in these watersheds. In order to obtain these optimized parameter values in above equations, the "Solver" tool in the EXCEL program was used. A detailed explanation regarding "Solver" algorithms and capabilities can be found in (http://www.frontsys.com).

The split-sample method was again used to obtain the optimized parameter values for each year in each model. For example, to obtain optimized parameter values for streamflow forecast in 1981, all the data in 1981 were deleted, and the optimized parameter values were obtained using the data from the remaining years 1982 to 2001 and then the same procedure was applied to each year sequentially. As in the case of

forecasts using SRM mass-balance model, two sets of forecasts were obtained, one using observed precipitation, and the other using a distribution of precipitation forecasts obtained by the ensemble method.

In order to get the streamflow forecasts from January 1st, February 1st, March 1st, the same procedure as that of streamflow forecasts using SRM mass-balance model was used. The two diagrams in **Figure 4-2** illustrate the general procedure for above two approaches to forecast volumetric streamflow amount from April 1st to September 30th in both watersheds.

4.3.7. Streamflow Forecasts Through Simple Index Variable and Streamflow Forecasts Made by NRCS

As mentioned above, two other streamflow forecasts are provided in this chapter. One comes from simple index-variable method which uses only the SWE measured in the SNOTEL stations, and the other is the streamflow forecasts made from NRCS. In the case of simple index-variable method, the linear regression between historical average SWE in the 1st day of each month (January, February, March and April) at several SNOTEL stations located in the 3rd zone and streamflow volumes from April 1st to September 30th from 1981 to 2001 were used. **Figure 4-3** shows these linear relationships using the data from all the years in both watersheds. Meanwhile, in the case of NRCS naturalized streamflow forecasts, which are only available in the Rio Grande watershed from 1990 to 2001, they also use the linear regression between variables significantly affecting streamflow amounts such as SWE and soil moisture and

streamflow volume along with some calibration techniques. They provide the streamflow forecasts having 10%, 30%, 50%, 70% and 90% exceedance probabilities (http://www.wcc.nrcs.usda.gov/wsf/). However, streamflow forecasts having 50% exceedance probability are used in here because this streamflow forecast is most probable one.

4.4 Results

4.4.1. Streamflow Forecasts Using Observed Precipitation on April 1st

Figure 4-4 shows the linear relationships between several variables which are important in the above mass balance equations in both watersheds. Through this investigation, it is possible to determine which years have different hydrologic characteristics compared to other years and whether good linear relationship exists between the variables which are closely related to each other in the watershed. The relationships are significant except the relationship between total average precipitation amount from April 1st to September 30th and streamflow volume from April 1st to September 30th in both watersheds. It is also possible to see that several points are far away from linear regression lines in the other two relationships, and the years having these points can be believed to show different hydrologic characteristics compared to other years.

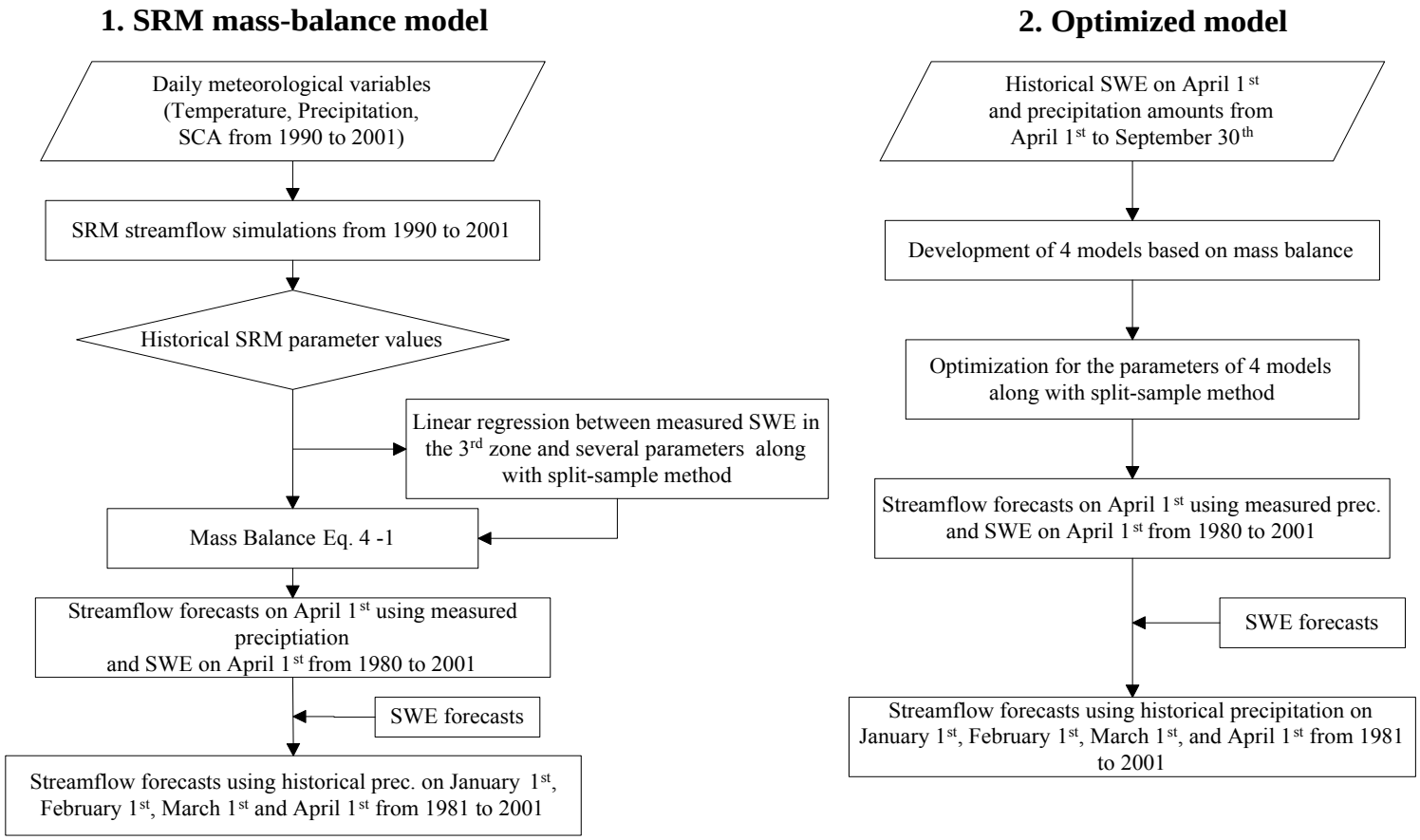

Figure 4-2. General procedures for two types' mass-balance models

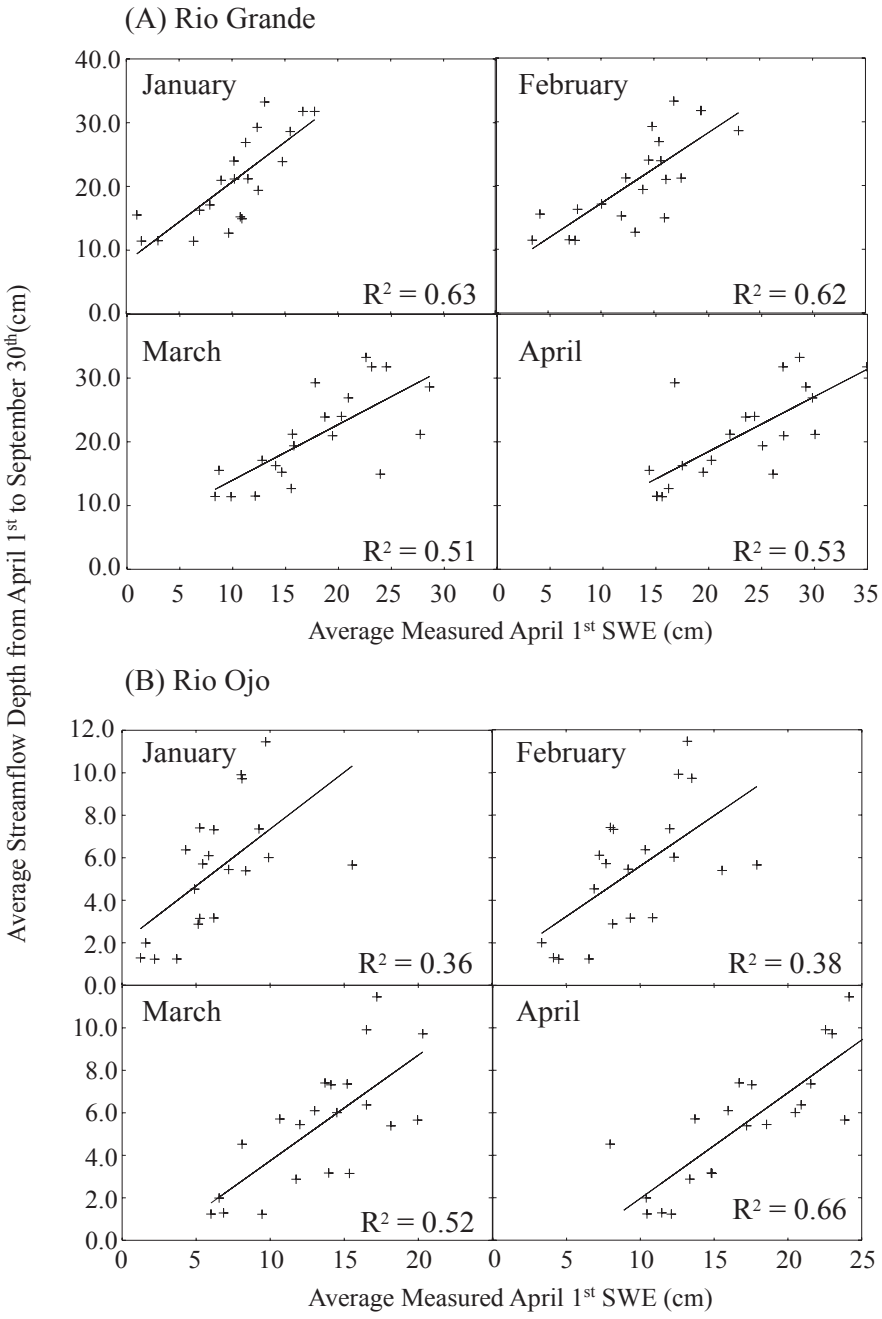

Figure 4-3. Relationships between historical average SWE on the 1st day of each month and streamflow volume from April 1st to September 30th in both watersheds

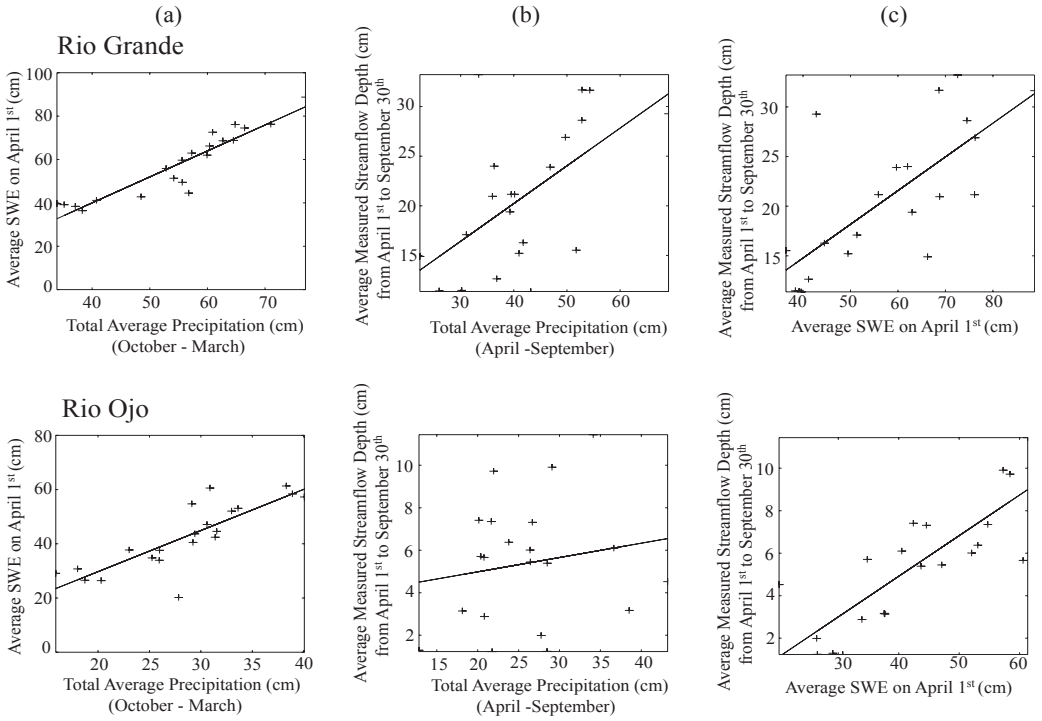

Figure 4-4. Linear relationships between several variables which are important in the above mass-balance models. a) Relationship between average SWE (cm) on April 1st and total average precipitation (cm) from October to March. b) Relationship between total average precipitation (cm) from April 1st to September 30th and average measured streamflow depth (cm) from April 1st to September 30th. c) Relationship between average SWE (cm) on April 1stand average measured streamflow depth (cm) from April 1st to September 30th

Table 4-2. Averages and standard deviations of optimized parameters in the models and average C_p values between the optimized and measured streamflow volumes

Model	Parameter	Average ± standard deviation		Average C_p[3]	
		Rio Grande	Rio Ojo	Rio Grande	Rio Ojo
Model 1	C_S	0.226 ± 0.019	0.131 ± 0.002	0.70	0.61
	C_R	0.196 ± 0.027	0.001 ± 0.003		
Model 2	a	0.264 ± 0.015	0.003 ± 0.012	0.80	0.74
	b	0.033 ± 0.021	0.217 ± 0.065		
	$C_S = a + b \cdot HW$	0.283 ± 0.007	0.099 ± 0.010		
	c	-0.109 ± 0.007	-0.011 ± 0.066		
	d	0.483 ± 0.028	0.195 ± 0.039		
	$C_R = c + d \cdot P$	0.092 ± 0.009	0.030 ± 0.013		
Model 3	C_S	0.381 ± 0.020	0.244 ± 0.005	0.66	0.61
	C_R	0.202 ± 0.028	0.001 ± 0.003		
	e[1]	0.255 ± 0.003	0.227 ± 0.002		
	f[2]	0.650 ± 0.006	0.591 ± 0.004		
Model 4	a	0.377 ± 0.098	0.424 ± 0.187	0.68	0.74
	b	0.098 ± 0.126	1.102 ± 0.426		
	c	0.122 ± 0.118	-0.163 ± 0.073		
	d	0.157 ± 0.166	0.449 ± 0.140		
	$C_{S,1} = a + b \cdot HW_1$	0.373 ± 0.112	0.027 ± 0.045		
	$C_{S,2} = a + b \cdot HW_2$	0.395 ± 0.086	0.102 ± 0.063		
	$C_{S,3} = a + b \cdot HW_3$	0.424 ± 0.059	0.691 ± 0.084		
	$C_{R,1} = c + d \cdot P_1$	0.163 ± 0.075	0.022 ± 0.004		
	$C_{R,2} = c + d \cdot P_2$	0.171 ± 0.068	0.030 ± 0.005		
	$C_{R,3} = c + d \cdot P_3$	0.177 ± 0.062	0.036 ± 0.005		
	e[1]	0.224 ± 0.012	0.054 ± 0.030		
	f[2]	0.578 ± 0.022	0.069 ± 0.045		

[1]Proportion between 1st and 3rd zonally-averaged SWE.

[2]Proportion between 2nd and 3rd zonally-averaged SWE.

[3]Average C_p values between measured and optimized streamflow after optimization.

Table 4-2 shows the averages and standard deviations of parameter values obtained by optimizing separately for each year according to the split-sample method in the two watersheds. Because there is no model structure which exactly matches to that of SRM mass-balance model, it is not appropriate to compare the parameter values used in SRM mass-balance model with those in optimized models. One interesting phenomenon is that optimized C_R values for the Rio Ojo watershed were almost zero in all years in models 1 and 3. This situation is caused by the fact that precipitation does not have any function in predicting the streamflow amounts in the Rio Ojo while apparently it has some function in the Rio Grande watershed.

The coefficient of prediction (C_p), which can be used for determining the accuracy of streamflow forecasts in a model, is calculated as follow.

$$C_p = 1 - \frac{\frac{1}{n}\sum_{i=1}^{n}(\Re_i - \Re'_i)^2}{s^2} \qquad (4.2)$$

$\Re_i$: Observed streamflow volume in the year *i*

$\Re'_i$: Forecasted streamflow volume in the year *i*

n: Number of years

s^2: Variance of observed streamflow volume in all the years

However, the C_p values for measured and optimized streamflow volumes during the optimization process using the split-sample method were first calculated. Therefore, "forecasted" streamflow volume in the above equation is replaced with "optimized"

streamflow volume and following modified form of above equation is used for calculating the C_p values between measured and optimized streamflow volume.

$$C_p(i) = 1 - \frac{\frac{1}{n}\sum_{j \neq i}^{n} (\Re_j - \Re'_j)^2}{s_i^{\,2}} \qquad \text{where} \quad s_i^{\,2} = \frac{1}{n}\sum_{j \neq i}^{n} (\Re_j - \overline{\Re})^2 \qquad (4.3)$$

$\Re_j$: Measured streamflow volume in the year *j*

$\Re'_j$: Optimized streamflow volume in the year *j*

$\overline{\Re}$: Average of streamflow volume in all the years except year *i*

n: Number of years

Through this calculation, it is possible to infer which models are more appropriately conceptualized in the watershed, and which years show different hydrological characteristics compared to other years. **Figure 4-5** shows the time variations of this C_p value in both watersheds and the average C_p values are given in **Table 4-2**. Models 2 and 4 have the highest C_p values in the Rio Grande and Rio Ojo watersheds, respectively, although models 2 and 4 in the Rio Ojo watershed have almost the same average C_p values. Therefore, these two models show the best performance of model conceptualization for hydrological conditions in both watersheds. The C_p values for 1987 and 1999 are significantly increased in the Rio Grande watershed, indicating hydrologically different characteristics compared to other years. Meanwhile, in the case of Rio Ojo watershed, 1984 and 1985 have different characteristics compared to other years. In the Rio Ojo watershed, the same C_p values are obtained for models 1 and 3 and

almost the same values when models 2 and 4 are used like mentioned above. From this, it can be inferred that although the variables (SWE and precipitation) to be optimized in the Rio Ojo watershed are separated into 3 zones in the models 3 and 4, this separation does not affect the improvement of model conceptualization in the Rio Ojo watershed. Moreover, while the conceptualization performance order of models in the Rio Grande watershed is model 2>model 1>model 4>model 3, models 2 and 4 show significant increases in the performance of model conceptualization compared to models 1 and 3 in the Rio Ojo watershed.

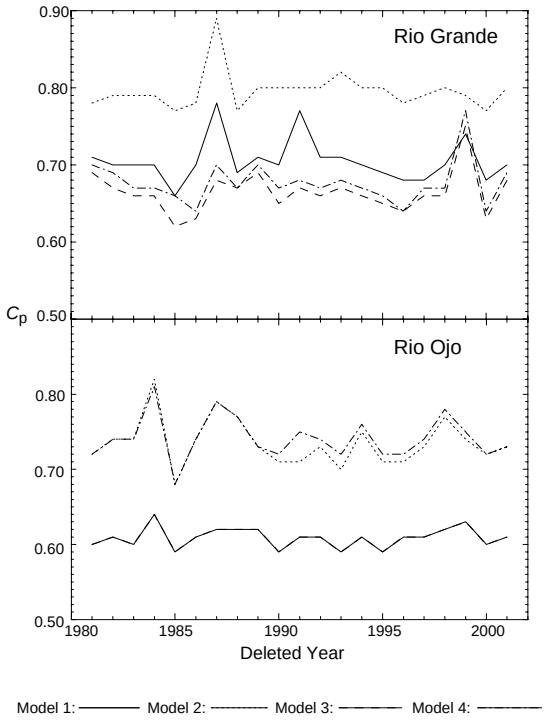

Figure 4-5. Time variation of C_p values between measured and optimized streamflow in both watersheds. Note that models 1 and 3 overlap in the Rio Ojo watershed

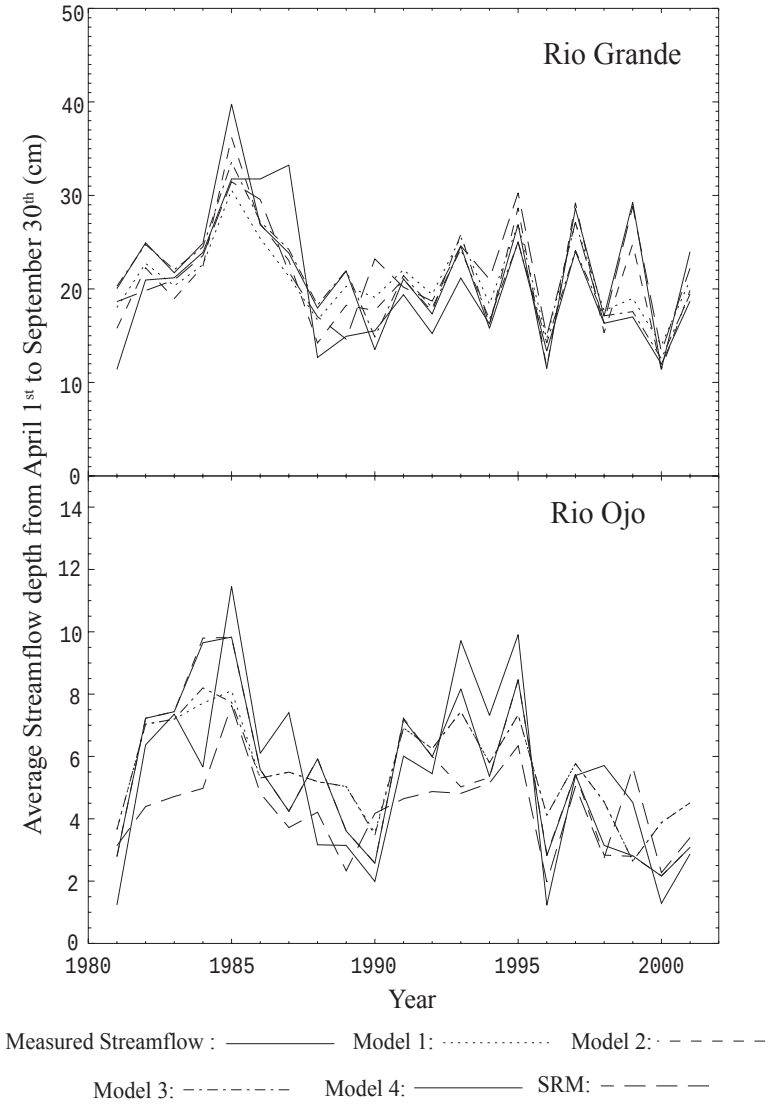

Figure 4-6. Streamflow forecasts using SRM mass-balance model and optimized models with observed precipitation in the year of interest

In order to compare and evaluate the performance of SRM mass-balance model and optimized models in the two watersheds, one needs to compute C_p value of streamflow forecasts using the observed rather than forecasted precipitation from April 1st to September 30th in the forecasted year. This comparison examines the functionality of the models apart from the effect of uncertain precipitation and models' sensitivity to precipitation. The long-dashed lines in **Figure 4-6** and **Table 4-3** show the streamflow forecasts and C_p values using SRM mass-balance model with observed precipitation in both watersheds on April 1st, respectively. From this point, C_p value is calculated using Eq. (4.2). That is, forecasted streamflow is used instead of optimized streamflow. As can be seen, satisfactory streamflow forecasts are obtained for the Rio Grande but less satisfactory for the Rio Ojo watershed. This situation seems to be related to two factors. The first one is related to high variation of parameter values in the Rio Ojo watershed compared to those in the Rio Grande as mentioned above, and the second is the weak relationships between average observed SWE in the 3rd zone and other parameter values in the Rio Ojo watershed (**Figure 4-1**) which were used in the above mass-balance Eq. (4.1).

Table 4-3. C_p values and standardized root mean squared error (SRMSE) between measured and forecasted streamflow volumes using observed precipitation in the year of interest

C_p	Model 1	Model 2	Model 3	Model 4	SRM
Rio Grande	0.57	0.75	0.55	0.47	0.68
Rio Ojo	0.58	0.52	0.56	0.65	0.40

SRMSE[1]	Model 1	Model 2	Model 3	Model 4	SRM
Rio Grande	0.23	0.17	0.23	0.25	0.20
Rio Ojo	0.35	0.36	0.37	0.31	0.42

[1]SRMSE is calculated like the following.

$$SRMSE = \sqrt{\frac{1}{n}(\sum_{i=1}^{n}(\Re_i - \Re_i'))^2} \; / \; \mu_{\Re}$$

where $\Re_i$: Measured streamflow volume in the year *i*

$\Re_i'$: Forecasted streamflow volume in the year *i*

$\mu_{\Re}$: Average of measured streamflow volume in all the years

n: Number of years

Figure 4-6 and **Table 4-3** also illustrates the streamflow forecasts and C_p values using each optimized model with observed precipitation in the year of interest, respectively. Model 2 and model 4 show the most satisfactory streamflow forecasts in the Rio Grande and Rio Ojo watersheds, respectively. From this result, it can be inferred that the use of linear functions of SWE and precipitation amount instead C_S and C_R, respectively, improves model performance in both watersheds. Meanwhile, the differences of model conceptualization in the Rio Ojo watershed between models 1, 3

and models 2, 4 are decreased when the observed precipitation in the forecasted year is used, which is related to the sensitivity of model to the precipitation.

When the streamflow forecast obtained using optimized parameter values are compared with those using SRM mass-balance model, the latter is the second-best one in the Rio Grande watershed. It is also interesting to see that the separation of zones decreases slightly the performance of model 3 as compared to model 1 and significantly decreases the performance of model 2, making model 4 the most unsatisfactory in the Rio Grande watershed. Zonal separation may give too many additional degrees of freedom in the optimization process, making it difficult to obtain adequate parameter values. This situation can be seen by comparing the standard deviations of corresponding optimized parameters between model 1 and model 3 and between model 2 and model 4 in **Table 4-2**. Models having zonal separation of variables have higher standard deviations of parameter values. In the case of Rio Ojo watershed, the same situation happens in the relationship between model 1 and model 3. However, in the case of model 2 and model 4, reverse situation happens. That is, the additional degrees of freedom of model 4 give some improvement of model 2. Therefore, it can be inferred that the increase of standard deviation of parameter values does differently affect model performance depending on the watershed. Related to the streamflow forecasts using the SRM mass-balance model, SRM mass-balance model shows the most unsatisfactory results compared to optimized models in the Rio Ojo watershed (**Table 4-3**).

Another technically interesting phenomenon can be seen in the comparison of **Figure 4-6** and **Table 4-3**. That is, almost the same range of C_p values can be obtained

in the Rio Ojo watershed compared to the Rio Grande watershed although visual inspection shows better streamflow forecasts in the Rio Grande watershed. This situation is caused by the method to calculate C_p. When C_p values are calculated, the denominator of C_p is the variance of measured streamflow amounts in all the years, and therefore the higher variation of measured streamflow amounts in the Rio Ojo watershed makes C_p have almost the same range of values compared to that of Rio Grande watershed. This fact can be confirmed when the SRMSE values, which don't consider the variance of measured streamflow, between both watersheds are compared (**Table 4-3**).

4.4.2. Streamflow Forecasts Using Ensemble-Forecasted Precipitation

4.4.2.1. Streamflow Forecasts on April 1st Using Ensemble-Forecasted Precipitation

Although the investigation about which model is more appropriate with observed precipitation in the forecasted year was discussed above, it is not the real forecasting situation. So, the historical precipitation amounts from April 1st to September 30th from 1981 to 2001 except the precipitation data of the year of interest were used to determine the ensemble of forecasted streamflow amounts from April 1st to September 30th on April 1st. After getting the ensemble of forecasted streamflow, the "best" streamflow forecast which is the arithmetic average of the ensemble of forecasted

streamflow was obtained for each year and the C_p values between "best" forecasted streamflow and measured one for all the years were calculated.

Six streamflow forecasts using the four optimized models, SRM mass-balance model, and simple index-variable model using only SWE are shown for both watersheds in **Figure 4-7** and **Figure 4-8**. Because the streamflow forecasts from NRCS are only available from 1990 and 2001, NRCS streamflow forecasts are not included in **Figure 4-7**. However, **Table 4-4** includes the C_p values for all the models including NRCS streamflow forecasts.

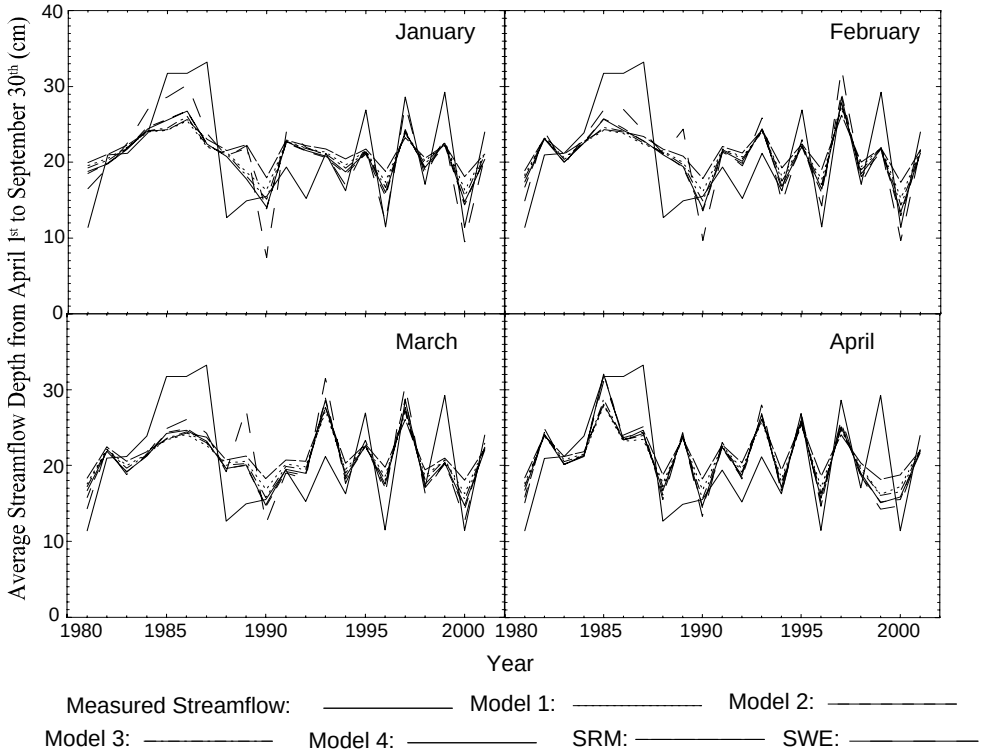

Figure 4-7. Streamflow forecasts for six models on January 1st, February 1st, March 1st and April 1st in the Rio Grande watershed

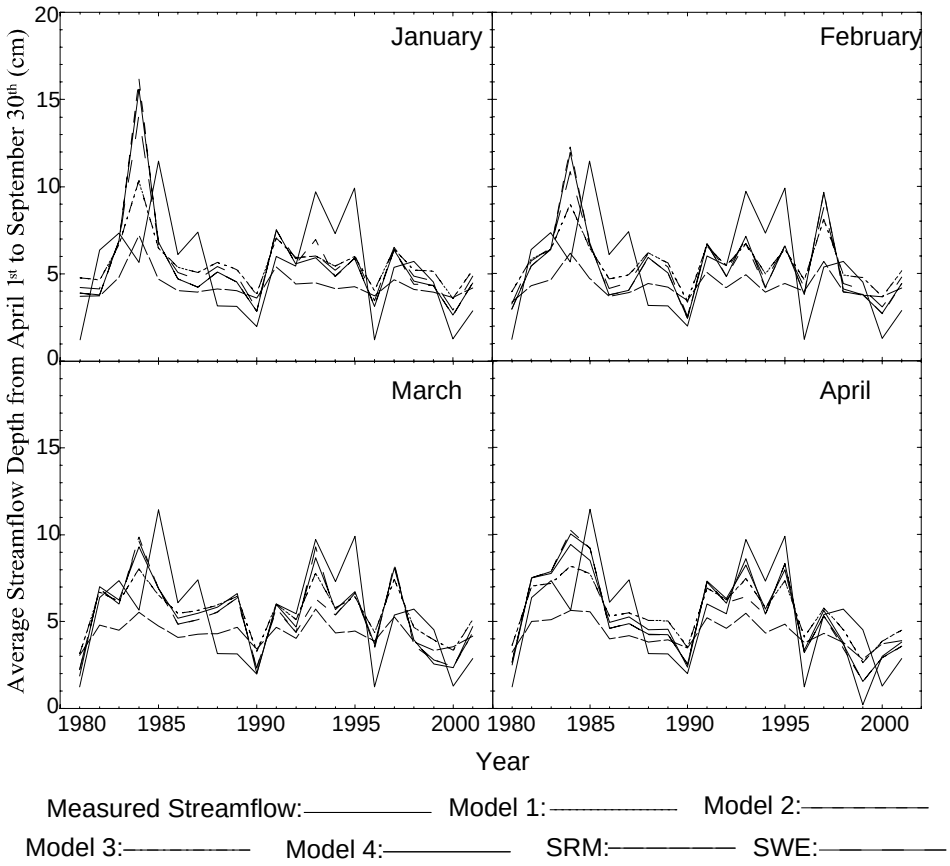

Figure 4-8. Streamflow forecasts for six models on January 1st, February 1st, March 1st and April 1st in the Rio Ojo watershed

Table 4-4. C_p values for streamflow forecasts for all the models with ensemble-forecasted precipitation on January 1st, February 1st, March 1st and April 1st

Rio Grande	Model 1	Model 2	Model 3	Model 4	SRM	SWE	NRCS
January 1st	0.44	0.50	0.48	0.53	0.35	0.57	0.20
February 1st	0.47	0.56	0.51	0.55	0.41	0.55	0.25
March 1st	0.43	0.52	0.47	0.50	0.38	0.43	0.26
April 1st	0.40	0.48	0.44	0.44	0.38	0.46	0.26

Rio Ojo	Model 1	Model 2	Model 3	Model 4	SRM	SWE
January 1st	0.23	-0.17	0.23	-0.13	0.02	0.02
February 1st	0.28	0.09	0.28	0.13	0.04	0.23
March 1st	0.43	0.35	0.43	0.43	0.13	0.44
April 1st	0.56	0.54	0.56	0.62	0.22	0.57

In the case of Rio Grande watershed, model 2 shows slightly better performance compared to the other models although not as much better as was the case for observed precipitation. Again, the use of a linear relation between SWE and precipitation instead of C_S and C_R in model 2 improves the performance of streamflow forecasts on April 1st when ensemble-forecasted precipitation is used. It is also interesting to consider the deterioration of streamflow forecasts using the SRM mass-balance model compared to that using observed precipitation. The SRM mass-balance model seems to have more sensitivity to the accuracy of the precipitation, and this can be confirmed by examining the average of standard deviations of the ensemble of forecasted streamflow for each year on April 1st (**Table 4-5**). SRM mass-balance model shows the highest standard

deviation of the ensemble of forecasted streamflow for each year on April 1st compared to other models, and therefore using the average of the ensemble of forecasted streamflow deteriorates the performance of model. However, this does not mean that the standard deviation of the ensemble of forecasted streamflow should be small to obtain good streamflow forecasts as measured by C_p value. For example, models 1 and 3 show the smaller standard deviations compared to model 2 although they show less satisfactory streamflow forecasts. This situation seems to be related to the fact that the variation of precipitation does not control the variation of streamflow. Meanwhile, in the case of Rio Ojo watershed, like the case of streamflow forecasts with the observed precipitation, model 4 shows the highest C_p value and SRM mass-balance model shows the lowest one although the differences among all the models except SRM mass-balance model are small. The relationship between the standard deviation of ensemble forecasted streamflow for each year and performance of model can be clearly seen in this watershed. Because optimized C_R coefficients have almost zero values in models 1 and 3 in the Rio Ojo watershed as mentioned above, the ensemble-forecasted precipitation does not affect the streamflow variation which makes the standard deviation almost zero. Therefore, in order to obtain good streamflow forecasts using the ensemble of forecasted streamflow, the standard deviation of the ensemble of forecasted streamflow should be apparently of moderate size.

Table 4-5. Average of standard deviation (cm) of ensemble of forecasted streamflow depth for each year on April 1st in both watersheds

	Model 1	Model 2	Model 3	Model 4	SRM
Rio Grande	2.15	3.58	2.24	2.60	4.29
Rio Ojo	0.01	0.74	0.01	0.65	1.11

Notice also the difference in the effect of using ensemble-forecasted precipitation compared to the observed one between the two watersheds. In the Rio Grande watershed, streamflow forecasts made using the ensemble-forecasted precipitation are worse than those using observed precipitation. However, the model performance is almost the same in the Rio Ojo watershed. This situation is again related to very small optimized C_R parameter values in the Rio Ojo watershed which make the effects of the precipitation negligible.

4.4.2.2. Streamflow Forecasts in Winter Months (January 1st, February 1st, March 1st) Using Ensemble-Forecasted Precipitation

Although streamflow forecasts on April 1st are important, forecasts on January 1st, February 1st and March 1st are even more valuable because these winter-time streamflow forecasts provide more time to water users to make use of the information. Because all the models except the streamflow forecasts using only SWE are based on a mass balance, the linear regressions between observed SWE on January 1st, February 1st, March 1st and observed SWE on April 1st in each SNOTEL station were used to estimate SWE on April 1st in each month. This estimated SWE at each SNOTEL station was averaged to obtain representative estimate of April 1st SWE. Other procedures are the same as streamflow forecasts on April 1st. **Figure 4-9** shows these linear regressions in one SNOTEL station for each watershed. As can be seen, the SWE on January 1st, February 1st and March 1st is well correlated to the SWE on April 1st and this good relationship was also applicable to other SNOTEL stations in both watersheds.

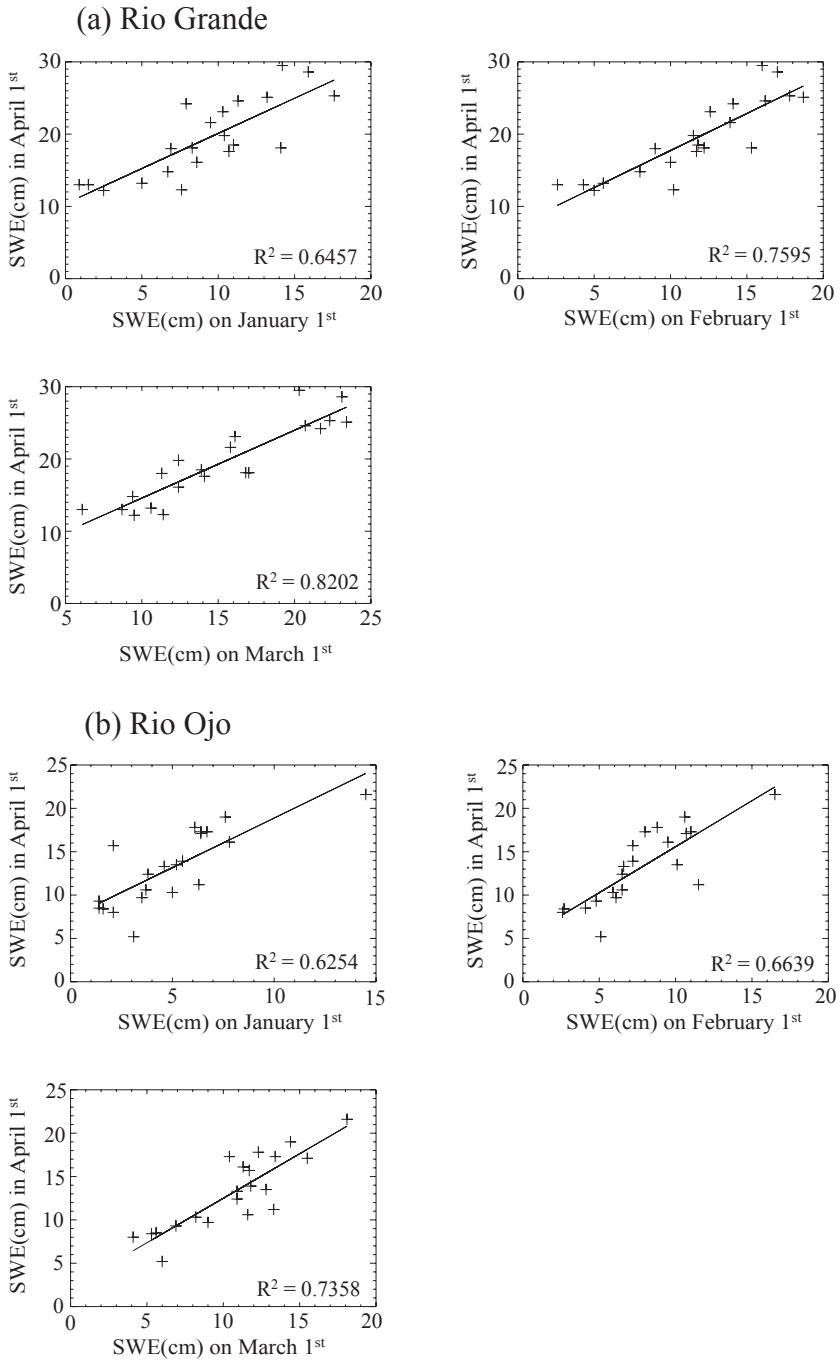

Figure 4-9. Linear relationships between historical SWE from 1981 to 2001 on January 1st, February 1st, March 1st and April 1st in a SNOTEL station (Middle Creek) in the Rio Grande watershed (a), and in a SNOTEL station (Bateman) in the Rio Ojo watershed (b)

Figure 4-7 and **Figure 4-8** illustrate the comparisons of streamflow forecasts in the Rio Grande and Rio Ojo watersheds, respectively, and **Table 4-4** lists C_p for each model from January 1st to March 1st. As can be seen, for the Rio Grande watershed, models 2 and 4 have slightly better C_p values than models 1 and 3 among those using optimized parameter values, and these models are better than the simple index-variable model only on March 1st. The use of a linear relationship instead of C_S and C_R again improves the performance of streamflow forecasts in winter months. Notice also that streamflow forecasts for the Rio Grande from early months (January 1st, February 1st) show higher C_p values than those from later months (March 1st, April 1st). This situation seems to be related to the climatological seasonal precipitation. That is, although April 1st is the closest day to the period of our interest for the streamflow forecasts, the streamflow amount from April 1st to September 30th in the Rio Grande watershed is more closely related to the SWE on January 1st or February 1st. This situation can be observed in the linear regressions between average measured SWE on the 1st day of each winter month and streamflow amounts from April 1st to September 30th (**Figure 4-2**). In the case of Rio Ojo watershed, models 1 and 3 generally have higher C_p values and have much more stable C_p values among the months compared to other models. With respect to forecast accuracy as a function of the date of the forecast, unlike the Rio Grande watershed, streamflow forecasts are improved with time.

The NRCS streamflow forecasts perform poor results compared to other models. However, NRCS streamflow forecasts are for the naturalized streamflow, not the measured streamflow in the streamflow gauge. Therefore, it is not appropriate to make a

simple comparison between NRCS streamflow forecasts and those using other models. However, they provide an indication of how much accurate the streamflow forecasts made by our models are.

4.5. Conclusions

This chapter presented an investigation of the forecasting of April 1st to September 30th streamflow volume using a mass-balance model which uses the parameter values obtained from SRM streamflow stimulations (called the SRM mass-balance model), mass-balance models of various complexities which have optimized parameter values, and a simple index-variable model using only SWE. Because there were only 21 years of data available in the watersheds, all the models used split-sample method. The streamflow forecasts were conducted using two precipitation conditions. One case used observed precipitation in the forecasted years even though it is not a true forecast, and the other used ensemble-forecasted precipitation from 1981 to 2001 excluding the observed precipitation in the year of interest. Observed precipitation in the forecasted years was used because the errors of precipitation forecasts can dominate the forecast errors, making it difficult to see the utility of the model itself for streamflow forecasts. Meanwhile, the reason to apply the ensemble-forecasted precipitation was that it is difficult to obtain reliable long-term precipitation forecasts, and therefore this method was used to overcome this limitation in the actual forecasting mode.

First, although a true forecast can not use observed precipitation in the forecasted year, the SRM mass-balance model in the large snowmelt-dominated Rio

Grande watershed showed some forecast value even without optimization if dependable precipitation forecasts are available. Meanwhile, ensemble-forecasted precipitation gave worse streamflow forecasts because of the high sensitivity of model to the precipitation. Therefore, the SRM mass-balance model for seasonal streamflow forecast in the Rio Grande watershed can be used under the condition that dependable precipitation forecasts are provided. The SRM mass-balance model in the drier and small Rio Ojo watershed provided no satisfactory forecasting results in either condition. This situation appears to be related to two main factors. The first is higher variation of parameter values obtained through the streamflow simulations, and the second is weaker relationships between average measured SWE and other parameter values which are used in the SRM mass-balance model compared to those in the Rio Grande watershed (**Figure 4-1**).

In the optimized models, the replacement of linear functions of SWE and precipitation for the C_S and C_R, respectively, significantly improved model conceptualization obtained through the relationship between measured and optimized streamflow (**Figure 4-5**), and in the model forecasting on April 1st when observed precipitation in the year of interest was used in both watersheds (**Figure 4-6**). The zonal separation of variables (SWE and precipitation) in the optimized models, however, showed different effects to the model performance between the two watersheds when observed precipitation in the year of interest was used. That is, while zonal separation of variables in the Rio Grande watershed decreased the performance in model 2, making model 4 have the worst performance among the optimized models, this separation

improved model 2, making model 4 show the best performance among the optimized models in the Rio Ojo watershed.

In the case of streamflow forecasts on January 1st, February 1st, March 1st and April 1st using ensemble forecasted precipitation in the Rio Grande watershed, models 2 and 4 had slightly better C_p values compared to the models 1 and 3 among the models using optimized parameter values, and these models showed almost the same performance as that of simple index-variable model. Meanwhile, in the Rio Ojo watershed, models 1 and 3 showed higher C_p values and much more stability in the C_p values among the months compared to other models.

However, when the C_p values of streamflow forecasts on April 1st using observed precipitation were compared with the streamflow forecasts of simple index-variable model using only SWE, there was significant improvement in model 2 in the case of the Rio Grande watershed and some improvement in model 4 in the case of the Rio Ojo watershed. Therefore, our optimized models showed potential to improve the accuracy of streamflow forecasts on April 1st especially in the Rio Grande watershed. However, this potential largely depends on the accuracy of precipitation forecast.

Finally, when the streamflow forecasts using above models were compared to the forecasts for naturalized streamflow made from NRCS, although the direct comparison is not appropriate because of the differences in the range of available data and in the streamflow forecasted, there were significant improvements in the optimized models.

CHAPTER V

GENERAL CONCLUSIONS AND RECOMMENDATIONS

In this dissertation, three hydrological perspectives on the improvement of long-term streamflow forecasting were investigated in the snowmelt-dominated URG basin of Colorado and New Mexico. The first chapter presented an investigation of the effects of ENSO on two important climatic factors, temperature and precipitation, along with streamflow volumes and estimates of SWE at snowcourse stations over the years of 1952-1999. This investigation demonstrated that ENSO modulates temperature and precipitation across the URG basin, affecting snow accumulation and melt and the resulting streamflow. Comparing this research with previous works highlights some important characteristics concerning temperature and precipitation responses to ENSO episodes specific to the URG. First, temperature differences between the three ENSO phases are not uniform throughout the entire winter, but are concentrated at its beginning and end – i.e., during November and March. Second, in El Niño years as compared to neutral years, the URG experiences lower temperatures especially in its northern and eastern sections. Third, during La Niña years, March temperatures are warmer across the entire basin. With respect to temperature at least, it can be said that ENSO in the URG affects the length of winter rather than its severity. Meanwhile, statistically significant increases in monthly precipitation totals during El Niño years were found to occur only during November. Significantly lower precipitation occurred

in La Niña years during December and March. So, climatological precipitation differences during El Niño, neutral, and La Niña years are confined to certain months, predominantly at the beginning and end of the winter season.

Differences in SWE among ENSO phases were found to exist during only March. Thus March during La Niña years is the critical month in determining differences in annual hydrograph in the URG. Higher temperatures and lower precipitation result in lower, and usually earlier, streamflow, compared to that of neutral and El Niño years. March therefore needs to be given special attention when modeling scenarios of streamflow under altered climatic conditions.

There are variable time lags between ENSO-modulated differences in temperature and precipitation and the resultant streamflow. Colder temperatures and greater precipitation in November of El Niño may result in more snow storage over the winter and higher streamflow during the following snowmelt season – a time lag of several months. However, the impact of warmer and drier conditions during March of La Niña years on streamflow is more immediate, with almost no lag time occurring between ENSO modulated meteorological differences and the resultant streamflow.

La Niña years experience decreased annual streamflow compared to both El Niño and neutral water years. However, examination of the reduction of runoff during La Niña phase on a monthly basis reveals different responses at different stations. With the exception of the Rio Grande at Embudo and Rio Pueblo, the peak streamflow month at the studied stations during La Niña years is earlier, though the size of the volume differences varies. At the Rio Grande near Del Norte, the effect of ENSO is rather slight,

matching small differences in SWE between El Niño and La Niña years in this drainage basin. At the Rio Grande at Embudo and at Rio Pueblo, winter streamflow during La Niña years is greatly increased and the spring peak is attenuated.

The second chapter approached the improvement of long-term streamflow forecasts in the URG basin by an investigation of the efficacy of the newly available MODIS snowcover product. The usefulness of the MODIS snowcover product was evaluated by the comparison of streamflow simulations using it and the NOHRSC snowcover product with the widely-used SRM in the two sub-watersheds (Rio Grande, Rio Ojo) located inside the URG basin. Differences in mapped snow cover during the melt season lead to differences in the simulated runoff and zonally averaged SWE. The MODIS product was found to generally map more snow at higher elevations in the two studied watersheds than did the NOHRSC product, while both products mapped similar snow amounts at lower elevations. The greater amount of snow mapped by MODIS lead to higher simulated discharge volumes from April to September in SRM simulations than when NOHRSC snow depletion curves were used. Similarly, the calculated zonally averaged April 1st SWE from MODIS was higher than that calculated using NOHRSC snow maps. MODIS-derived snow maps showed more consistent patterns of snow cover retreat with respect to elevation than did the NOHRSC snow maps, and no significant effect of aspect on differences between the two products in mapped snowcover was found.

For the larger and wetter of the two watersheds, the Rio Grande, satisfactory simulations were obtained by using representative parameter values obtained from 1990

– 2001 SRM streamflow simulations. The MODIS-based simulations showed higher discharge simply because MODIS mapped more snow in the watersheds. Meanwhile, SRM was unable to satisfactorily simulate observed streamflow in the smaller Rio Ojo watershed because of much drier condition and smaller size compared to the Rio Grande. The observed differences in MODIS- and NOHRSC-based simulated streamflow for both watersheds were traced to spatial-temporal differences in SCA in a single SRM zone, the 2nd zone, within each watershed. This zone comprises approximately 50% of the area of both watersheds, and in this zone of both watersheds, MODIS consistently mapped more snow. Because this zone occupies a high proportion of each watershed's area, small fractional SCA differences lead to some differences in simulated streamflow.

Total basin April 1st SWE calculated using MODIS-based snow depletion curves showed a little more difference compared to the difference in the amount of simulated streamflow. Again, the 2nd zone in each watershed contributes most significantly. The differences between SRM zonally averaged SWE and SNOTEL measured SWE located in the uppermost (3rd) zone in both watersheds were judged to be small when the fact that the SWE measurement is a point one is considered. However, snowcover information obtained from MODIS and NOHRSC maps and discharge simulated using the SRM was generally quite comparable both in terms of total seasonal discharge and in daily streamflow variations for two tributary basins of the URG. Thus it appears that MODIS snowcover product can provide SCA information of sufficient quality for streamflow simulation using SRM in snowmelt-dominated watersheds.

Finally, the fourth chapter presented an investigation of the forecasting of April 1st to September 30th streamflow volume using a mass-balance model with the parameter values obtained from SRM streamflow stimulations, four mass-balance models of various complexities which have optimized parameter values, and a simple index-variable model using only SWE and naturalized streamflow forecasts made by NRCS. The streamflow forecasts were conducted using two precipitation conditions. One case used observed precipitation in the forecasted years even though it is not a true forecast, and the other used ensemble-forecasted precipitation from 1981 to 2001 excluding the observed precipitation of the year of interest.

The results of this investigation were as follows. First, although it is not a real forecasting situation to use observed precipitation in the forecasted year, the SRM mass-balance model in the larger snowmelt-dominated Rio Grande watershed showed some forecast value even though no optimization process was involved if dependable precipitation forecasts are provided. Meanwhile, the application of ensemble-forecasted precipitation gave worse streamflow forecasts than when observed precipitation was used because of the high sensitivity of model to the precipitation. The use of SRM mass-balance model in the drier and smaller Rio Ojo watershed did not give any satisfactory forecasting results in either condition. This situation was related to two main factors. The first is higher variation of parameter values obtained through the streamflow simulations, and the second is weaker relationships between average measured SWE and other parameter values compared to those in the Rio Grande watershed.

Considering the results for the optimized models, the replacement of C_S and C_R with linear functions of SWE and precipitation, respectively, gave significant improvement in the model fit to the observed streamflow in the case of observed precipitation of the year of interest in both watersheds. The zonal separation of variables (SWE and precipitation) in the optimized models, however, showed different effects to the model performance between the two watersheds, with the Rio Grande showing the deterioration of model performance and the Rio Ojo showing the improvement of model performance. Meanwhile, using the ensemble-forecasted precipitation decreased the forecasting differences among different models including simple index-variable model, making all the models except SRM mass-balance model have almost the same forecasting results in both watersheds.

When the C_p values of streamflow forecasts on April 1st using observed precipitation were compared with the streamflow forecasts of simple index-variable model using only SWE on April 1st, there was significant improvement in model 2 in the Rio Grande watershed and some improvement in model 4 in the Rio Ojo watershed. Therefore, optimized models 2 and 4 showed potential to improve the accuracy of streamflow forecasts in the Rio Grande and Rio Ojo watersheds, respectively, although this potential largely depends on the accuracy of precipitation forecast.

Finally, when the streamflow forecasts using above models were compared to the forecasts for naturalized streamflow made from NRCS, although the direct comparison is not appropriate because of the differences in the range of available data

and in the streamflow forecasted, there were significant improvements in the optimized models.

The following recommendations are proposed for the future research.

1. In addition to the ENSO teleconnection, much research about the relationships between Pacific Decadal Oscillation (PDO) or Arctic Oscillation (AO) and regional climate variables has been conducted. Accordingly, future studies could extend this ENSO analysis to these other indices. This would add to the understanding of the effects that teleconnections between global atmospheric circulations and regional climate have on hydrologic, ecologic and geomorphologic processes, and it might be ultimately possible to provide more accurate long-term streamflow forecasts in regional basis with a long lead-time.

2. Although the relative differences between simulated streamflow using NOHRSC and newly available MODIS snowcover product were investigated in chapter III, it would be also interesting to evaluate the accuracy of MODIS snowcover product by comparing it with that obtained using higher resolution remotely-sensed data sources such as Landsat, SPOT or ASTER under various conditions in these and other watersheds.

3. In chapter IV, ensemble-forecasted precipitation were used in order to provide the long-term precipitation because there are currently no such available long-term precipitation forecasts. However, the Climate Prediction Center (CPC) of NOAA currently provides 3-month precipitation forecasts at various lead-times. Accordingly, it

would be also interesting to examine the performance of above optimized models using these actual precipitation forecasts issued by the CPC.

REFERENCES

Ackerman SA, Strabela KI, Menzel PWP, Frey RA, Moeller CC and Gumley LE, 1998. Discriminating clear sky from clouds with MODIS. *Journal of Geophysical Research* **103**(D24): 32,141-32,157.

Armstrong RL, Brodzik MJ. 2001. Recent northern hemisphere snow extent: A comparison of data derived from visible and microwave satellite sensors. *Geophysical Research Letters* **28**: 3673-3676.

Bartolino JR, Cole JC. 2002. *Ground-water Resources of the Middle Rio Grande Basin*. US Geological Survey Circular 1222. Reston, Virginia.

Barton JS, Hall DK, Riggs GA. 2000. Remote sensing of fractional snow cover using Moderate Resolution Imaging Spectroradiometer (MODIS) data. In *Proceedings of the 57th Eastern Snow Conference*, Syracuse, New York; 171-183.

Baumgartner MF, Seidel K, Martinec J. 1987. Toward snowmelt runoff forecast based on multisensor remote-sensing information. *IEEE Transactions on Geoscience and Remote Sensing* **25**: 746-750.

Bergstrom S. 1975. The development of a snow routine for the HBV-2 model. *Nordic Hydrology* **6**: 73-92.

Bitner D, Carroll T, Cline D, Romanov R. 2002. An assessment of the differences between three satellite snow cover mapping techniques. *Hydrological Processes* **16**: 3723-3733.

Brown RD. 1998. El Niño and North American snow cover. In *Proceedings of the 55th Eastern Snow Conference*, 2-3 June 1998, Jackson, New Hampshire; 165-171.

Cayan DR. 1996. Interannual climate variability and snowpack in the western United States. *Journal of Climate* **9**: 928-948.

Cayan DR, Redmond KT, Riddle LG. 1999. ENSO and hydrologic extremes in the western United States. *Journal of Climate* **12**: 2881-2893.

Cayan DR, Webb RH. 1992. El Niño/Southern Oscillation and streamflow in the western U.S. In *Historical and Paleoclimatic Aspects of the Southern Oscillation*, Diaz HF, Markgraf V (eds). Cambridge University Press. New York; 29-68.

Chang ATC, Foster JL, Hall DK. 1987. Nimbus-7 SMMR derived global snow cover parameters. *Annals of Glaciology* **9**: 39-44.

Chiew FHS, Piechota TC, Dracup JA, McMahon TA. 1998. El Niño/Southern Oscillation and Australian rainfall, streamflow and drought: links and potential for forecasting. *Journal of Hydrology* **204**: 138-149.

Chiew FHS, Zhou SL, McMahon TA. 2003. Use of seasonal streamflow forecasts in water resources management. *Journal of Hydrology* **207**: 135-144.

Clark MP, Serreze MC, McCabe GJ. 2001. Historical effects of El Niño and La Niña events on the seasonal evolution of the montane snowpack in the Columbia and Colorado river basins. *Water Resources Research* **37**: 741-757.

Cline DW, Carroll TR. 1999. Inference of snow cover beneath obscuring clouds using optical remote sensing and a distributed snow energy and mass balance model. *Journal of Geophysical Research* **104**(D16): 19, 631-19,644.

Clyde GD. 1931. *Snow Melting Characteristics*. Utah Agricultural Experiment Station, Bulletin No. 231: Logan, Utah.

Collins, EH. 1934. Relationship of degree-days above freezing to runoff. *Transactions of the American Geophysical Union* **15**: 624-629.

Compagnucci RH, Vargas WM. 1998. Inter-annual variability of the Cuyo rivers' streamflow in the Argentinean and Andean Mountains and ENSO events. *International Journal of Climatology* **18**: 1593-1609.

Davis, JC. 1986. *Statistics and Data Analysis in Geology*. Wiley: New York.

Dewalle DR, Henderson Z, Rango A. 2002. Spatial and temporal variations in snowmelt degree-day factors computed from SNOTEL data in the Upper Rio Grande basin. In *Proceedings of the 70th annual Western Snow Conference*, Sol Vista, Corolado; 73-81.

Dey B, Goswami DC, Rango A. 1983. Utilization of satellite snow-cover observations for seasonal streamflow estimates in the western Himalayas. *Nordic Hydrology* **14**: 257-266.

Dracup JA, Kahya E. 1994. The relationship between U.S. streamflow and La Niña events. *Water Resources Research* **30**: 2133-2141.

Ferguson RI. 1999. Snowmelt runoff models. *Progress in Physical Geography* **23**: 205-227.

Garen DC. 1992. Improved techniques in regression-based streamflow volume forecasting. *Journal of Water Resources Planning and Management* **118**: 654-670.

Gershunov A. 1998. ENSO influence on intraseasonal extreme rainfall and temperature frequencies in the contiguous United States: implications for long-range predictability. *Journal of Climate* **11**: 3192-3203.

Gershunov A, Barnett TP. 1998. ENSO influence on intraseasonal extreme rainfall and temperature frequencies in the contiguous United States: observations and model results. *Journal of Climate* **11**: 1575-1586.

Groisman PY, Eastering DR. 1994. Variability and trends of total precipitation and snowfall over the United States and Canada. *Journal of Climate* **7**: 184-205.

Hall DK, Martinec J. 1985. *Remote Sensing of Ice and Snow*. Chapman and Hall: New York.

Hall DK, Riggs GA, Salomonson VV. 1995. Development of methods for mapping global snow cover using moderate resolution imaging spectroradiometer data. *Remote Sensing of Environment* **54**: 127-140.

Hall DK, Andrew BT, James LF, Alfred TCC, Milan A. 2000. Intercomparison of satellite-derived snow-cover maps. *Annals of Glaciology* **31**: 369-376.

Hall DK, Riggs GA, Salomonson VV, Barton JS, Casey K, Chien JYL, DiGirolamo NE, Klein AG, Powell HW, Tait AB. 2001. *Algorithm Theoretical Basis Document (ATBD) for the MODIS Snow and Sea Ice-Mapping Algorithms*. http://modis-snow-ice.gsfc.nasa.gov/atbd01.html (last accessed: July 13, 2003).

Hall DK, Riggs GA, Salomonson VV, DiGirolamo NE, Bayr KJ. 2002. MODIS snow-cover products. *Remote Sensing of Environment* **83**: 181-194.

Hamlet AF, Huppert D, Lettenmaier DP. 2002. Economic value of long-head streamflow forecasts for Columbia River hydropower. *Journal of Water Resources Planning and Management* **128**: 91-101.

Hartman RK, Rost AA, Anderson DM. 1996. *Operational Processing of Multi-Source Snow Data*, Paper presented at Third International Conference/Workshop on Integrating Geographic Information Systems and Environmental Modeling. National Center for Geographic Information and Analysis, Santa Barbara, California.

Justice C, Vermote E, Townshend JRG, Defries R, Roy DP, Hall DK, Salomonson VV, Privette J, Riggs G, Strahler A, Lucht W, Myneni R, Knjazihhin Y, Running S, Nemani R, Wan Z, Huete A, van Leeuwen W, Wolfe R, Giglio L, Muller J-P, Lewis P, Barnsley M. 1998. The Moderate Resolution Imaging Spectroradiometer (MODIS): Land remote sensing for global change research. *IEEE Transactions on Geoscience and Remote Sensing* **36**: 1228-1249.

Kahya E, Dracup JA. 1993. U.S. streamflow patterns in relation to the El Niño/Southern Oscillation. *Water Resources Research* **29**: 2491-2503.

Kaufman YJ, Kleidman RG, Hall DK, Martins JV, Barton JS. 2002. Remote sensing of subpixel snow cover using 0.66 and 2.1 μm channels. *Geophysical Research Letters* **29**: 28-1 – 28-4.

Klein AG, Barnett AC. 2003. Validation of daily MODIS snow cover maps of the Upper Rio Grande river basin for the 2000-2001 snow year. *Remote Sensing of Environment* **86**: 162-176.

Kustas WP, Rango A, Uijlenhoet R. 1994. A simple energy budget algorithm for the snowmelt runoff model. *Water Resources Research* **30**: 1515-1527.

Landesa EG, Rango A. 2002. Operational snowmelt runoff forecasting in the Spanish Pyrenees using the snowmelt runoff model. *Hydrological Processes* **16**: 1583-1591.

Leaf CF. 1967. Areal extent of snow cover in relation to streamflow in central Colorado, In *Proceedings of the International Hydrology Symposium*, Fort Collins, Colorado; 157-164.

Lettenmaier DP, Garen DC. 1979. Evaluation of streamflow forecasting methods. In *Proceedings of the 47th Western Snow Conference*, Sparks, Nevada; 48-55.

Lettenmaier DP, Wood EF, Parkinson DB. 1990. Operating the Seattle water system during the 1987 drought. *Journal of American Water Works Association* **82**: 55-60.

Maidment DR. 1992. *Handbook of Hydrology*. McGraw-Hill: New York.

Martinec J. 1975. Snowmelt-runoff model for stream flow forecasts. *Nordic Hydrology* **6**: 145-154.

Martinec J and Rango A. 1981. Areal distribution of snow water equivalent evaluated by snow cover monitoring. *Water Resources Research* **17**: 1480-1488.

Martinec J. 1985. Snowmelt runoff models for operational forecasts. *Nordic Hydrology* **16**: 129-136.

Martinec J, Rango A. 1986. Parameter values for snowmelt runoff modeling. *Journal of Hydrology* **84**: 197-219.

Martinec J, Rango A. 1987. Interpretation and utilization of areal snow-cover data from satellites. *Annals of Glaciology* **9**: 166-169.

Martinec J. 1991. Areal modeling of snow water equivalent based on remote sensing techniques. Snow, Hydrology and Forests in High Alpine Areas. In *Proceedings of the Vienna Symposium*. IAHS Publication. no. 205. IAHS Press: Wallingford, UK; 121-129.

Martinec J, Rango A. 1995. Seasonal runoff forecasts for hydropower based on remote sensing. In *Proceedings of the 63rd Western Snow Conference*, Reno, Nevada; 10-20.

Martinec J, Rango A, Robert R. 1998. *Snow Runoff Model (SRM) User's Manual*. http://hydrolab.arsusda.gov/cgi-bin/srmhome (last accessed: July 13, 2003).

Maurer EP, Rhoads JD, Dubayah RO, Lettenmaier DP. 2003. Evaluation of the snow-covered area data product from MODIS. *Hydrological Processes* **17**: 59-71.

Maxson RW, Allen MW, Szeliga TL. 1996. Theta – Image Classification by Comparison of Angles Created between Multi-channel Vectors and an Empirically Selected Reference Vector. http://www.nohrsc.nws.gov/html/papers/theta/theta.htm (last accessed: October 20, 2001).

McCuen, RH. 1998. *Hydrologic Analysis and Design*, 2nd edn. Prentice-Hall: Upper Saddle River, New Jersey; 189-190.

Mitchell KM, DeWalle DR. 1998. Application of the snowmelt runoff model using multiple-parameter landscape zones on the Towanda creek basin, Pennsylvania. *Journal of the American Water Resources Association* **34**: 335-346.

Potts HL. 1937. Snow surveys and runoff forecasting from photographs. In *Proceedings of South Continental Divide Snow-Survey Conference*, Denver, Colorado; 658-660.

Ramsay B. 2000. Prospects for the interactive multisensor snow and ice mapping system (IMS), In *Proceedings of the 57th Eastern Snow Conference*, Syracuse, New York; 161-170.

Rango A, Martinec J. 1979. Application of a snowmelt-runoff model using Landsat data. *Nordic Hydrology* **10**: 225-238.

Rango A. 1980. Operational applications of satellite snow cover observations. *Water Resources Bulletin* **16**: 1066-1073.

Rango A, Martinec J. 1981. Accuracy of snowmelt runoff simulation. *Nordic Hydrology* **12**: 265-274.

Rango A. 1985. Assessment of remote sensing input to hydrologic models. *Water Resources Bulletin* **21**: 423-432.

Rango A. 1986. Progress in snow hydrology remote-sensing research. *IEEE Transactions on Geoscience and Remote Sensing* **24**: 47-53.

Rango A, van Katwijk V. 1990. Development and testing of a snowmelt-runoff forecasting technique. *Water Resources Bulletin* **26**: 135-144.

Rango A. 1992. Worldwide testing of the snowmelt runoff model with applications for predicting the effects of climate change. *Nordic Hydrology* **23**: 155-172.

Rango A, Martinec J. 1995. Revisiting the degree-day method for snowmelt computations. *Water Resources Bulletin* **31**: 657-669.

Rango A. 1996. Spaceborne remote sensing for snow hydrology applications. *Hydrological Science* **41**: 477-494.

Rango A, Martinec J. 1997. Water storage in mountain basins from satellite snow cover mapping. In *Remote Sensing and Geographical Information Systems for Design and Operation for Water Resources System*, Baumgartner MF, Schultz GA and Johnson AI (eds). IAHS Publication no. 242. IAHS Press: Wallingford, UK; 83-91.

Rango A, Landesa EG, Bleiweiss M. 2002. Comparative satellite capabilities for remote sensing of snow cover in the Rio Grande basin. In *Proceedings of the 70th Western Snow Conference*, Sol Vista, Colorado; 21-26.

Rango A, Landesa EG, Bleiweiss M, Havstad K, Tanksley K. 2003. Improved satellite snow mapping, snowmelt runoff forecasting, and climate change simulations in the Upper Rio Grande basin. *World Resource Review* **15**: 26-41.

Redmond KT, Koch RW. 1991. Surface climate and streamflow variability in the western United States and their relationship to large-scale circulation indices. *Water Resources Research* **27**: 2381-2399.

Richard C, Gratton DJ. 2001. The importance of the air temperature variable for the snowmelt runoff modeling using the SRM. *Hydrological Processes* **15**: 3357-3370.

Riggs G, Hall DK. 2002. Reduction of cloud obscuration in the MODIS snow data product. In *Proceedings of the 59th Eastern Snow Conference*, Stowe, Vermont; 205-212.

Rodriguez JY. 1994. An operational forecasting snowmelt model with objective calibration. *Nordic Hydrology* **25**:79-100.

Romanov P, Gutman G, Csiszar I. 2000. Automated monitoring of snow cover over North America with multispectral satellite data. *Journal of Applied Meteorology* **39**: 1866-1880.

Ropelewski CF, Halpert MS. 1986. North American precipitation and temperature patterns associated with the El Niño/Southern Oscillation (ENSO). *Monthly Weather Review* **114**: 2352-2362.

Ropelewski CF, Halpert MS. 1989. Precipitation patterns associated with the high index phase of the southern oscillation, *Journal of Climate* **2**: 268-284.

Ropelewski CF, Jones PD. 1987. An extension of the Tahiti-Darwin southern oscillation index. *Monthly Weather Review* **115**: 2161-2165.

Scharfen GR, Hall DK, Riggs GA. 1997. MODIS snow and ice products from the NSIDC DAAC, In *Proceedings of the SPIE*, San Diego, California; 143-147.

Shafer BA, Jones EB, Frick DM. 1982. *Snowmelt Runoff Simulation Using the Martinec-Rango Model on the South Fork Rio Grande and Conejos River in Colorado*. AgRISTARS Report. Goddard Space Flight Center, Greenbelt, Maryland.

Stedinger JR, Grygier J, Yin H. 1989. Seasonal streamflow forecasts based upon regression in computerized decision support systems for water managers, Labadie JW, Brazil LE, Corbu I, Johnson LE (eds), In *Proceedings of the 3rd Water Resources Operations Management Workshop*, ASCE, New York; 266-279.

Thorn CR, McAda DP, Kernodle JM. 1993. *Geohydrologic Framework and Hydrologic Conditions in the Albuquerque Basin, Central New Mexico*. US Geological Survey Water-Resources Investigations Report 93-4149, US Department of the Interior, US Geological Survey, Denver.

Twedt TM, Schaake JC, Peck EL. 1977. National Weather Service extended streamflow prediction. In *Proceedings of the 45th Western Snow Conference*, Albuquerque, New Mexico; 52-57.

van Katwijk VF, Rango A, Childress AE. 1993. Effect of simulated climate change on snowmelt runoff modeling in selected basins. *Water Resources Bulletin* **29**: 755-766.

Vogelmann JE, Howard SM, Yang L, Larson CR, Wylie BK, van Driel N. 2001. Completion of the 1990s national land cover data set for the conterminous United States from Landsat Thematic Mapper data and ancillary data sources. *Photogrammetric Engineering and Remote Sensing* **67**:650-662.

Woolhiser DA, Keefer TO, Redmond KT. 1993. Southern Oscillation effects on daily precipitation in the southwestern United States. *Water Resources Research* **29**: 1287-1295.

VITA

Song-Weon Lee was born in 1970 in Seoul, South Korea. He is the son of Inbok Lee and Youngae Kim. He received a B.A. in forestry science from Kyunghee University, Seoul, South Korea, in 1996 and an M.E. from Texas A&M University in 1999. He entered the doctoral program in Civil Engineering at Texas A&M University on January 2000.

Selected Publications

Songweon Lee, Andrew Klein, Thomas Over, 2004. Effects of the El Nino-southern oscillation on temperature, precipitation, snow water equivalent and resulting streamflow in the Upper Rio Grande river basin. *Hydrological Processes*. **18**: 1053-1071.

Songweon Lee, Andrew Klein, Thomas Over, 2004. Comparison of MODIS and NOHRSC snowcover products for simulating streamflow using snowmelt runoff model. *Hydrological Processes*. (in review).

Songweon Lee, Thomas Over, Andrew Klein, 2004. Potential and limitations of mass-balance models for forecasting long-term streamflow volume in the Upper Rio Grande basin. *Water Resources Bulletin*. (in review).

His permanent mailing address: 442-3 Pulkwang-3 Dong, Enupyung-Gu,

Seoul 122-043

South Korea